Université catholique de Louvain

École polytechnique de Louvain (EPL)

Study of the Performance of a Natural Gas HCCI Engine Coupled with an Organic Rankine Cycle

Dissertation presented by
Corentin MICHEL and **Arnaud PAQUET**

for obtaining the Master's degree in
Mechanical Engineering

Supervisors
Hervé JEANMART, Maxime POCHET

Readers
Tony ARTS, Yann BARTOSIEWICZ

Academic year 2017-2018

"Remember to look up at the stars and not down at your feet. Try to make sense of what you see and wonder about what makes the universe exist. Be curious."

Stephen Hawking

Abstract

Homogeneous Charge Compression Ignition (HCCI) combustion is a promising way to combine both the advantages of the traditional Spark Ignition (SI) and Compression Ignition (CI) engines. Similarly to SI engines, a homogeneous charge is used, providing low NO_x formation, and is compressed to auto-ignition as in diesel engines, resulting in a high efficiency and reduced CO_2 emission.

The objective of this thesis is to study the performance of a stationary HCCI engine running on natural gas. Particularly, three methods have been reviewed in order to achieve higher power: turbocharging, exhaust gas recirculation (EGR) and coupling with an Organic Rankine Cycle (ORC).

Towards that goal, a test bench was implemented and used to experimentally study the influence of the intake conditions on the engine performance. Experiments were conducted on a four-cylinder HCCI engine operating with natural gas. Furthermore, a turbocharger and an EGR system were added to the test bench in order to analyse their impact on the engine power.

An HCCI 0-Dimensional model was developed and used together with experimental results to evaluate the optimum performance of the HCCI engine. A mathematical model was implemented for the theoretical study of the ORC in order to estimate the final performance of the HCCI-ORC system.

Results showed that when coupling with the Organic Rankine Cycle, the whole system could achieve an overall efficiency of 50.2%, which makes it quite competitive with the SOFC-MGT system and its 55% efficiency. Despite some assumptions made in the frame of this thesis, the HCCI-ORC system seems to be a promising technology in stationary power generation.

Acknowledgements

First of all, we would like to express our sincere gratitude to our thesis supervisors Prof. Hervé Jeanmart and Maxime Pochet for giving us the opportunity to work on such an interesting subject. Thank you for helping us to conduct this thesis in the best conditions throughout the year. Your guidance, availability and patience were essential to the quality of this work.

We would also like to thank Prof. Tony Arts and Prof. Yann Bartosiewicz for kindly accepting to be reader and jury member.

We would like to address our special thanks to the great technical staff of the TFL department, Julien, Frank, Lily and François, for their help in the implementation of the test bench and for accommodating so many of our unforeseen requests.

Finally, we would like to heartily thank our families and friends for their presence and support through this thesis and all these university years.

CONTENTS

NOMENCLATURE

ABBREVIATIONS

BDC	Bottom Dead Center
BMEP	Brake Mean Effective Pressure
CA10	Crank angle at which 10% of the combustion heat has been released
CA50	Crank angle at which 50% of the combustion heat has been released
CA90	Crank angle at which 90% of the combustion heat has been released
CA_{90-10}	Burn duration = CA90 − CA10
CAD	Crank Angle Degree
CI	Compression Ignition
CoV	Coefficient of Variation
EGR	Exhaust Gas Recirculation
EVC	Exhaust Valve Closing
EVO	Exhaust Valve Opening
FMEP	Friction Mean Effective Pressure
FuelMEP	Fuel Mean Effective Pressure
HCCI	Homogeneous Charge Compression Ignition
HR	Heat Release
ICE	Internal Combustion Engine
IMEPg	Gross Indicated Mean Effective Pressure
IMEPn	Net Indicated Mean Effective Pressure
IVC	Intake Valve Closing
IVO	Intake Valve Opening
LHV	Lower Heating Value
MEP	Mean Effective Pressure
MPRR	Maximum Pressure Rise Rate
NG	Natural Gas
NO_x	Nitrogen Oxide
ORC	Organic Rankine Cycle

PCP	Peak Cylinder Pressure
PCT	Peak Cylinder Temperature
PMEP	Pumping Mean Effective Pressure
QemisMEP	Emission Mean Effective Pressure
QexhMEP	Exhaust Mean Effective Pressure
QhrMEP	Heat Released Mean Effective Pressure
QhtMEP	Heat Transfer Mean Effective Pressure
QlossMEP	Heat Loss Mean Effective Pressure
RoHR	Rate of Heat Release
RPM	Revolutions Per Minute
SI	Spark Ignition
TDC	Top Dead Center
VGT	Variable Geometry Turbocharger
WHR	Waste Heat Recovery

SYMBOLS

A	Area
B	Cylinder bore
c	Specific heat
c_p	Specific heat at constant pressure
c_v	Specific heat at constant volume
h	Heat transfer coefficient
h_i	Sensible specific enthalpy of species i
L	Connecting rod length
m	Mass
$\dot{m}$	Mass flow rate
m_a	Mass of air
m_{a1}	Stoichiometric air-fuel ratio
m_b	Mass of burned gas
m_f	Mass of fuel
M_i	Molecular mass of species i
n	Number of moles, number of consecutive cycles
N	Crankshaft rotational speed
P	Power
p	Pressure, cylinder pressure
p_{exh}	Exhaust pressure of the turbine
p_{in}	Intake pressure
p_{out}	Exhaust pressure of the engine
Q	Heat transfer
Q_{exh}	Exhaust losses
Q_{gross}	Gross heat release

Q_{ht}	In-cylinder heat transfer losses
Q_{loss}	In-cylinder heat loss
Q_{net}	Net heat release
r	Crankshaft radius
R	Universal gas constant $= 8.3145\ \mathrm{J \cdot mol^{-1} \cdot K^{-1}}$
R_i	Specific gas constant of species i
S	Piston stroke
T	Temperature, cylinder temperature
T_{exh}	Exhaust temperature of the turbine
T_{in}	Intake temperature
T_{out}	Exhaust temperature of the engine
U	Internal energy
V	Volume, cylinder volume
$\dot{V}$	Volumetric flow rate
V_{a1}	Stoichiometric air-fuel ratio expressed in terms of $\mathrm{m}^3_{s,air}/\mathrm{m}^3_{s,fuel}$
V_c	Clearance volume
V_{cyl}	Single-cylinder displaced volume
V_d	Total displacement volume
W	Work transfer
(i)	Mass fraction of species i
$[i]$	Molar fraction of species i
α	EGR rate
γ	Specific heat ratio $= c_p/c_v$
ε_{exh}	Relative exhaust losses
ε_{ht}	Relative in-cylinder heat transfer losses
η_b	Brake efficiency
η_c	Combustion efficiency
η_{ge}	Gas exchange efficiency
η_{gen}	Generator efficiency
η_{ig}	Gross Indicated efficiency
η_{in}	Net Indicated efficiency
η_{mec}	Mechanical efficiency
η_{mTC}	Mechanical efficiency of the turbocharger
η_{net}	Net efficiency
η_{ti}	Thermodynamic efficiency
η_{siC}	Compressor isentropic efficiency
η_{siT}	Turbine isentropic efficiency
η_{vol}	Volumetric efficiency
θ	Crank angle
θ_b	Duration of the burning process
θ_s	Start of the burning process
λ	Air-fuel equivalence ratio

λ_{EGR}	Air-fuel equivalence ratio with EGR
ρ	Density
τ	Compression ratio
ϕ	Fuel-air equivalence ratio
ϕ_{EGR}	Fuel-air equivalence ratio with EGR
ω	Angular velocity

LIST OF FIGURES

LIST OF TABLES

INTRODUCTION

Homogeneous Charge Compression Ignition (HCCI) combustion is a promising way to combine both the advantages of the traditional Spark Ignition (SI) and Compression Ignition (CI) engines. Similarly to SI engines, a homogeneous charge is used, providing low NO_x formation, and is compressed to auto-ignition as in diesel engines, resulting in a high efficiency and reduced CO_2 emission.

The combustion process in HCCI engines relies on auto-ignition that arises during the compression stroke when the gas temperature increases. However, while SI engines use a spark-plug and CI engines rely on fuel injection timing, HCCI engines have no direct control on the auto-ignition. The combustion being only driven by chemical kinetics, a major challenge of this technology is to ensure a proper control of all the parameters that influence kinetics in order to maintain an optimum combustion phasing. Furthermore, HCCI engines are characterized by a very fast combustion as the homogeneous mixture burns almost instantly. Very lean mixtures, hence low power density, are then used to prevent important mechanical stresses that could result in ringing phenomenon.

In the frame of this thesis, three methods have been investigated to extend the upper load limit of a stationary natural gas HCCI engine, thereby increasing its efficiency: turbocharging, Exhaust Gas Recirculation (EGR) and coupling with an Organic Rankine Cycle (ORC). The purpose of this work is to evaluate the overall efficiency of an HCCI-ORC system with both turbocharging and EGR. Such a combined cycle could then be compared to other hybrid systems, such as the Solid Oxide Fuel Cell-Micro Gas Turbine (SOFC-MGT) system characterized by an overall efficiency of 55%.

The first chapter of this work presents the fundamentals concepts to understand the technology behind HCCI combustion, turbocharging, EGR and ORC. The second chapter details the methodology used in the frame of this thesis in order to effectively analyse the performance of the system. This includes the HCCI 0D model, the experimental setup and the mathematical modeling of the ORC. The final chapter discusses the results obtained in this work: the influence of intake conditions on HCCI engine performance and the coupling between the engine and the Organic Rankine Cycle, with an estimation of its overall efficiency.

CHAPTER 1

THEORETICAL CONCEPTS

This chapter presents the fundamentals underlying concepts of this work: HCCI combustion, turbocharging, Exhaust Gas Recirculation (EGR) and Organic Rankine Cycle (ORC). First, a brief overview is made to understand the technology behind Internal Combustion Engines (ICE). Then, the HCCI combustion principle as well as its advantages and limitations are analysed. In the third and fourth sections, the turbocharging technology and the influence of EGR on HCCI combustion are discussed. Finally, the basic concepts regarding the ORC are summarized.

1.1 A brief overview of IC engines

IC engines, which stands for internal combustion engines, are an integral part of society for their place in the automotive and stationary power generation industries. Internal combustion means that the combustion of the fuel occurs with an oxidizer inside a combustion chamber. The heat released by the combustion is then converted into a useful mechanical work by the piston. Nowadays, there are mainly two types of IC engines: Spark Ignition (SI) and Compression Ignition (CI) engines. Both technologies have their advantages and disadvantages particularly in terms of efficiency and pollutant emissions.

1.1.1 SI engine

SI engines, more commonly referred to Otto or gasoline engines, are characterized by the combustion of a homogeneous air-fuel mixture. The fuel is premixed with air and injected at the intake port before being compressed by the piston. The liquid fuel used in SI engines being highly volatile, the mixture is ignited by a spark-plug at a predetermined position near the Top Dead Center (TDC). The combustion results in a flame front which expands from the spark towards the rest of the unburned fuel. To guarantee a high flame propagation speed and a proper operation of the three-way catalytic converter, SI engines must use stoichiometric mixtures. In Eq. (1.1), the fuel-air equivalence ratio ϕ is defined as the ratio between the fuel-to-air ratio, m_f/m_a, and the stoichiometric fuel-to-air ratio, $(m_f/m_a)_{st}$.

$$\phi = \frac{m_f/m_a}{(m_f/m_a)_{st}} \tag{1.1}$$

Such stoichiometric and homogeneous mixtures are characterized by very low nitrogen oxide (NO_x) and soot emissions. Nevertheless, a throttle valve is needed at the intake to regulate the air supply, leading to additional pumping losses. Furthermore, the compression ratio, defined as $\tau = \frac{V_{BDC}}{V_{TDC}}$, is limited in SI engines to prevent from knocking. Knocking phenomenon occurs when auto-ignition conditions are met during the compression before the spark ignition. This results in shock waves propagation that can lead to resonance and destructive pressure peaks for the engine. Therefore, low compression ratios and fuels that resist to auto-ignition, hence fuels with a high octane number, are used in SI engines. In view of thermodynamics, the thermal efficiency depends on both τ and ϕ and is given in Eq. (1.2), where x is a declining function of ϕ.

$$\eta_{th} = 1 - \frac{1}{\tau^x} \qquad \text{with } x = f(\tau, \phi) \tag{1.2}$$

Thermal efficiency thus rises with the compression ratio and decreases with the fuel-air equivalence ratio. Therefore, a major drawback of SI engines is their lower efficiency.

1.1.2 CI engine

CI engines, also referred to diesel engines, are characterized by high compression ratios and fuels with low octane number to trigger the combustion by compression ignition. In these engines, only air is compressed to high temperatures by the piston while the fuel is injected in the hot air at the end of the compression, leading to its spontaneous auto-ignition. NO_x are formed in the presence of oxygen and nitrogen at very high temperatures. In the absence of premixing, the fuel-air mixture is non-homogeneous and the consequent charge stratification in CI engines results through diffusion process in very lean and hot areas where NO_x are produced. Therefore, high NO_x emissions are characteristic of diesel engines. However, higher compression ratios along with typical fuel-air equivalence ratios less than 0.6 give CI engines better thermal efficiencies than SI engines, resulting in lower fuel consumption and reduced CO_2 emissions.

1.1.3 Definition of MEP and efficiencies

The chemical energy contained in a fuel is not entirely transformed into useful work for the engine. The energy conversion chart from the fuel energy content to the mechanical work in an IC engine is presented in Figure 1.1. Each step is defined by its own efficiency and all the energy quantities can be normalized as Mean Effective Pressures (MEP). This method allows to compare engine performances independently of the engine size. The MEP is defined as the ratio between the energy and the displacement volume, and is expressed in bar, having the units of a pressure.

First of all, the chemical energy contained in the fuel can be determined thanks to its Lower Heating Value

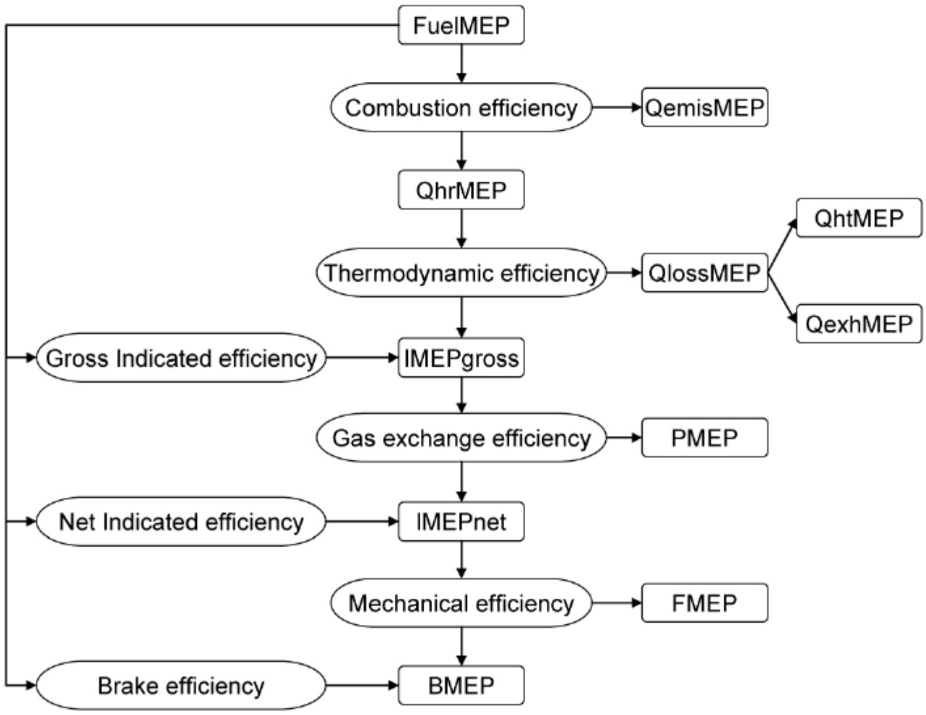

Figure 1.1: Energy conversion chart from fuel energy to brake work expressed as MEP [1].

(LHV) and its mass per engine cycle, m_f. By normalizing it with the total displacement of the engine V_d, the FuelMEP can be expressed as follows:

$$\text{FuelMEP} = \frac{m_f \text{ LHV}}{V_d} \tag{1.3}$$

The fuel is then burned in order to produce a maximum of heat. The combustion efficiency, η_c, is defined as the ratio between the heat released by the combustion and the fuel energy content. The QhrMEP being the normalized value of the heat release, the combustion efficiency can be written as:

$$\eta_c = \frac{\text{QhrMEP}}{\text{FuelMEP}} \tag{1.4}$$

Because there are still unburned compounds after the combustion, a part of the chemical energy of the fuel is lost in the exhaust gases. These losses are represented by the QemisMEP (Emission MEP).

The thermodynamic efficiency converts the heat release, QhrMEP, into a cyclic work on the piston, IMEPg (Indicated MEP gross). Losses occurring during this conversion include heat transfer losses, QhtMEP, and exhaust losses, QexhMEP. The thermodynamic efficiency, η_{ti}, is given in Eq. (1.5).

$$\eta_{ti} = \frac{\text{IMEPg}}{\text{QhrMEP}} = 1 - \underbrace{\frac{\text{QhtMEP}}{\text{QhrMEP}}}_{\varepsilon_{ht}} - \underbrace{\frac{\text{QexhMEP}}{\text{QhrMEP}}}_{\varepsilon_{exh}} \tag{1.5}$$

In this equation, ε_{ht} and ε_{exh} are respectively the relative in-cylinder heat transfer losses and the relative exhaust losses.

The gross indicated efficiency, η_{ig}, can also be derived:

$$\eta_{ig} = \frac{\text{IMEPg}}{\text{FuelMEP}} \tag{1.6}$$

After that, the IMEPn (Indicated MEP net) can be deduced from the IMEPg by subtracting the pumping losses, PMEP (Pumping MEP). The PMEP can be estimated as the difference between the exhaust and intake pressures.

$$\text{PMEP} \simeq p_{out} - p_{in} \tag{1.7}$$

The admission stroke of the piston is easier as the intake pressure increases, while the exhaust stroke takes more work from the crankshaft when the exhaust pressure increases. Therefore, negative pumping losses occur when the exhaust pressure is lower than the intake pressure, creating a positive work on the piston. In contrast, a positive PMEP deteriorates the engine efficiency.

The next step in the conversion chart concerns the mechanical friction inside the engine, FMEP (Friction MEP). The mechanical work available for the crankshaft, BMEP (Brake MEP), is obtained by subtracting the FMEP to the IMEPn. The mechanical efficiency, η_{mec}, is therefore the ratio between the BMEP and the IMEPn.

$$\eta_{mec} = \frac{\text{BMEP}}{\text{IMEPn}} = 1 - \frac{\text{FMEP}}{\text{IMEPn}} \tag{1.8}$$

Finally, the brake efficiency η_b indicates the efficiency of the engine in converting the fuel energy content, FuelMEP, into useful work, BMEP.

$$\eta_b = \frac{\text{BMEP}}{\text{FuelMEP}} \tag{1.9}$$

All these mean effective pressures and efficiencies will be used to characterize the performance of the engine in Part 3.

1.2 HCCI combustion

Homogeneous Charge Compression Ignition (HCCI) engines constitute an alternative to the traditional SI and CI engines as they combine advantages of both. The concept is based on the spontaneous auto-ignition by compression, like in CI engines, of a homogeneous fuel-air mixture, like in SI engines. A schematic representation of these combustion modes is shown in Figure 1.2. The interest in this new combustion process has grown because of the increasingly stringent standards regarding NO_x emissions from IC engines, and the desire to reduce fuel consumption as well as production of greenhouse gases like CO_2. In fact, HCCI combustion is a hybrid between SI and CI that basically achieves the best trade-off between these two traditional combustion modes: the low NO_x emission of SI engines and the high efficiency, hence low fuel consumption and reduced CO_2 production, of CI engines. The summary made in this section on the concepts behind HCCI combustion is inspired by the works of Rouanet [2] and Boveroux and Gramme [3].

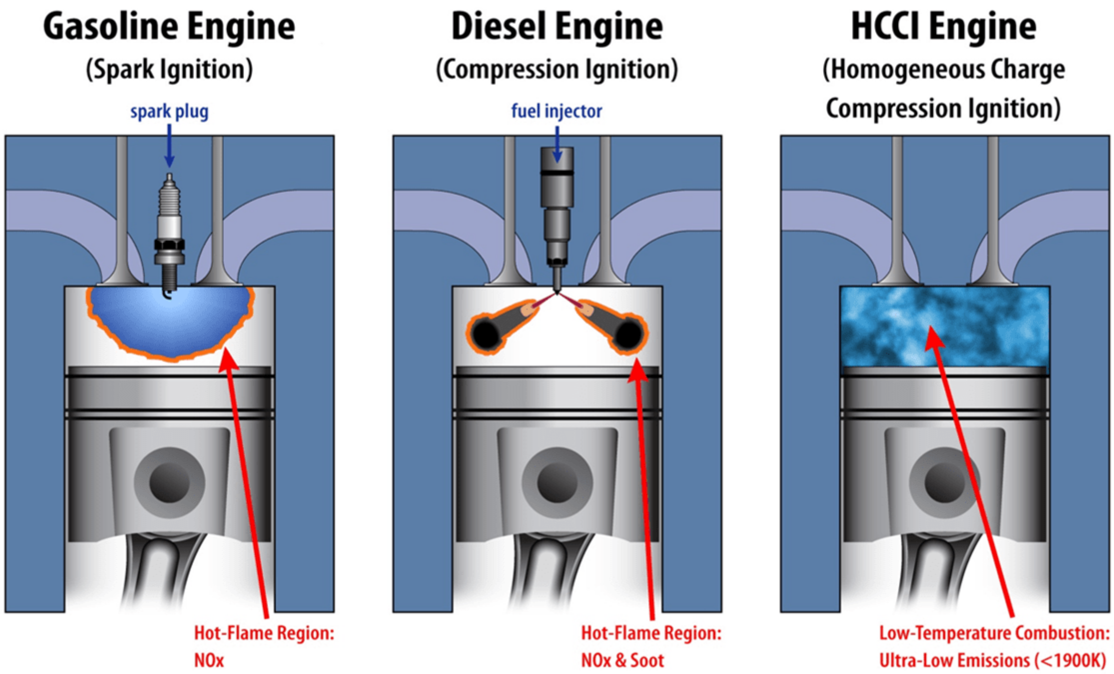

Figure 1.2: Schematic representation of the combustion in SI, CI and HCCI engines.[1]

1.2.1 Auto-ignition phenomenon

In an HCCI engine, the combustion is triggered when auto-ignition conditions are fulfilled. These are reached during the compression stroke when the gas temperature increases and chemical reactions release heat and reactive radicals, thereby causing a chain reaction which results in the total combustion of the fuel. Since the fuel is premixed with air, pressure and temperature are globally homogeneous inside the combustion chamber. Therefore, the auto-ignition arises simultaneously at many points in the cylinder causing a very fast combustion and a high pressure rise rate. Furthermore, no flame propagation like in SI engines or diffusion process like in CI engines could slow down the heat release. To prevent important mechanical stresses, HCCI engines use very lean mixtures, in other words a high fuel dilution.

A major challenge in HCCI combustion concerns its lack of ignition timing control. The combustion phasing is optimum near the TDC, allowing the piston to produce more mechanical work. However, while the combustion in SI engines is triggered by the spark plug, and the combustion in CI engines is initiated by the timing of fuel injection, HCCI combustion is only driven by chemical kinetics. Therefore, the auto-ignition timing depends on all the parameters that influence kinetics: temperature, pressure, equivalence ratio, fuel composition, EGR rate, compression ratio, engine rotational speed, cylinder wall temperature, etc.

The temperature is the parameter that influences the most the combustion phasing, as chemical kinetics is highly temperature-dependent. The auto-ignition temperature is the temperature that is required to trigger the combustion at the TDC. Because kinetics is less influenced by other parameters, typical auto-ignition temperature ranges can be defined for a given fuel type, regardless of the other parameters. Concerning the fuel type, methane, the main component of natural gas, is known to have one of the highest octane number, about 120, and will thus be more difficult to auto-ignite in an HCCI engine. When using natural gas or methane in an HCCI engine, a preheating of the air is therefore necessary. Based on the work made by

[1] http://green-group.mit.edu/hcci-engines/, accessed on May 25, 2018.

Aceves and Flowers [4], an intake temperature of 380 K would be required at $\tau = 18$ to allow natural gas to burn effectively. For pure methane, the intake temperature would increase up to 400 K. Indeed, the other compounds in natural gas, such as hydrocarbons, have lower octane numbers and thus help promoting its earlier auto-ignition.

Same trends about the strong influence of the temperature have been observed by Amneus et al. [5]. They measured the influence of temperature, pressure and fuel-air equivalence ratio on the auto-ignition timing in a natural gas HCCI engine. They found out that an increase of each parameter leads to an advance in the combustion timing while a decrease of them shows a delayed auto-ignition. However, the most influential parameter is the temperature as an increase of it by only 0.6% contributes to advance the auto-ignition by 1 crank angle degree (CAD). In contrast, an increase of the pressure by 11% or an increase of ϕ by 10% should be made to produce the same result.

In 2011, Kobayashi et al. [6] have experimentally investigated the possibility of turbocharging on a natural gas HCCI engine. Experiments were performed at a compression ratio of 17 and a boost pressure of 2.5 bar, while varying the intake temperature and the fuel-air equivalence ratio. Their results are given in Figures 1.3 and 1.4. As a first observation, the combustion efficiency increases with T_{in} and ϕ. Indeed, a higher cylinder temperature allows a better oxidation of the residual CO into CO_2, hence increasing the heat release and the combustion efficiency. An increase in ϕ has both kinetic and thermal effects. Richer mixtures auto-ignite more readily than leaner ones because the speed of reaction is proportional to the concentration of reactants. At low ϕ, less reactive radicals are created, thereby limiting propagation and combustion rate. Also, increasing the equivalence ratio provides higher cylinder temperatures resulting from the higher heat release.

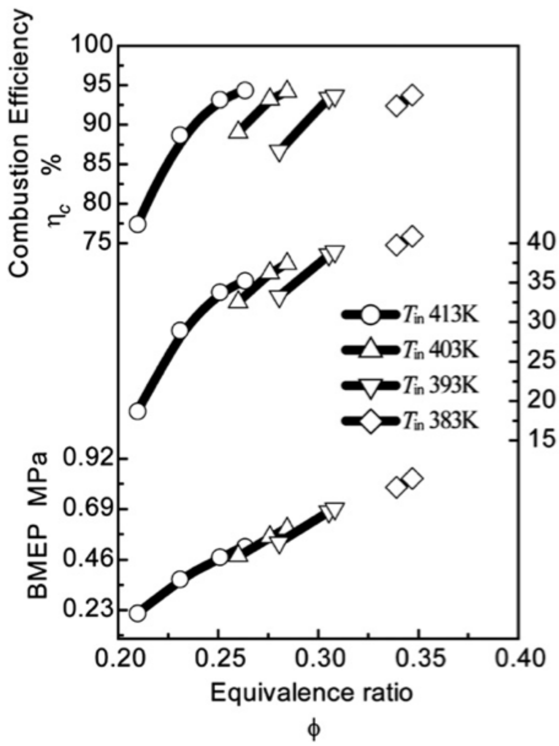

Figure 1.3: Influence of T_{in} and ϕ on BMEP, combustion efficiency η_c and brake efficiency η_e [6].

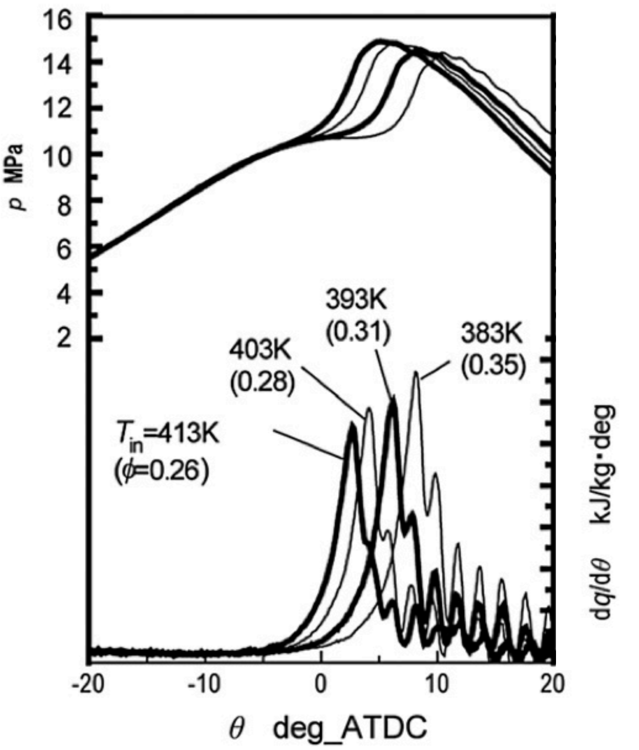

Figure 1.4: Influence of T_{in} and ϕ on cylinder pressure p and RoHR [6].

Figure 1.3 also shows that both the BMEP and brake efficiency appear to reach their maximum at high ϕ and low T_{in}. An increase in the equivalence ratio leads to higher power output, hence higher BMEP while the part of mechanical losses becomes less important in the efficiency. Lower temperatures increase the mixture density and provide a higher amount of fuel at constant ϕ, improving the BMEP. But temperatures also have a strong influence on the pressure trace and the Rate of Heat Release (RoHR), as seen in Figure 1.4. A decrease in T_{in} delays the auto-ignition as more time is needed to reach the auto-ignition temperature during the compression stroke. This results in a reduced Peak Cylinder Pressure (PCP), allowing therefore the use of higher equivalence ratios while respecting the limit on the PCP. To a lesser extent, the increase of the brake efficiency at low T_{in} can also be explained by the reduction of the wall heat losses, resulting from the lower temperature profile. As a conclusion, Kobayashi et al. [6] showed that a low intake temperature was beneficial to both power and efficiency of an HCCI engine.

1.2.2 Advantages

HCCI engines use homogeneous fuel-air mixture with high fuel dilution and are characterized by a low combustion temperature, leading to very poor NO_x emissions. Figure 1.5 depicts the temperature-equivalence ratio couples that lead to NO_x and soot formation, and the areas where diesel and RCCI (Reactivity Controlled Combustion Ignition, similar to HCCI) engines work. Diesel engines produce high NO_x and soot quantities due to their charge stratification. Since NO_x begin to form at temperatures above 2100 K, it is thus essential to maintain a low combustion temperature in HCCI engines, by working with lean mixtures. As will be explained in Section 1.4, the use of EGR is a way to limit the temperature even at higher fuel-air equivalence ratios.

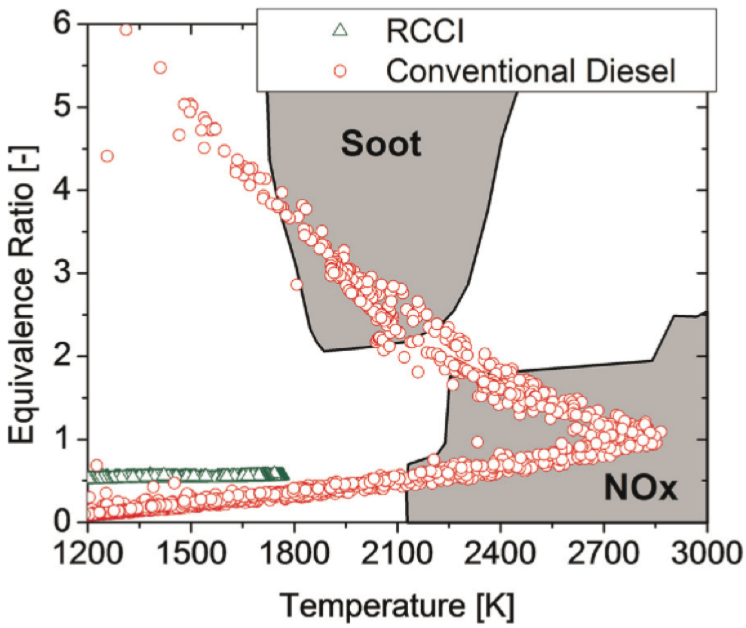

Figure 1.5: NO_x and soot emissions as functions of peak cylinder temperature and equivalence ratio for diesel and RCCI ($\approx$ HCCI) engines [7].

The second advantage of HCCI engines is their high efficiency, similar to the one of CI engines. Because HCCI combustion is based on the auto-ignition mechanism, high compression ratios are used for the temperature at the TDC to be sufficiently high to trigger the combustion. As seen in Section 1.1, a higher τ results in a higher thermal efficiency and a lower fuel consumption. On the other hand, there is no need for a throttle valve like in SI engines since fuel-air mixtures are very diluted to prevent high mechanical stresses.

One last advantage of HCCI combustion is its multifuel adaptability. Whereas SI and CI engines need very specific fuels to work properly, an HCCI engine can basically run with any liquid or gaseous fuel, under the condition that all parameters are adapted accordingly. Nowadays, a lot of research is done on HCCI combustion with alternative fuels, such as biomass syngas in the work of Bhaduri [8], or ammonia-hydrogen blends in the works of Pochet et al. [9, 10].

1.2.3 Disadvantages and limitations

The characteristic cold combustion of HCCI engines, which is around 1500 to 1800 K, also has disadvantages. Although NO_x emissions are considerably reduced, the mixture might burn incompletely due to low cylinder temperatures, producing large amounts of residual CO and unburned hydrocarbons (HC). Because CO and HC have a high residual energy content that could not be converted as heat release, the combustion efficiency is negatively impacted and is lower in HCCI engines, typically under 95%.

Another disadvantage is the absence of direct control on the auto-ignition timing like the spark-plug in gasoline engines or the fuel injection timing in diesel engines. Therefore, one challenge in HCCI combustion is to control in real time all the parameters that influence kinetics in order to obtain the optimum combustion phasing.

Finally, HCCI engines are characterized by a limited operating range as shown in Figure 1.6. At low load, the auto-ignition of very lean mixtures is difficult due to low fuel concentration. The heat released is thus not sufficient to sustain the chain reaction propagation, resulting in an incomplete combustion with low efficiency. This unstable combustion is characterized by large cyclic variations measured by the Coefficient of Variation (CoV).

At high load, the upper limit is determined by the combustion noise. Compared to SI and CI engines, HCCI combustion is very fast as the whole homogeneous mixture auto-ignites approximately at the same time, resulting in a fast pressure increase. This rise in pressure is quantified by the Maximum Pressure Rise Rate (MPRR), expressed in bar/CAD. At higher load, hence richer mixtures, the MPRR increases and induces large pressure waves in the cylinder, resulting in high mechanical stresses and loud combustion noises. This phenomenon is called *ringing* in HCCI engines and is similar to knocking in SI engines. Maximum values for the MPRR typically lie between 10 bar/CAD (Bhaduri [8]) and 20 bar/CAD (Christensen et al. [11]). While the high load limit is usually determined by the MPRR, turbocharged engines could also be limited by the maximum peak cylinder pressure (PCP).

As a conclusion, one of the main challenges of HCCI combustion is to extend its operating range. To this end, several strategies have been developed: variable compression ratio, fuel composition, variable valve timing, turbocharging, EGR. The present work will focus on turbocharging and exhaust gas recirculation as two ways to extend the upper load limit of a stationary HCCI engine an achieve higher specific power.

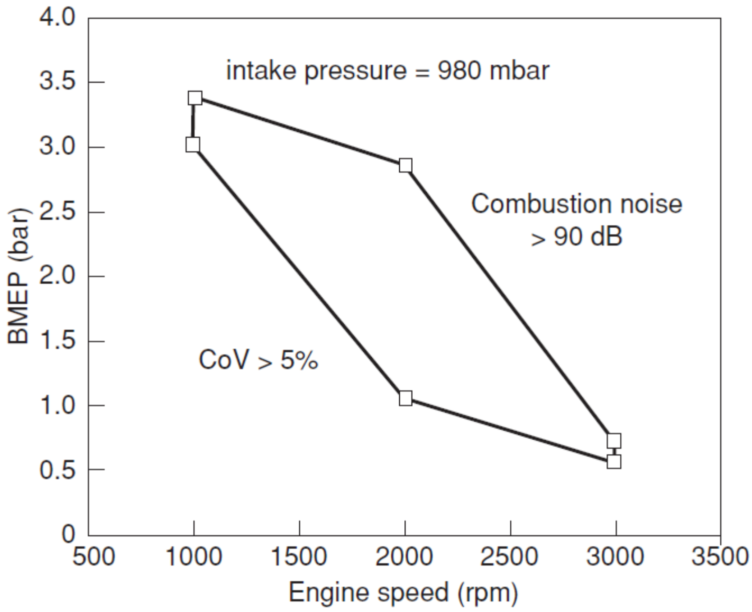

Figure 1.6: Limited working zone in HCCI combustion [7].

1.3 Turbocharging

The content of this section is mainly based on the book "Fundamentals of turbocharging" of Baines [12] and the work of Rouanet [2]. The basic principle of turbocharging is discussed, followed by the compressor and turbine thermodynamic equations. The theoretical study is concluded by a brief description of the concept behind the variable geometry turbocharger (VGT).

1.3.1 Principle of turbocharging

The main goal of turbocharging is to increase the specific power of the engine, represented by the Indicated Mean Effective Pressure net (IMEPn), and expand in the same time the engine operating range. The IMEPn, introduced in Section 1.1.3, is the ratio between the net amount of work done by the expansion of hot gases on the pistons during one engine cycle, known as the indicated work W_{ind}, and the displacement volume, V_d. Its expression for a gaseous fuel is given in Eq. (1.10).

$$\begin{aligned} W_{ind} &= \eta_{ti}\eta_c m_f \text{LHV} - (p_{out} - p_{in})\, V_d \\ &= \eta_{ti}\eta_c\eta_{vol}\rho_{in}\frac{V_{a1}}{V_{a1}+\phi}\frac{\phi\ \text{LHV}}{m_{a1}}\, V_d - (p_{out} - p_{in})\, V_d \\ \text{IMEPn} &= \eta_{ti}\eta_c\eta_{vol}\rho_{in}\frac{V_{a1}}{V_{a1}+\phi}\frac{\phi\ \text{LHV}}{m_{a1}} - \text{PMEP} \end{aligned} \tag{1.10}$$

In this formula, the volumetric efficiency η_{vol} accounts for the non-perfect filling of the cylinder during the intake stroke, and ρ_{in} is the charge density in the intake manifold.

The principle of turbocharging consists to increase the IMEPn by acting on the mass of fuel that enters the cylinder during each engine cycle. A compressor is used to boost the intake pressure, resulting in an increase of the intake charge density ρ_{in}. In some cases, the hot compressed air can be cooled down through an intercooler in order to counter the decrease in density due to the temperature rise during the compression. At a constant equivalence ratio, as more air has entered the cylinder, the corresponding amount of fuel is higher and results in a higher IMEPn.

In the case where the compressor is mechanically coupled to the engine crankshaft, the engine is said to be supercharged. Although being more reliable than turbocharging, supercharging has a cost in terms of power, as the energy needed by the compressor is directly taken on the engine crankshaft, resulting in a lower global efficiency. Rouanet [2] has showed that an HCCI engine running at $p_{in} = 2$ bar, $T_{in} = 130°\text{C}$, and $\phi = 0.35$ would lost 15% of its mechanical power to the supercharger, with a net indicated efficiency decreasing from 40% to 32%.

In the case of turbocharging, the energy needed by the compressor is supplied by a turbine along the same shaft which recovers a part of the exhaust gases residual energy. The concept of turbocharging is illustrated in Figure 1.7. Typically, the relative exhaust losses ε_{exh} are about 35% in an IC engine, and a part of it will be used by the turbine to drive the compressor. Although the turbine creates a back-pressure, causing high pumping losses, the increase in mechanical power output reduces in the same time the relative part of the friction losses in the efficiency, that could even result in an increase of the efficiency. As a conclusion, turbocharging seems to be the best solution to overcome the characteristic low specific power of HCCI engines.

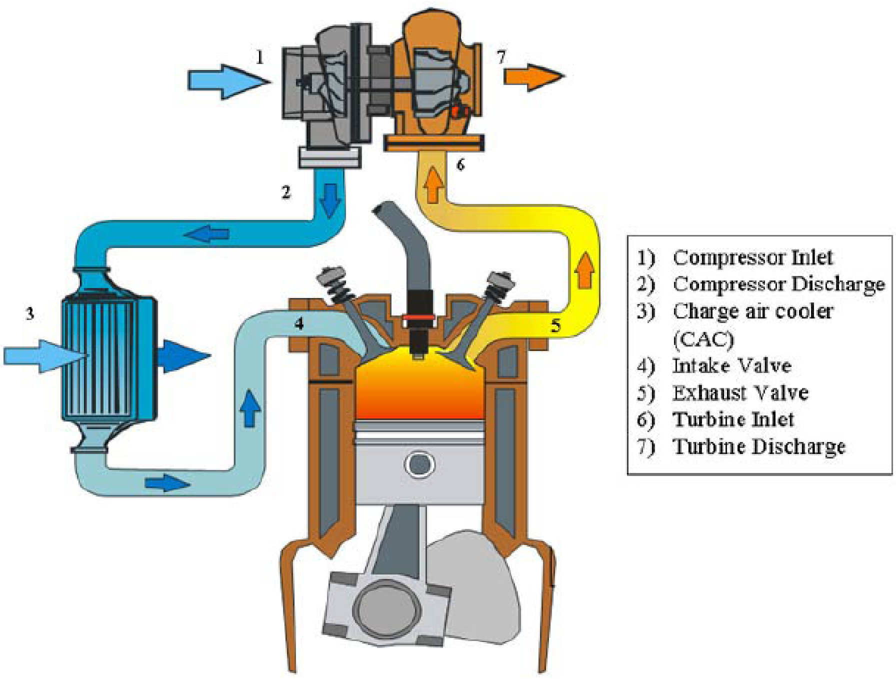

Figure 1.7: Schematic of a turbocharged engine with intercooler [2].

1.3.2 Thermodynamic equations

This section briefly summarizes the thermodynamic equations of the compressor and turbine that will be used in Part 3. The states numbering follows the one of Figure 1.7.

Both compressor and turbine performances are characterized by their isentropic efficiency, which are directly related to the isentropic relation between pressure and temperature. The formula of an isentropic compression is given in Eq. 1.11, where indices 1 and 2 refer to the locations upstream and downstream of the compressor. The temperature T_{2s} stands for temperature after the compressor if the compression was isentropic. The coefficient γ_C is the mean specific heat ratio of the gas during the compression.

$$\frac{p_2}{p_1} = \left(\frac{T_{2s}}{T_1}\right)^{\frac{\gamma_C}{\gamma_C - 1}} \tag{1.11}$$

The isentropic efficiency of the compressor, η_{siC}, is derived in Eq. 1.12 and is defined as the ratio between the minimum input work that would be sufficient if the compression was isentropic, and the actual input work.

$$\eta_{siC} = \frac{W_{mC,s}}{W_{mC}} = \frac{h_{2s} - h_1}{h_2 - h_1} \approx \frac{T_{2s} - T_1}{T_2 - T_1} \tag{1.12}$$

The input power of the compressor P_C, given in Eq. 1.13, is the power required for the compressor to boost a mass flow rate $\dot{m}$ from a pressure p_1 to a higher pressure p_2. In this equation, c_{pC} is the mean specific heat during the compression.

$$P_C = \dot{m} c_{pC} (T_2 - T_1) \tag{1.13}$$

The formula of an isentropic expansion is the same as for a compression and is given in Eq. 1.14, were indices 6 and 7 refer to the locations upstream and downstream of the turbine. The coefficient γ_T is the mean specific heat ratio of the gas during the expansion and is different from γ_C since the composition and temperature of the exhaust gases are different from that of the intake load.

$$\frac{p_6}{p_7} = \left(\frac{T_6}{T_{7s}}\right)^{\frac{\gamma_T}{\gamma_T - 1}} \tag{1.14}$$

The isentropic efficiency of the turbine, η_{siT}, is shown in Eq. 1.15 and is defined as the ratio between the actual work done by the fluid on the turbine, and the work that would have been done if the expansion was isentropic.

$$\eta_{siT} = \frac{W_{mT}}{W_{mT,s}} = \frac{h_6 - h_7}{h_6 - h_{7s}} \approx \frac{T_6 - T_7}{T_6 - T_{7s}} \tag{1.15}$$

The output power of the turbine P_T, developed in Eq. 1.16, is proportional to the engine exhaust temperature T_6. This temperature is lower in HCCI combustion than in other IC engines and this will have large consequences. Regarding Eq. 1.14, the turbine will have to work with higher expansion ratios to compensate for the lower exhaust temperature.

$$P_T = \dot{m} c_{pT} (T_6 - T_7) \tag{1.16}$$

Finally, friction losses occurring in the bearing of the shaft are represented through the mechanical efficiency of the turbocharger $\eta_{m,TC}$. This efficiency is the ratio between the compressor input power and the turbine output power, as given in Eq. 1.17.

$$P_C = \eta_{m,TC} P_T \tag{1.17}$$

1.3.3 Variable geometry turbocharger

A turbine only operates optimally for predetermined couples of mass flow rates and expansion ratios. This can be very limiting as the required mass flow rate and expansion ratio are determined separately by the compressor and the engine. The use of a variable geometry turbocharger (VGT) is a way to regulate the turbine behavior to make it fit a larger engine operating range. The concept behind the VGT is to modify the effective turbine wheel inlet area in order to shift its characteristic curve, thus expanding its operating region.

For a given exhaust mass flow, reducing the cross-sectional area raises the velocity when the exhaust gases encounter the turbine wheel. Therefore, the turbine characteristic is shifted downwards and its power is increased at low mass flow rate. The side-effect is that the flow speed enters the wheel more tangentially, resulting in a reduced maximum flow capacity since the effective inlet area is reduced. This phenomenon is observed in Figure 1.8 by the flattening of the curve at lowest inlet area (0% or closed).

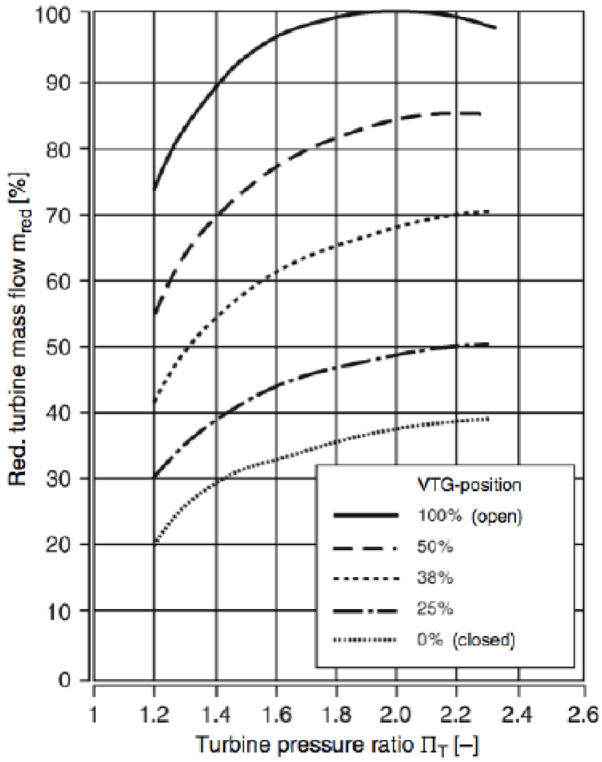

Figure 1.8: Variation of the turbine characteristic with the VGT position [13].

1.4 Exhaust Gas Recirculation

While the use of Exhaust Gas Recirculation (EGR) for NO_x reduction in commercial diesel engines is the most known reason for applying EGR, its potential extents to other applications as well. Especially, EGR has been widely used as a way to control HCCI combustion and expand its operating range. This section, based on the works of Bhaduri [8] and Rouanet [2], first discusses the various existing techniques of EGR, before investigating the influence of EGR on HCCI combustion.

1.4.1 Comparison between EGR techniques

Exhaust Gas Recirculation can be implemented in various ways. EGR can be done through residual gas trapping, called internal EGR, or externally by recycling gases from the exhaust and mixing them with the fresh load at the engine intake. Internal EGR is naturally present in engines since there is always a small amount of exhaust gases that are trapped and remain in the cylinder after the exhaust valve closing (EVC). By playing on the exhaust valve timing, the control on the internal EGR rate becomes possible. The main interest of using hot internal EGR in HCCI combustion is to avoid the need of an additional preheating system. This is not particularly interesting since the intake temperature and EGR rate could not be controlled separately.

External EGR is easier to implement and allows a separate control of the intake temperature and EGR rate. Therefore, external EGR could be used for its damping properties, independently from the temperature regulation. Furthermore, external EGR can be either cooled or not, allowing an additional control on the intake temperature. For these reasons, external EGR seems to be more suitable for the present application.

When using external EGR, two options are possible with a turbocharged engine. These two techniques are the high pressure (HP) and low pressure (LP) EGR loops, both represented in Figure 1.9.

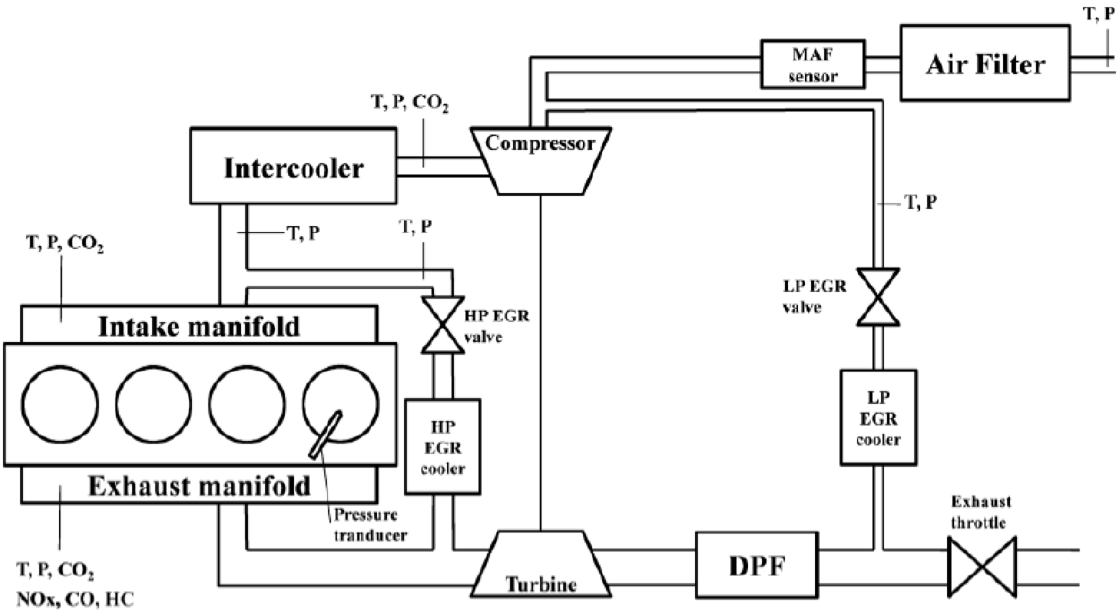

Figure 1.9: Illustration of LP and HP EGR loops on a turbocharged engine [14].

In the HP loop, the exhaust gases are directly recycled from the exhaust manifold and injected back in the intake manifold. Since HCCI combustion is characterized by high exhaust pressure, the recirculation if then driven by a positive pressure difference. Another advantage of the HP loop is its shorter length, resulting in an improved transient response. However, this is not particularly relevant for a stationary engine. The major drawback of the HP loop is that it bypasses the turbocharger. Therefore, the mass flow rate through the turbocharger decreases with the EGR rate, leading to a decrease of the turbine power output. Due to mass flow conservation, the compressor flow also decreases, resulting in a displacement of the turbocharger operating point. As a conclusion, the main problem with the HP EGR loop is the variation of the turbocharger operating point with the EGR rate. In contrast, the LP EGR loop does not impact the turbocharger mass flow rate. It is therefore possible to optimize the turbocharger while working at various EGR rates. The low pressure recirculation is managed by a throttle valve installed at the exhaust, causing an increase in the pressure downstream of the turbine.

1.4.2 Influence of EGR on HCCI combustion

The influence of EGR on HCCI combustion can be classified into five categories: dilution effects, thermal effects, influence on intake mixture temperature, influence on chemical kinetics and, to a lesser extent, re-burning effects.

Dilution effects occur when EGR is implemented in lean conditions with excess of air ($\phi < 1$). A certain amount of remaining air is thus recycled through EGR and injected at the engine intake. This results in a reduced fuel-air equivalence ratio from the original ϕ to the effective ϕ_{EGR}. Furthermore, by mass flow conservation, the presence in the cylinder of exhaust gases reduces the amount of fresh load aspirated during each cycle, hence reducing the total energy content of the intake mixture.

Thermal effects are associated to thermodynamic damping and constitute the main effect aimed to be exploited on HCCI combustion by the use of EGR. With high fuel dilution, exhaust gases consist mostly of O_2, N_2, CO_2 and H_2O. As shown in Figure 1.10, CO_2 and H_2O compounds have much higher heat capacities, resulting in an increase of the load thermal inertia.

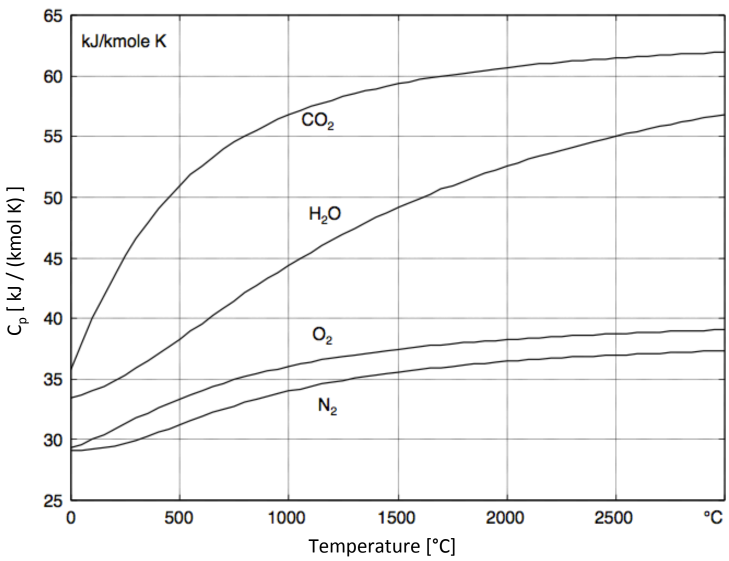

Figure 1.10: Heat capacity of the main EGR compounds [7].

The use of EGR, through its composition, reduces the temperature rise during the compression, causing a delay in the auto-ignition and a damping of the combustion process. This damping phenomenon causes the heat release to spread over more crank angle degrees (CAD). Therefore, by decreasing the rate of heat relase (RoHR), a lower MPRR is achieved, thus allowing the use of higher fuel-air equivalence ratios. The damping effects on the cylinder pressure are observed in Figure 1.11, where both the PCP and the MPRR decrease with the EGR rate. As a conclusion, the use of EGR is particularly interesting for its potential to decrease the

MPRR and extend therefore the operating range of an HCCI engine by achieving higher IMEPg along with good efficiencies.

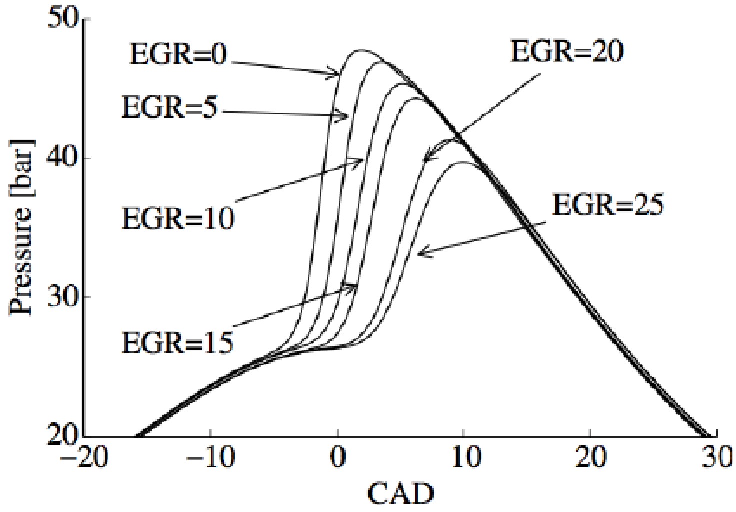

Figure 1.11: Illustration of EGR thermal effects. Experimental results obtained for biomass syngas HCCI combustion, at $T_{\mathrm{EGR}} = T_{in} = 523$ K, and constant energy content [15].

The EGR may also influence the temperature of the intake charge, depending on which form the EGR is implemented in. In the case of external cooled EGR, delayed combustion with lower RoHR are observed, resulting in very poor NO_x emissions. In contrast, hot internal EGR provides an increase of the intake temperature, hence advancing the auto-ignition timing.

The recirculation of gases such as CO_2, H_2O, CO, HC or NO_x may influence the HCCI combustion through chemical kinetics. Indeed, products of a non-ideal combustion like CO, HC and NO are very reactive species and tend to reduce the global activation energy of the intake charge, thus leading to an earlier auto-ignition. On the other hand, high quantities of CO_2 and H_2O in the intake mixture along with a lower relative O_2 concentration tend to slow down the oxidizing reaction, thereby reducing the RoHR.

Finally, since HCCI combustion is characterized by quite low combustion efficiency ($< 95\%$), the use of EGR could recycle the unburned compounds contained in the exhaust gases by injecting them back in the intake manifold and give them a second opportunity to effectively burn.

1.5 Organic Rankine Cycle

A growing interest has been shown towards the use of Waste Heat Recovery (WHR). This attention results from the increasingly stringent regulations regarding fuel consumption and carbon dioxide (CO_2) emissions. Compared to other WHR technologies such as absorption cycle air-conditioning and thermo-electricity, the Organic Rankine Cycle (ORC) is considered by Shu et al. [16] to be the most suitable technology in order to convert low and medium temperature heat source into electricity thanks to its higher efficiency and the low boiling point of the organic fluid. Indeed, according to Rettig et al. [17], an ORC can convert thermal energy at low temperatures in the range of 80 to 350°C into electricity. For all these reasons, the ORC seems to be particularly adapted for waste heat recovery in HCCI engines. This section first presents the overall description of the cycle. Then, a brief overview of the characteristics of the working fluids is made, followed by a comparison between subcritical and supercritical ORC. Finally, the coupling with an HCCI engine is discussed.

1.5.1 Overall description

The Organic Rankine Cycle works similarly to the traditional Rankine cycle except that the working fluid is not water but an organic fluid. An ORC is thus a thermodynamic cycle designed to produce electricity from industrial or waste heat acting as the hot source, with an organic working fluid which can be refrigerants, solvents hydrocarbons or other organic substances. The cycle includes a feeding pump, a boiler or steam generator, a turbine and a condenser. The schematic and T-s diagram of a typical ORC are given in Figures 1.12 and 1.13.

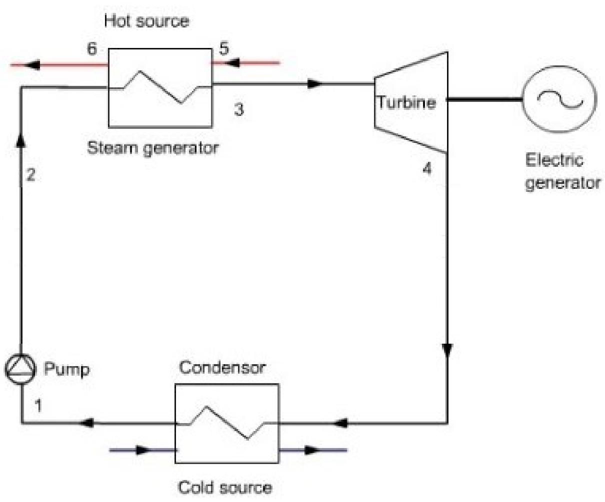

Figure 1.12: Schematic of an Organic Rankine Cycle without regenerator [18].

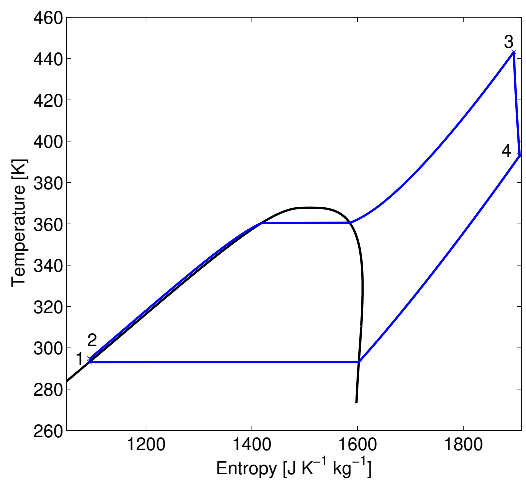

Figure 1.13: T-s diagram of an Organic Rankine Cycle working with the R1234yf fluid.

Pump

The role of the feeding pump is to provide to the fluid the desired pressure at the intake of the boiler while allowing its circulation in the cycle.

Boiler

The steam generator heats up the organic fluid which undergoes a phase transformation from liquid to superheated vapour state. The boiler being the hot source of the cycle, it must produce a certain amount of heat by burning a fuel or recovering heat from an external source. In the case of waste heat recovery, this heat is taken from an external system such as engine exhaust gases.

Turbine

Composed of one or several stages, the turbine expands the vapour in order to produce a mechanical work.

For all the working fluids, the vapour fraction after the turbine must be higher than a threshold value, to prevent formation of too much liquid that can damage the turbine blades through cavitation phenomenon.

Condenser

The condenser cools down the vapor flow after the expansion in order to bring it back to its liquid state. The condenser conditions are fixed by the temperature of the cold source.

Regenerator

A more complex configuration of the ORC can be used to take advantage of regeneration and reheating principles. Indeed, in an ORC, the working fluid must be heated up in order to flow into the turbine in gaseous state. After its expansion in the turbine, the fluid must be condensed to liquid state in order to enter the pump and start the cycle again. Because the heating step comes with a cost, a solution would be to add a heat exchanger within the cycle between the heating and condensing parts in order to reduce the energy consumption, therefore increasing the power and the total energetic efficiency of the cycle. The ORC coupled with a regenerator is shown in Figure 1.14.

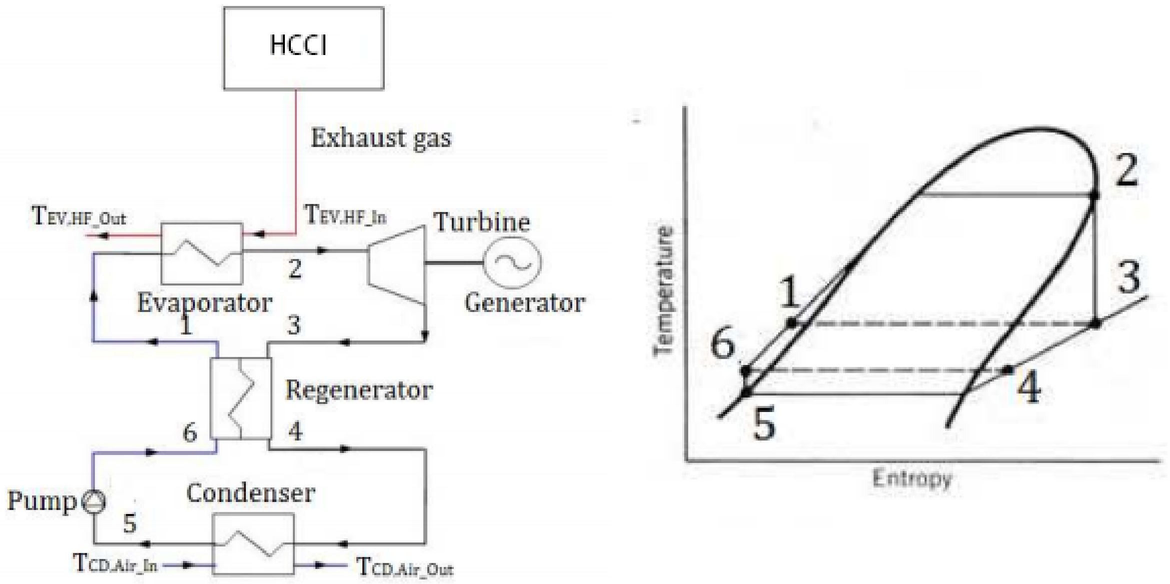

Figure 1.14: Schematic and T-s diagram of an Organic Rankine Cycle with a regenerator [18].

1.5.2 Working fluid

The choice of the working fluid and the corresponding operating conditions are vital to get optimal cycle performance, corresponding to high efficiency, but also to low environmental impact and economic viability. Many working fluids have been studied in the literature and some of them have been rejected because of environmental concerns and protocols [19]. While the choice of the working fluid for the ORC will be developed in Section 2.4.2, fluid characteristics and behaviors will be discussed in this section.

Organic fluids have many different characteristics from water. According to Chen et al. [20], the slope of the saturation curve of a working fluid in a T–s diagram can be positive (e.g. isopentane), negative (e.g. R22) or vertical (e.g. R11). These fluids are respectively called "wet", "dry" and "isentropic" fluids. Their T-s diagrams are plotted in Figure 1.15. Wet fluids like water usually need to be superheated, while other organic fluids, like dry or isentropic fluids, do not need superheating.

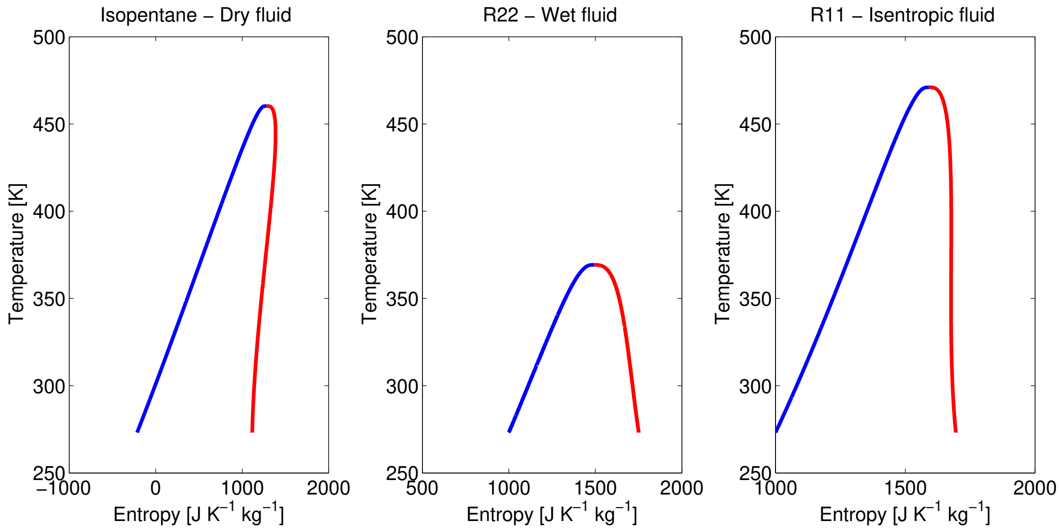

Figure 1.15: T-s diagram of the three types of organic fluids.

Another advantage of organic fluids is that the turbine built for an ORC typically requires only a single-stage expansion, resulting in a simpler, more economical system in terms of capital costs and maintenance. The choice of the ORC fluid is done according to three types of criteria [21]: thermodynamics criteria, security and environment criteria and technological, operational and economical criteria.

- **Thermodynamic criteria**: The total energetic efficiency and/or the output power should be as high as possible for a given heat source. The thermodynamic performance of the Organic Rankine Cycle depends heavily on the thermodynamics properties of the working fluid, including specific heat, density, critical point, etc. Thus, in order to find the optimum working fluid in terms of thermodynamic performance, it is necessary to simulate the cycle with various working fluids thanks to a mathematical model and to compare their output power and/or their total energetic efficiency.

- **Security and environment criteria**: Safety is a key parameter of energy industry and involves both toxicity and flammability. The environmental aspect includes low Ozone Depleting Potential (ODP), low Greenhouse Warming Potential (GWP) and Atmospheric Lifetime (ALT). Because of this, several working fluids were unusable and phased out. Regarding the Kyoto Protocol, the Belgian refrigerant fluids regulation prohibits the utilization and possession of CFC (chlorofluorocarbone) fluids since January 1, 1998, and prohibits HCFC (hydrochlorofluorocarbone) since January 1, 2015 [2]. The choice of the working fluid according to the second criteria can be made with Figure 1.16.

- **Technological, operational and economical criteria**: This criterion imposes several constraints on the working fluid properties to guarantee the economical and technological feasibility of the ORC cycle. The vapour density of the working fluid plays an essential role because a low density leads to higher volumetric flow rates, resulting in an increase of the turbine size and a higher pressure drop

[2] http://www.mcvs.be/reglementation2013fr.pdf, accessed on June 3, 2018.

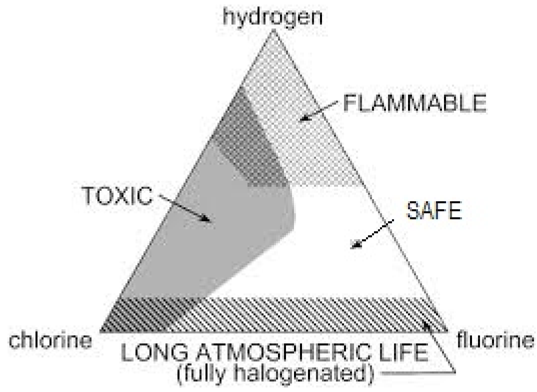

Figure 1.16: Safety and environment characteristics of hydro-chloro-fluoro-carbon compounds according to their composition [22].

in the heat exchangers. Therefore, the fluid density has a great impact on the cycle performance and the installation costs. The evaporation pressure of the fluid should not be too high in order to prevent greater complexity and higher cost, while the condensation pressure should be higher than the atmospheric pressure to avoid air infiltration. The working fluid should also have good aerodynamic and thermal properties. Therefore, the fluid viscosity must be low while the thermal conductivity must be high in order to maintain low friction losses and high heat transfer coefficients.

1.5.3 Subcritical and supercritical ORC

According to Karellas et al. [23], the use of supercritical fluid parameters in an ORC seems to be very attractive as it results in lower exergy destruction together with enhanced heat utilization. Moreover, from a pure thermodynamics point of view, by considering a constant fluid flow, as the pressure ratio rises, more work will be performed by the turbine, resulting in a higher power output for the cycle. For these reasons, there is a growing interest in supercritical Organic Rankine cycles.

A supercritical ORC is a cycle where the organic fluid is at supercritical state before the turbine. This state is reached by the ORC fluid when the couple pressure-temperature is higher than its critical pressure and temperature. The fluid in supercritical state presents intermediate physics properties like density, diffusivity and viscosity between gaseous and liquid states. On the contrary, a subcritical ORC is a cycle where the organic fluid is at subcritical state before the turbine meaning that either the inlet pressure or either the temperature of the turbine is smaller than the critical pressure or temperature. The T-s diagrams of both cycles are represented on Figure 1.17.

As it can be observed on Figure 2.9 where the temperature is displayed in function of the transferred heat, the two curves are much closer in the supercritical conditions. Therefore, the exergy losses due to the heat transfer are smaller than in the subcritical case. However, the more the two curves are close, the more the logarithmic temperature difference (LMTD) between organic fluid in each point and the heat source is smaller, resulting in a lower heat exchanger thermal efficiency [23]. So in order to transfer the same heat flux and achieve the same live vapour temperature, it is necessary to increase the heat transfer area, conferring the same heat exchanger efficiency for both cases represented on Figure 2.9.

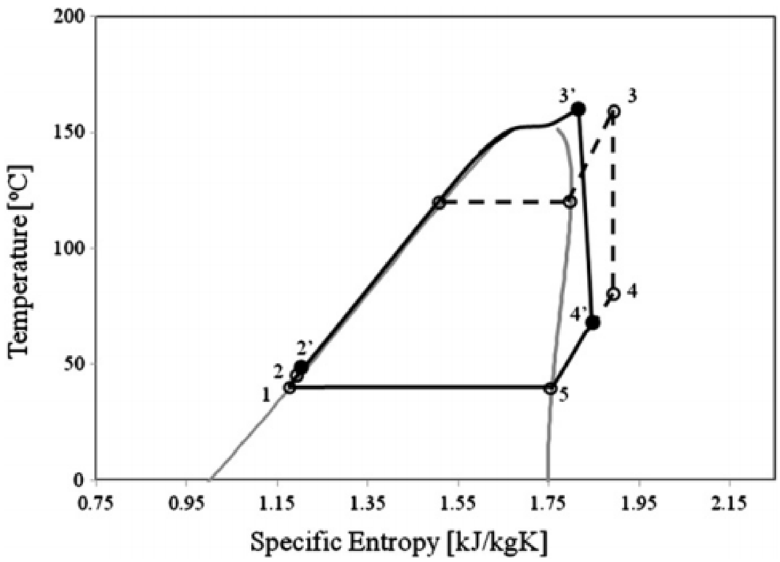

Figure 1.17: Illustration of subcritical (dash line) and supercritical (solid line) ORC with the R245fa fluid [23].

1.5.4 Coupling with an HCCI engine

As mentioned above, the coupling with a WHR unit could reduce the exhaust losses in an HCCI engine, resulting in an increase of its specific power and efficiency. The temperature of the exhaust gases being higher than the evaporating temperature of many ORC fluids, it is therefore possible to recover a large fraction of the exhaust enthalpy. The combination of an HCCI engine and an ORC is displayed in Figure 1.18. In this case, the WHR unit takes the role of a counter-current heat exchanger. Because the engine exhaust is directly connected to the WHR, the mass flow of burned gas is conserved and the gas temperature at the WHR input is equal to the temperature at the engine output.

Figure 1.18 shows that the WHR unit contains an economizer E, an evaporator V and a superheater S. The heating fluid are the exhaust gases of the HCCI engine which are at state 4g before entering in the WHR and at the state 5g at the WHR exit. Between these two states, the exhaust gases transfer their heat to the organic fluid. The operation of the WHR unit within the ORC cycle is the following. First, the organic fluid is at liquid state and flows through the economizer where it is heated up. Then comes the evaporator loop that returns the dry saturated fluid to the drum from which it exits in the direction of the superheater. And finally, the superheater brings the fluid into a superheated steam state. The operation of the WHR can be studied thanks to the heat exchanger diagram displaying the temperature along the y-axis and the heat fraction transferred to the consider section of the heat exchanger along the x-axis.

Figure 1.19 depicts the evolution of the organic fluid from its liquid state to its superheated vapour state. The graph also shows the drop in the gas temperature between the states 4g and 5g. The minimum difference between the temperatures of the fluid and the gases will be reached when the fluid is at saturated liquid state. Therefore, the exchanger pinch is obtained from:

$$\Delta T_p = T_p - T_{2'} \tag{1.18}$$

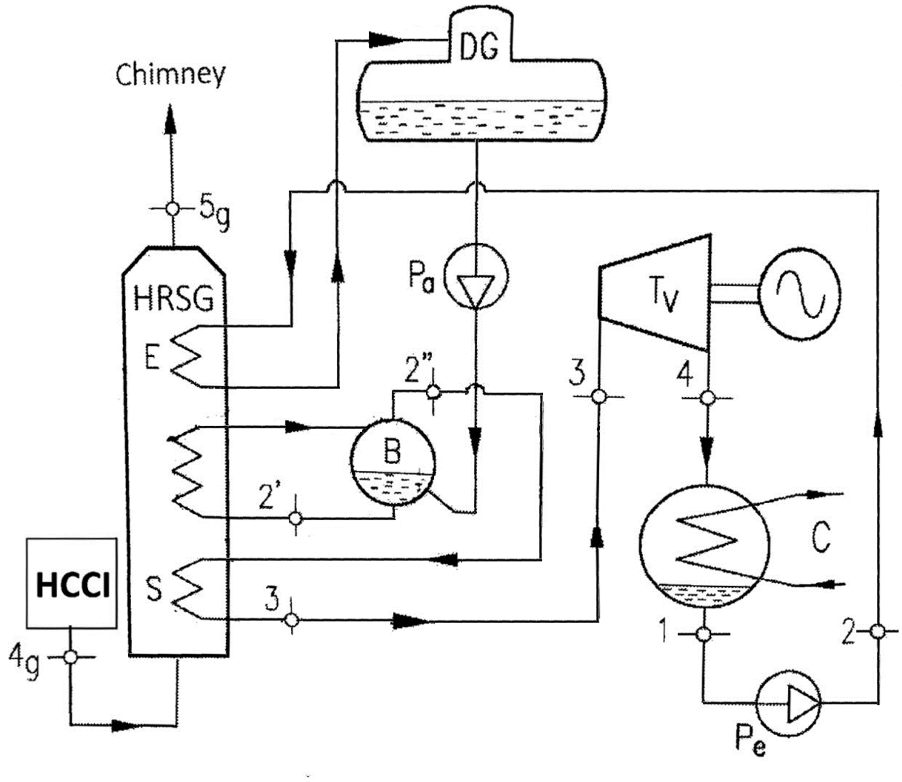

Figure 1.18: Schematic of a single pressure level combined cycle between an HCCI engine and an ORC.[3]

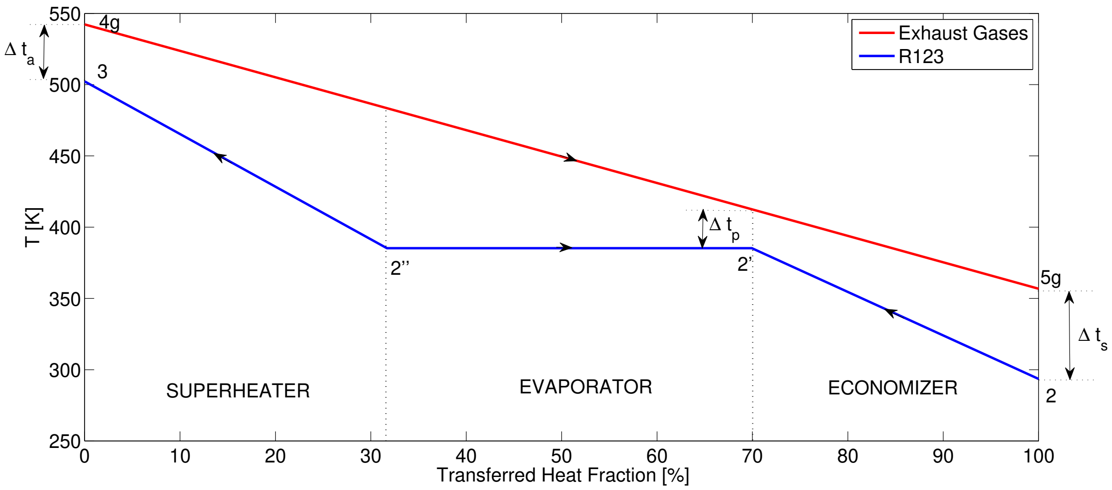

Figure 1.19: Heat exchanger diagram displaying the temperature agasint the heat fraction transferred for the R123 fluid.

Under normal conditions of the WHR, the value of the pinch is around 15°C [24]. The pinch and the choice of vaporization pressure will determine the temperatures $T_{2'}$ and T_p. Then, the temperature difference between the superheated steam temperature T_3 and the gas temperature T_{4g} is taken into account by a pinch ΔT_a whose value is usually contained between 20 and 50°C.

$$\Delta T_a = T_{4g} - T_3 \tag{1.19}$$

[3]Schematic adapted from [24].

CHAPTER 2

METHODOLOGY

This chapter details the methodology used in this work to obtain the final results. First, the 0D model of the engine is explained. Secondly, the experimental setup is presented. Modifications made on the test bench in the frame of this thesis are explained. The post-processing of experimental data is also briefly discussed while this chapter is concluded by the mathematical modeling of the Organic Rankine Cycle.

2.1 0D model for engine cycle simulation

The elaboration of the 0-Dimensional model is based on the previous work done by Rouanet [2]. The model is used to simulate the processes that occur in the engine during the compression and power strokes, from Intake Valve Closing (IVC) to Exhaust Valve Opening (EVO). Its primary purpose is to estimate the cycle thermodynamic efficiency, the cylinder wall losses and the remaining enthalpy in the exhaust gases.

2.1.1 Cylinder pressure

The knowledge of the in-cylinder pressure in function of the crankshaft angle is essential to model a finite energy release. The pressure trace can be obtained from a simple ODE model using the first principle of thermodynamics and the perfect gas law.

The first law of thermodynamics in a closed system states that the internal energy variation ΔU in the cylinder is equal to the amount of heat Q received by the load, plus the amount of work W received by the load from its surrounding.

$$\Delta U = Q + W \tag{2.1}$$

As mentioned above, this equation is only valid for a closed system, i.e. with conservation of mass. In IC engines, the system is considered as closed between the IVC and the EVO. The first principle is then expressed in terms of derivatives with respect to the crank angke θ. Because the mixture within the cylinder is considered as a perfect gas, Eq. (2.1) can be written as follows:

$$nC_v \frac{dT}{d\theta} = \frac{dQ}{d\theta} - p\frac{dV}{d\theta} \tag{2.2}$$

Where n is the number of moles and C_v the molar specific heat at constant volume. The perfect gas law, $pV = nRT$, can also be written in terms of crank angle derivatives:

$$p\frac{dV}{d\theta} + V\frac{dp}{d\theta} = nR\frac{dT}{d\theta} \tag{2.3}$$

By replacing this equation in Eq. (2.2), and using the Mayer's relation, $C_p - C_v = R$, and the definition of the specific heat ratio, $\gamma = \frac{C_p}{C_v}$, the ODE for the pressure trace is finally obtained.

$$\frac{dp}{d\theta} = -\gamma\frac{p}{V}\frac{dV}{d\theta} + \frac{\gamma - 1}{V}\frac{dQ}{d\theta} \tag{2.4}$$

2.1.2 Geometrical parameters

In view of Eq. (2.4), the computation of the pressure trace requires the knowledge of the cylinder volume an its derivative. The instantaneous volume depends on many geometrical parameters such as the compression ratio $\tau = \frac{V_{BDC}}{V_{TDC}}$, the single-cylinder displaced volume $V_{cyl} = \frac{V_d}{4}$, the length of the connecting rod L and the crankshaft radius r. Once these parameters are known, the cylinder volume and its derivative can be computed. A schematic of these geometrical quantities is displayed in Figure 2.1.

$$V = \frac{V_{cyl}}{\tau - 1} + \frac{V_{cyl}}{2}\left(\frac{L}{r} + 1 - cos\theta - \sqrt{\left(\frac{L}{r}\right)^2 - sin^2\theta}\right) \tag{2.5}$$

$$\frac{dV}{d\theta} = \frac{V_{cyl}\ sin\theta}{2}\left(1 + \frac{cos\theta}{\sqrt{(\frac{L}{r})^2 - sin^2\theta}}\right) \tag{2.6}$$

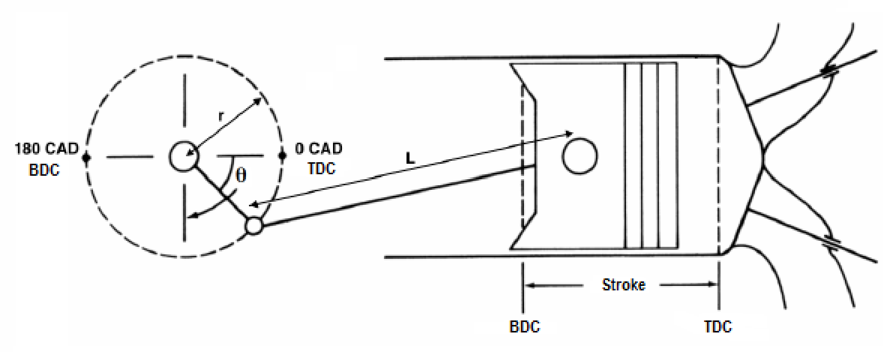

Figure 2.1: Schematic showing the geometrical parameters of the connecting rod-crankshaft system in an ICE [25].

2.1.3 Heat release

In Eq. (2.4), the heat Q represents the net heat release Q_{net}. It is only a part of the total heat released by the combustion, Q_{gross}, while the other part, Q_{loss}, characterizes the heat transfer losses.

$$Q_{gross} = Q_{net} + Q_{loss} \tag{2.7}$$

The gross heat release Q_{gross} is modeled as a simple cosine function starting in $\theta = \theta_s$ and with a burn duration of θ_b. The heat supply and its derivative are given below.

$$Q_{gross}(\theta) = \frac{1}{2}\left(1 - cos\left(\pi\frac{\theta-\theta_s}{\theta_b}\right)\right) Q_{gross,tot} \tag{2.8}$$

$$\frac{dQ_{gross}}{d\theta} = \frac{1}{2}\frac{\pi}{\theta_b} sin\left(\pi\frac{\theta-\theta_s}{\theta_b}\right) Q_{gross,tot} \tag{2.9}$$

Concerning the parameters θ_s and θ_b, they can either be computed experimentally, either be approximated through correlations.

2.1.4 In-cylinder heat loss

The in-cylinder heat transfer losses must be known in order to determine the HR. Because the temperature inside the cylinder and the environment are not the same, the load inside the cylinder continuously exchanges heat with its environment all along the cycle. The major part of the heat transfer occurs during the expansion phase of the piston and the heat transfer mode is mainly convection. Thus, in order to quantify this heat exchange, the Newton law describing convection heat flux is used.

$$\frac{dQ_{loss}}{dt} = hA(T - T_{wall}) \quad \text{[W]} \tag{2.10}$$

$$\frac{dQ_{loss}}{d\theta} = hA(T - T_{wall})\frac{1}{\omega} \quad \text{[J/CAD]} \tag{2.11}$$

In these equations, h represents the heat transfer coefficient expressed in W /(m^2 K), A the exchange surface in m^2 between the gas mixture and its environment, T and T_{wall} respectively, the temperatures in Kelvin of the load and the walls and finally, ω the engine angular velocity expressed in CAD / s.

The exchange surface is composed of three surfaces forming a cylinder: The cylinder head, the cylinder walls and the piston. The cylinder head and the piston surface are obviously constant but cylinder walls depend on crankshaft angle θ implying that the exchange area remains not constant. The total surface A depends therefore on the crank angle θ and can be determined thanks to the engine geometrical parameters.

Between all the empirical models for determining h, the Hohenberg's correlation is simple to implement and effective while, requiring no major tuning effort to match the geometry of the engine [8]. Although, the Woschni correlation is popular in SI and CI engines, it is not suited to HCCI engines [8]. Soyhan et al. [26] discussed the exiting models for HCCI engine and it results that the Hohenberg's model was the most suitable to represent the heat exchange at the HCCI engine cylinder walls. This model contains a scaling depending on engine geometrical parameters, the temperature and the equivalence ratio. The fact of the matter is that the scale factor has to be modified for each working point of the HCCI engine. For this reason, some sources as Broekaert and al. [27] tell that no model is suited to HCCI engine. It is thus difficult to determine accurately the value of the scale factor. But for the sake of consistency with previous master theses, the value of α_{exch} was fixed to 82 despite the potential imprecision that it could imply.

$$h_{Hohenberg} = \alpha_{exch} V^{-0.06} p^{0.8} T^{-0.4} (u + 1.4)^{0.8} \ \ [\text{W/}(m^2 \text{ K})] \tag{2.12}$$

Where V is the cylinder volume in m^3, p the in-cylinder pressure in bar, T the load temperature in K and u the mean speed of the piston in m/s.

2.1.5 Bulk gas temperature

In order to compute the HR, the wall temperature must be known. The latter can be approximated by the coolant temperature at the engine exhaust. The error caused by this assumption is relatively small because the difference between the cylinder walls temperature and the coolant temperature is rather small compared to the difference between the gas and the walls temperatures.

An assumption made to determine the temperature inside the cylinder is to consider the gas inside the cylinder behaves like a perfect gas.

$$p(\theta)V(\theta) = nRT(\theta) \qquad \forall\ \theta \in [IVC, EVO] \tag{2.13}$$

The number of mole inside the cylinder remains constant between the IVC and the EVO because the cycle is a closed system between these two positions.

2.1.6 Specific heat ratio

The adiabatic coefficient γ is defined as the specific heat ratio. The adiabatic coefficient depends both on temperature and composition of the gas mixture. As these two parameters remain not constant along the cycle, the adiabatic coefficient is therefore not constant during the cycle. Several methods exist in order to estimate the adiabatic coefficient value, going from the easiest to the most complicated. These methods were discussed in the thesis of Bhaduri [8]. The drawback of complex methods is the computation time. Indeed, in order to estimate accurately the adiabatic coefficient, these methods take the variations of chemical composition during the combustion into account. But the intrinsic problem of these methods is that the adiabatic coefficient is required to compute the HR and calculate thus the mixture composition afterwards. Consequently, complex methods need an iterative resolution which implies considerable computing resources so that the solver converges and are therefore not suitable for real time computations. This is the main reason, why a simpler model was used to estimate the value of the adiabatic coefficient γ in combustion engines. The model used was developed to compute the adiabatic coefficient on each step of integration (ode45).

$$\gamma(T) = \begin{cases} \dfrac{c_{p,r}(T)}{c_{p,r}(T) - R_r} & if \quad \theta < \theta_s + \dfrac{\theta_b}{2} \\ \dfrac{c_{p,e}(T)}{c_{p,e}(T) - R_e} & if \quad \theta > \theta_s + \dfrac{\theta_b}{2} \end{cases} \tag{2.14}$$

The subscript (r) means reactants and (e) means exhaust products. Eq. (2.14) shows that the homogeneous engine load composition instantaneously changes from reactants (r) to exhaust products (e) when the CA50 ($\theta_s + \frac{\theta_b}{2}$) is reached.

2.2 Experimental test bench

This section describes the conception and the implementation of the experimental test bench. First of all, the main characteristics of the engine are enumerated, then the fuel modification as well as the changes that it causes will be approached, after that, the different test bench configurations will be discussed in order to choose the best option according to the objectives of this thesis. Afterwards, the test bench will be described in its overview in order to have a general understanding of its operation, then the turbocharging and the EGR implementation will be explained and finally the different instruments of the test bench will be listed.

The P&ID of the installation is attached in Appendix A.2 to allow the reader to represent all the elements that constitute the test bench.

2.2.1 Engine specifications

The engine used for the experimental tests is a four-stroke CI engine with four cylinders developed by Yanmar (reference 4TNV98T-GGE). The latter is a stationary engine equipped with a turbocharger and is connected to a 55kW three-phase induction generator (model W22 IE2 from WEG) by means of a universal joint equipped with a flexible joint SGFlex-096.02, allowing a transmission of a maximum torque of 420 Nm. A non-exhaustive list containing the main characteristics of the engine, coming from its data sheet presented in Appendix A.1, is illustrated in the table 2.1.

2.2.2 Natural gas composition and characteristics

Natural gas composition

The fuel used in the HCCI engine is the UCL LNG whose composition is represented in Table 2.2.

Lower Heating Value

By definition, the lower heating value (LHV) of a fuel is the total heat released by a complete stoechiometric combustion of one quantity unit of fuel, when the water in the products is in vapour state. Because the

Yanmar 4TNV98T-GGE engine specifications	
Total displacement V_d	3.318 $[L]$
Piston stroke S	110 $[mm]$
Cylinder bore B	98 $[mm]$
Connecting rod length L	167 $[mm]$
Rotation speed N	1500 $[RPM]$
Inlet Valve Closing (IVC)	-127 $[CAD$
Exhaust Valve Opening (EVO)	150 $[CAD]$
Compression ratio τ	18.1 $[/]$
Peak Cylinder Pressure (PCP)	150 $[bar]$
Maximum Pressure Rate Rise (MPRR)	15 $[bar/CAD]$

Table 2.1: Engine specifications.

$[CH_4]$	$[C_2H_6]$	$[C_3H_8]$	$[C_4H_{10}]$	$[CO_2]$	$[N_2]$
82.70	3.88	0.86	0.38	1.37	10.81
(CH_4)	(C_2H_6)	(C_3H_8)	(C_4H_{10})	(CO_2)	(N_2)
71.05	6.25	2.03	1.18	3.24	16.25

Table 2.2: UCL natural gas composition expressed in %

combustion is isobaric, the heat of combustion under constant pressure is given by the following equations.

$$LHV = \Delta H^f + \int_{T_s}^{T_{in}} \Delta c_p \, dT$$

Where H^f are the compounds enthalpy of formation at the standard state and c_p the heat capacities at constant pressure. This gaseous mixture can be considered as a perfect gas. Because only the hydrocarbons C_nH_m take part in the combustion, the LHV of the fuel is given by:

$$LHV_{fuel} = \sum [C_nH_m] \, LHV_{C_nH_m} \tag{2.15}$$

The values for the standard enthalpies of formation and heat capacities at 298.15 K can be found in thermodynamic tables. By considering a temperature inside the laboratory where experimental tests are performed of 296K, the molar LHV of the natural UCL gas is obtained. The mass LHV is achieved by the division of the molar LHV with its molar mass. All the natural gas parameters computed are displayed in the table 2.3.

Air demand

The air-demand is the exact amount of air needed for the combustion of one quantity unit of fuel. The air-demand of the fuel is given by:

$$m_{a1,fuel} = (CH_4)\, m_{a1,CH_4} + (C_2H_6)\, m_{a1,C_2H_6} + (C_3H_8)\, m_{a1,C_3H_8} + (C_4H_{10})\, m_{a1,C_4H_{10}}$$

The m_{a1} of every hydrocarbons is obtained through their complete stoechiometric combustion reactions:

$$m_{a1,fuel} = \frac{n_{air} M_{m,air}}{n_{fuel} M_{m,fuel}}$$

For gaseous fuels, it is more common to express the air-demand in m_s^3 of air per m_s^3 of fuel, where the index s denotes the standard conditions: $T_s = 298.15\ K$, $p_s = 1\ atm$.

LHV_{molar} $[\frac{MJ}{kmol_{fuel}}]$	LHV_{mass} $[\frac{MJ}{kg_{fuel}}]$	$M_{m,fuel}$ $[\frac{kg}{kmol}]$	$m_{a1,fuel}$ $[\frac{kg_{air}}{kg_{fuel}}]$	$m_{a1,fuel}$ $[\frac{m^3_{s,air}}{m^3_{s,fuel}}]$
746.63	40.089	18.6244	13.756	8.8452

Table 2.3: Natural gas properties

Combustion equation

The complete combustion of the fuel occurring in the HCCI engine with an EGR fraction α is the following:

$$\begin{aligned}\sum_{n=1}^{4}[C_nH_{2n+2}] + 0.0137CO_2 + 0.1081N_2 + \lambda w(O_2 + 3.76N_2) + \\ \alpha(a_0O_2 + (a_1 + 0.0137)CO_2 + a_2H_2O + (a_3 + 0.1081)N_2) \\ \rightarrow a_0O_2 + (a_1 + 0.0137)CO_2 + a_2H_2O + (a_3 + 0.1081)N_2\end{aligned}$$

a_0	a_1	a_2	a_3
$\frac{w(\lambda-1)}{1-\alpha}$	$\frac{0.9456+0.0137\ \alpha}{1-\alpha}$	$\frac{1.8238}{1-\alpha}$	$\frac{3.76\ \lambda w+0.1081\ \alpha}{1-\alpha}$

Table 2.4: Product molar coefficient

Equivalence ratio

As the EGR rate causes a dilution of the load (see Section 1.4.2), the excess air coefficient during combustion decreases with the fraction of EGR. The formula for calculating the excess air ratio actually involved in the combustion is:

$$\lambda_{EGR} = \lambda + \frac{\alpha a_0}{w} = \frac{\lambda - \alpha}{1 - \alpha}$$

The equivalence ratio being defined as the opposite of the excess air coefficient:

$$\phi_{EGR} = \frac{1}{\lambda_{EGR}} = \frac{1-\alpha}{\lambda - \alpha} = \frac{1-\alpha}{\frac{1}{\phi} - \alpha} \tag{2.16}$$

2.2.3 Configuration of the test bench

A significant change in the experimental test bench compared to previous year is that natural gas coming from UCL network will be used in the HCCI engine instead of pure methane present in bottles. However, for all the tests performed in this thesis, the inlet pressure of the HCCI engine will be higher than the pressure of the natural gas network. Therefore, natural gas has to be compressed in order to get the desired pressure at the inlet engine for the all the experimental tests. In the previous thesis, the methane was already pressurized into bottles and it was thus not necessary to compress it. In order to achieve this new constraint three possible configurations have been intended for the HCCI test bench. The experimental test bench from the previous year was took as starting point.

Case 1

The first case is schematized on Figure 2.2 on the left. In this configuration, the air first flows through the compressor and is then warmed up in the heating resistance. After these two steps, the air is at the required pressure and temperature for the test. After that, the air and the compressed natural gas which is previously compressed at the same pressure as the air by means of a natural gas compressor are mixed together before to flow in the engine. As the natural gas flow is much smaller than the air flow, the load temperature and the air temperature are the same.

Advantages: Compared to configuration 2, the main advantage of configuration 1 and three is that they have a higher effective efficiency. The formula (1.13) shows that the compressor power increases when the inlet temperature rises. The turbine power will therefore rises which implies a higher turbine pressure inlet. This higher inlet turbine pressure means that pumping losses raises because of the higher amount of work performed by the piston. The mechanical energy available at the crankshaft is therefore reduced which decreases the engine effective efficiency. Another advantage is the absence of natural gas in the heating resistance. Therefore the gas inflammation into the heating resistance is avoided.

Drawbacks: This configuration requires a natural gas compressor which was not present on the installation of the previous year. Thus, as the UCL does not have a natural gas compressor, it will be necessary to buy it. Moreover, with the addition of the natural gas compressor, the piping of the experimental test bench will be slightly modified.

Case 2

The second case is schematized on Figure 2.2 in the center. In this configuration, the air is first warmed up into the heating resistance then the air and the natural gas which is not yet compressed are mixed together. Again, as the natural gas flow is much smaller than the air flow, the temperature of the load is the same as the air temperature. After, the gas mixture flows through the compressor to reach the desired inlet pressure and finally, the pressurized mixture at the required temperature flows into the HCCI engine.

Advantages: The two great advantages of this configuration are first that the experimental test bench does not require a natural gas compressor, so it is no more necessary to buy one. And secondly, exactly the same advantage as for the first case, in this configuration the natural gas does not flow through the heating resistance thus inflammation of natural gas through the heating resistance is avoided.

Drawbacks: The biggest drawback of this configuration is that the thermodynamic efficiency of the HCCI engine is the smallest one of the three configurations. Indeed, In this configuration, the heating resistance is located before the compressor which implies a higher compressor inlet temperature. As explained in case 1, this temperature rise will cause higher pumping losses which will reduce the effective engine efficiency.

Case 3

The third case is schematized on Figure 2.2 on the right, in this configuration the air and the not compressed natural gas are directly mixed together. Then the mixture flows into the compressor in order to reach the required engine inlet pressure. After that the gas mixture is warmed up in the heating resistance and finally, the pressurized mixture at the desired temperature enters into the engine.

Advantages: The first advantage of this case is that the thermodynamic efficiency is the highest one. Secondly, This setting does not require a natural gas compressor which is the same advantage as configuration 2 compared to the first one. And furthermore, with this configuration the piping of the experimental text bench will remain nearly the same. Consequently, this configuration will cause the less piping modification on the previous year test bench.

Drawback: The main drawback of this configuration compared to the others is the presence of hot spots in the heating resistance which may not be certificated ATEX. Thus, if the heating resistance is not ATEX, a hot spot can ignite the natural gas into the heating resistance and make an explosion that can damage or worse break the experimental test bench.

In order to determine the configuration that best suits the objectives of this master thesis, some criteria were establish. The first and the most important criteria is that the effective efficiency of the HCCI engine is the highest as possible to be coherent with the aims of this thesis. To check this criteria, the effective efficiency of the three configurations were computed through a mathematical model by keeping the same output conditions at the engine inlet.

From a thermodynamic point of view, configuration 1 and 3 are equivalent because in both configurations, the air flow is first compressed before to be heated. The only difference between configuration 1 and 3 is the place where the natural gas is injected. But this difference has no impact on the thermodynamic efficiencies simulated through the 0D model. All the efficiencies of configurations 1 and 2 are presented in Table 2.5.

	Configuration 1&3	Configuration 2
P_{fuel}	38.7 kW	35.5 kW
η_c	0.95	0.95
η_{ti}	0.586	0.585
$\eta_{pumping}$	0.838	0.759
η_{in}	0.467	0.422
η_{mec}	0.85	0.85
η_{eff}	0.397	0.359
P_{eff}	15.3 kW	12 kW

Table 2.5: Engine specifications.

Table 2.5, clearly shows that the effective efficiency of the first and the third configurations is greater than the effective efficiency of the second one. Therefore based on the thermodynamic criteria configurations one and three will be preferred. As the thermodynamic efficiency of configurations 1 and 3 is the same, the next criteria established to select the best configuration is to start the experimental tests as soon as possible. The configuration which best satisfied this constraint is thus the number 3 because it does not require a natural gas compressor.

As configuration three was chosen according to the previous criteria, now it is necessary to check the drawback of this configuration, that is, if the heating resistance is certificated ATEX. It was realized by calling the manufacturer of this resistance: Ohmewatt. Unfortunately, Ohmewatt confirmed that the heating resistance is not suitable for hot spots because it's not certificated ATEX. Thus the third configuration was given up in order to avoid a possible explosion in the resistance. In order to ensure the highest effective efficiency, it was decided to explore the possibility to realize the tests with the first configuration. For this configuration, it is necessary to have a natural gas compressor which fulfill all the requirements for the HCCI test bench. Five companies were contacted and only two offers were obtained. The cheapest offers got was from Atelier François. This offer consisted in a natural gas compressor and a electric motor. But its price largely overtook the budget of this master thesis, it was decided to give this solution up.

In conclusion, because of the constraint that the heating resistance have to be certificated ATEX and because of the thesis budget constraint it was forced to give the configuration 1 and 3 up. Therefore, to fulfill all the requirements, the only possibility is to make the experimental tests with the configuration 2 of the HCCI engine even if the effective efficiency will be smaller.

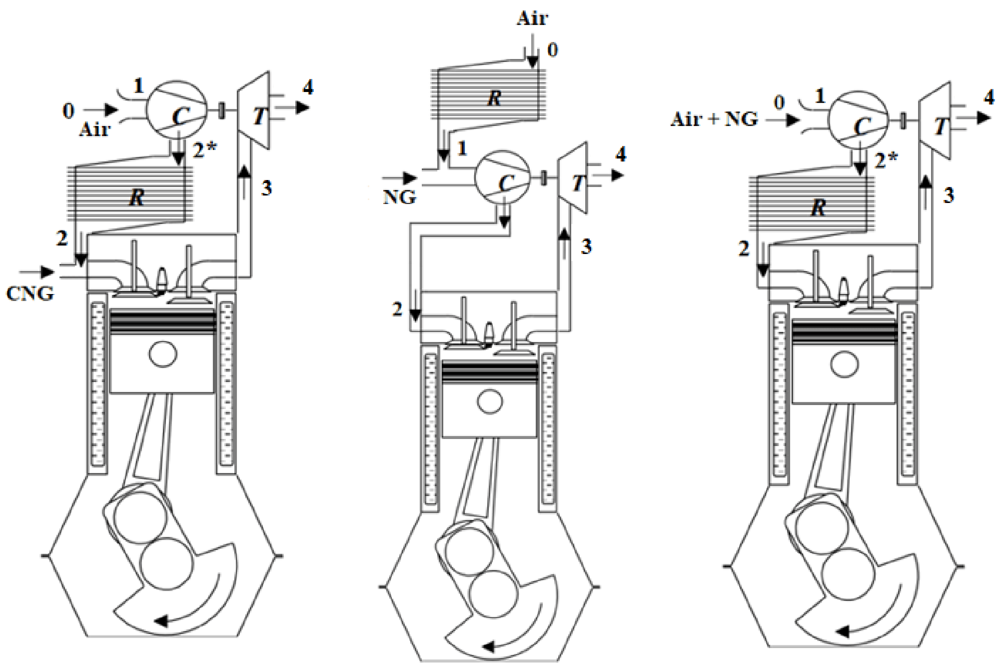

Figure 2.2: Schematic representation of different configurations of the test bench.[1]

2.2.4 Intake system

Diaphragm and intake box

In order to determine most of efficiencies and engine parameters, the air flow must be known. Thus to compute the air flow passing through the engine, a depressing device system consisting in a diaphragm placed at the top of a suction hose has been used. The air flow is computed by means of the ISO-5167 norm. Indeed,

[1] Schematic adapted from [7].

by knowing the ambient conditions, the geometry of the diaphragm, the arrangement of the sensors and the variation of pressure between upstream and downstream of this diaphragm, the norm ISO-5167 allows to determine the air flow.

However, the aspiration of the air into the engine is not smooth and match to a pulsed flow which contains peaks and dips of air flow. In the case of a direct measurement, it should therefore result in rather marked variations of air flow lecture. This variation of lecture should have a huge impact on the accuracy of the equivalence ratio of the load which is a main parameter of experimental tests and thus, could skew the results of the analyzes.

In this point of view, a box has been used to serve as a buffer tank, smoothing the phenomena of pulsed flow induced by the engine. The box used in the test bench is the same as in the previous master thesis. The intake box comes from an engine with a similar total displacement running at higher rpm, therefore the size of the intake box is sufficient to smooth the intake air flows of the HCCI engine. Thanks to the smoothing of the air flow measurement, the equivalence ratio control became easier and its measurement became more accurate.

Heating resistance

The heating resistance was already present on the former configuration of the HCCI test bench which provides the necessary heat input. With the combination of the heat provided by the heating resistance and the heat induced by the compressor, the load will reach the desired temperature inlet condition.

Natural gas pipe

By observing the P&ID of the HCCI test bench, it is shown that the natural gas pipe contains five different devices.

The first device of the gas line pipe is an emergency stop valve that closes when a security condition is no more respected. The security conditions are encoded in Labview and are checked with the information sent by the sensors present on the HCCI test bench.

Because the natural gas of the UCL network is pressurized with a 0.290 bar boost pressure, a zero pressure gas regulator was installed in the natural gas pipe to reduce its pressure up to the atmospheric pressure. This device will therefore allow the mixing of the natural gas with the air.

The knowledge and the control of the natural gas flow is essential to get desired and accurate results. The measurement of the natural gas flow is made through a gas meter which was present on another engine of the hall Stevin. The gas meter is a Krom schroder device which can measure the gas flow in a range from 0.06 to 10 [m^3/h] and with a maximal pressure of 1,2 bar. As the gas network pressure is bigger than the maximum allowable pressure of the gas meter, the zero pressure regulator must be placed on the gas line before the gas meter. The gas meter suits for all experimental tests of this thesis. Indeed, the gas flow of the experimental tests is always bigger than the minimum value of the gas meter. To check the upper limit, the theoretical maximum gas flow used in the experimental test is computed. The HCCI configuration giving this flow rate is the following: ϕ =0.46, T_{in}=170°C and p_{in}=1,4bar.

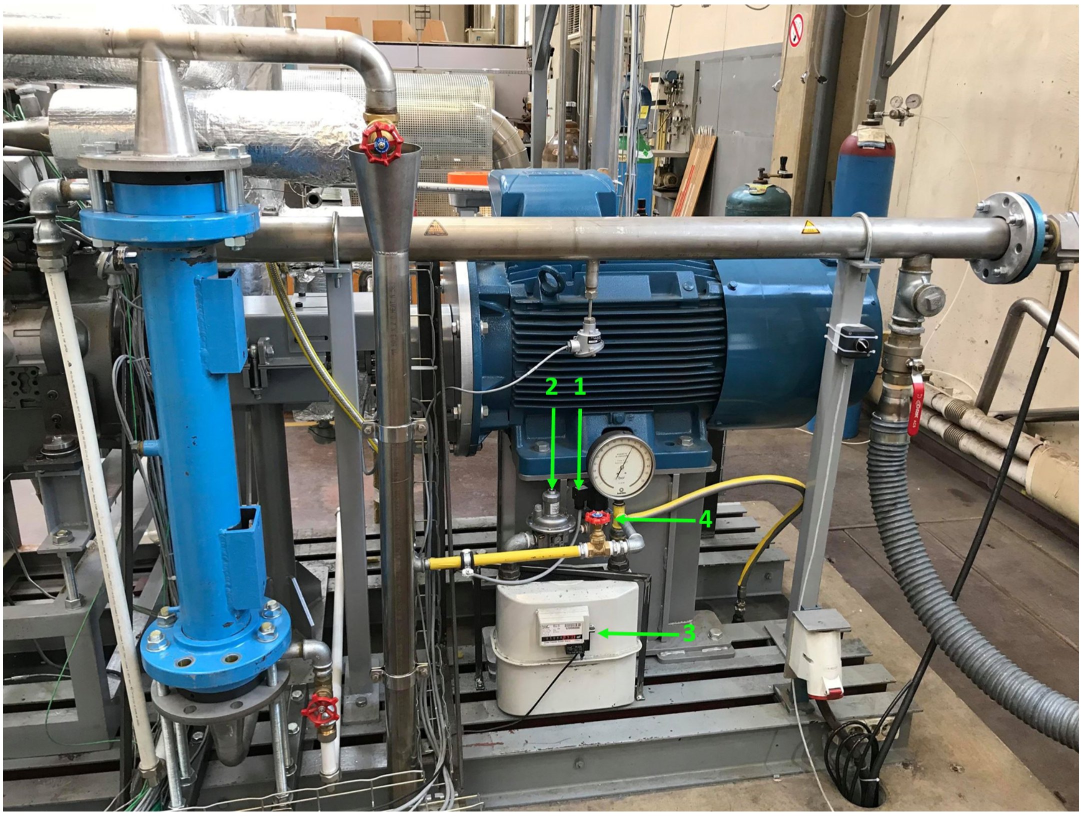

Figure 2.3: Natural gas pipe devices: (1) emergency stop valve, (2) zero pressure regulator, (3) Krom schroder gas meter, (4) slide valve.

By knowing both inlet temperature and pressure, the filling coefficient and the air flow rate can be easily computed:

$$r = \eta_{vol} \frac{p_2}{p_{ref}} \frac{T_{ref}}{T_2} \qquad \dot{m}_{air} = r \cdot \rho_0 \cdot V_c \cdot \frac{\omega}{120} \tag{2.17}$$

Where V_c is the total displacement, p_{ref} = 101325 Pa, T_{ref} = 296K and ω the number of rpm of the HCCI engine. By inserting the inlet parameters in the equations above, the NG mass flow rate is obtained.

$$\dot{m}_{fuel,max} = \frac{\phi \cdot \dot{m}_{air,max}}{m_{a1}} = 1,5[g/s] \tag{2.18}$$

This maximum natural gas flow is converted into a volume flow with the help of the perfect gas equation at the reference conditions. So the maximum volume flow of gas is 6.48 m^3_{ref}/h which is less than the maximum measurable value by the gas meter. The gas flow measure for the experimental tests was made through two different manners. The first way to measure the gas volume flow is by computer with the Labview software. Indeed, a pulse is sent by the gas meter to the CompactRIO each time 0.01 m^3 is consumed by the engine. Thus a Labview code was written in order to compute the natural gas flow over a certain period. Because of the fluctuation of the gas flow, to get a sufficiently accurate and fast measure, the computation period was fixed to a minimum of 30 seconds. The computing method used in Labview is the following.

$$\dot{V} = \frac{N_{pulse} \cdot 0.01}{T_{pulse}} \quad [m^3/s] \tag{2.19}$$

Where N_{pulse} is the number of pulse and T_{pulse} the computation period. The second way to measure the volume gas flow, is by hand. Indeed, each time 0.001 m^3 is consumed by the engine the the gas meter dials value is incremented by 1 on the gas meter. Thus, the volume gas flow can be obtained by measuring the number of incrementing of the gas meter over a determined time period. This method was realized by using a stopwatch. For both methods, the volume gas flow is easily converted into a mass gas flow with the reference density of the natural gas ρ_{ref}.

So that the experimental tests are done correctly, it's essential to be able to modify the equivalence ratio during each test. In the experimental test bench the control of the natural gas flow, therefore the equivalence ratio, is designed by means of a slide valve.

The last device of the natural gas pipe is a check valve. This experimental apparatus is essential for the security during experimental tests. Indeed, if an explosion occurs in the engine during a test, a pressure wave will be created and will go up in the test bench pipes. And with the check valve, the pressure wave will be stopped preventing damage or broken in the natural gas meter because it's maximum allowable pressure is lower than the pressure caused by the explosion.

Gas mixer

A gas mixer from the Heinzmann company is used to add the fuel to the hot air having circulated in the line of the heating resistance. This device uses the Venturi effect to mix gases from two lines. After this system, the mixture is very homogeneous and the loss of pressure is very small due to the almost ideal Venturi insert.

2.2.5 Cooling system

During the experimental tests, the temperature of the engine increases because of the heat lost at the cylinder walls and the heat generated by all the frictions in the engine. Thus the engine have a cooling system to void this heat. A mixture of water and coolant is used by the cooling system, flows into the engine to evacuate the heat towards a heat exchanger. The heat exchanger is a plate exchanger between the mixture water-coolant and the water coming from the distribution system. This system allows to cool down the mixture water-coolant coming from the engine without ever renewing it. To regulate the engine temperature, a thermostat is present at the output of the engine. A working temperature of approximately 90°C has been chosen in order to limit cylinder walls losses and in order not to damage the engine components with large thermal gradients. Rather than regulating the flow of cold water through the exchanger, a 3-way valve is used to control the proportion of hot water passing through the exchanger and the one short-circuiting it. If the engine temperature is too cold, the fraction of water circulating in a closed loop in the engine internal circuit without flowing in the heat exchanger increases. On the contrary, if the engine temperature is too hot, this water fraction decreases and the fraction of water flowing in the heat exchanger increases in order to reduce the engine temperature. As the HCCI combustion is pretty influenced by the cylinder walls temperature, it's important to have a good control on it in order to maintain this temperature the most constant as possible.

2.2.6 Variable geometry turbocharger

The exhaust manifold allows to collect the exhaust gases of the different cylinders and to direct them towards the turbine. The exhaust gases will flow through the turbine which will recover a part of the residual energy contained in the gases to ensure the operation of the compressor upstream. In order to control the inlet pressure given by the compressor, the turbine has a variable geometry which is composed of a system of adjustable fins. The variable geometry turbine control system is the same as the previous year.

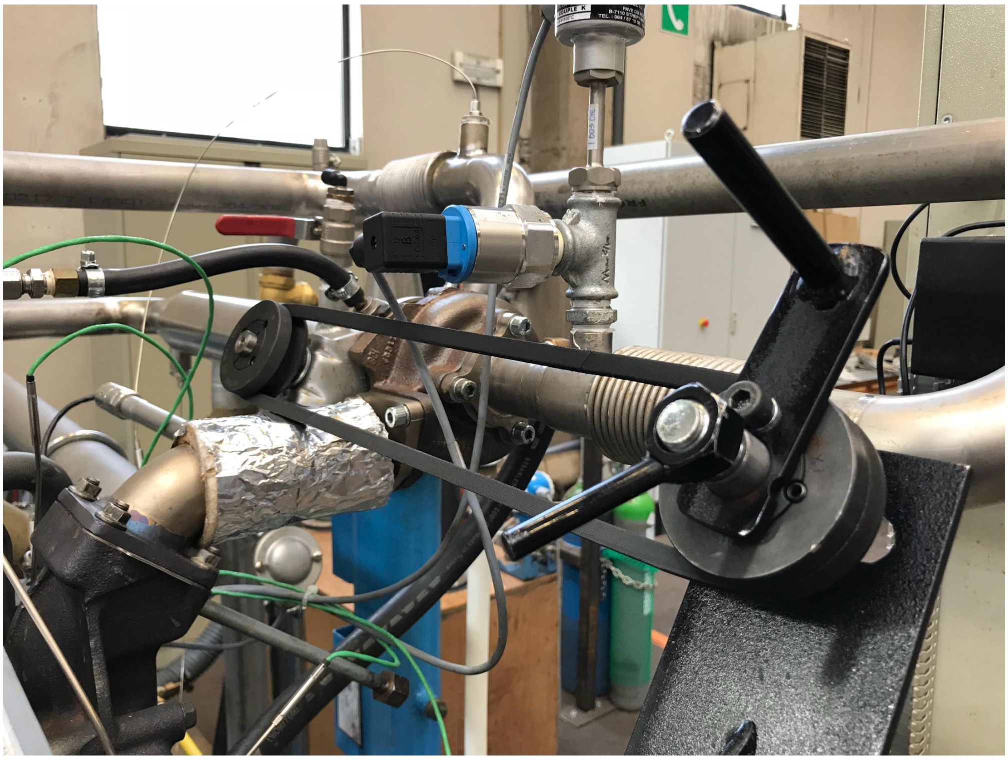

Figure 2.4: Variable geometry turbine command

This is a screw adjustment mechanism that induces the displacement of a threaded rod connected to the VGT command of the turbine. The screw thread is fine and a displacement of 1mm is made at every screw full rotation. To make the command more accessible, a belt and pulleys system was designed to rotate the screw without risking getting burned. The values studied in the continuation of the work are integer multiples of number of half turns made with the control pulley (and thus by 0.5 mm of displacement). Each pulley turn corresponds to a defined position of the VGT control ranging from 0 to 20. 0 is therefore the fully open position and 20 is the closed position.

2.2.7 EGR implementation

EGR configuration

EGR configuration of the experimental test bench is the same as the previous year and consists in an external low pressure loop EGR. This configuration was chosen mainly because the inlet temperature is much more easy to control. Moreover, EGR fraction does not influence the turbine flow which allows to choose the turbocharger with an optimal efficiency in the mass flow range of this thesis.

Air - EGR mixer

The system air - EGR of our HCCI test bench is exactly the same as the one present on the test bench of the previous year. After the expansion of smokes in the turbine, a part of smokes flows directly in the exhaust device and the other part flows into the EGR device. In order to implement the recirculation of the exhaust gases into the engine, a DN 40 elbow conveying burned gases has been inserted into the DN 65 inlet pipe (see Figure 2.5). The diameter of both EGR and air pipes were determined so that the passage section of the air and the EGR are at the same amount of magnitude for two reasons. First, to guarantee a sufficient air flow and second, to allow the use of a high fraction of EGR. If the EGR fraction is not sufficient enough, the counter pressure valve can be closed gradually to increase the exhaust gas flow.

EGR valve and cooler and counter-pressure valve

In order to control the EGR flow, a sliding valve was placed after the cooler on the pipe allowing the recirculation of cooled exhaust gases towards the admission. The EGR cooler serves to reduce the temperature of the exhaust gases before the reinsertion in order to respect the inlet temperature constraint. However, the compressor inlet temperature should remain high enough to avoid water condensation. A second valve is placed just before the exhaust and allows to adjust the counter-pressure at the exhaust in order to increase the EGR flow and the EGR fraction in the case of a too small output turbine pressure. The EGR system devices are represented on Figures 2.5 and 2.6.

Figure 2.5: Exhaust system:(1) Counter-pressure valve, (2) EGR valve, (3) EGR water valve.

Figure 2.6: Exhaust system: (1) EGR valve.

EGR implementation

Because it was not possible to directly measure the EGR flow rate notably because of the exhaust gases composition which was unknown, it was necessary to find another way to compute the EGR flow rate and therefore the EGR fraction.

In the experimental test bench, the fuel and the air flow rate are both known respectively thanks to the gas meter and the sensor located in the depressurized device. It is therefore possible to determine both EGR flow and EGR fraction by considering that the exhaust gases take replace the air in the engine without affecting the fuel and the total flow rate. However, the use EGR will allow a higher turbine power. This results in a higher filling coefficient which modifies the total flow rate of the engine. Consequently, this inlet pressure modification must be taken into account in the computation of the EGR flow rate. The EGR flow rate flowing in the HCCI engine is computed according to the following equation.

$$\dot{m}_{EGR} = \dot{m}_{air,without\ EGR} \cdot \frac{p_{in,with\ EGR}}{p_{in,without\ EGR}} - \dot{m}_{air\ with\ EGR} \tag{2.20}$$

$$(EGR) = \frac{\dot{m}_{EGR}}{\dot{m}_{air\ without\ EGR} \cdot \frac{p_{in,with\ EGR}}{p_{in,without\ EGR}}} \tag{2.21}$$

2.2.8 Instrumentation and control system

Compared to the previous year test bench [28], this year's bench is pretty similar but contains however two modifications. As mentioned in Section 2.2.4, the measure of the natural gas is made though the Krom schroder gas meter and no more with mass flow controllers which constitutes the first modification. And a temperature sensor was added on the load pipe located just before the EGR-load mixer. All the instrumentation and the control system of the present test bench are listed in the table 2.6. The Labview graphical interface used during the tests to control systems and displaying the measures sensors is represented in the appendix A.3.

2.3 Post-processing of experimental data

2.3.1 HR computation from experimental pressure curves

In Eq. (2.4), Q represents the useful heat which is converted into work and is thus renamed Q_{net}. The heat Q_{net} can be divided into two terms: Q_{gross} the heat released by the combustion of the fuel and Q_{loss} the heat loss to the cylinder walls.

$$Q_{net} = Q_{gross} - Q_{loss} \tag{2.22}$$

The Eq. (2.4) can then be rewritten by isolating the derivative from the heat release due to the combustion and allows to get the RoHR equation.

$$\frac{dQ_{gross}}{d\theta} = \frac{\gamma}{\gamma - 1} p \frac{dV}{d\theta} \cdot + \frac{1}{\gamma - 1} V \frac{dp}{d\theta} + \frac{dQ_{loss}}{d\theta} \tag{2.23}$$

By integrating this expression over a range of angle which contains the combustion field, the heat released Q_{gross} can be determined in function of the crank angle θ. From Q_{gross}, it's possible to find the angles CA10,

	Measured quantity	Instrumentations	Details
Fast acquisition	Cylinder pressures	Beru PSG (one per cylinder)	0-200 bar
	Angular position	Heidenhain ROD 426	Resolution 0.1 CAD
	Couple and rotating speed	HBM T40B	-500 à 500 Nm
Slow acquisition	Diaphragm upstream pressure	Kistler RAG25	0-10 barg
	Diaphragm upstream Temperature	PT100 probe	0-50° C
	Diaphragm differential pressure	Endress+Hauser PMD75	0 to 10 kPa
	Admission pressure	Kistler 4260	0-5 bar
	Admission temperature	Thermocouple type K	0-200°C
	Compressor inlet temperature	Thermocouple type K	0-200°C
	Exhaust pressure	Kistler 4260	0-5 bar
	Exhaust temperature for each cylinder	Thermocouples type K	0-500°C
	Cooling liquid temperature	PT100 probe	0-150°C
	Oil pressure	Pressure switch Yanmar	ON/OFF
	Oil temperature	Thermocouple type K	0-150°C
Slow control	Admission temperature	Heating resistance Ohmewatt	15-200°C ; 15 kW
	Exchanger flow rate	Three-way valve	0-100%
	Rotating speed	Mitsubishi variator	0-1500 rpm ; 55 kW

Table 2.6: Instrumentation and control systems of the test experimental bench

CA50 and CA90 but also the combustion timing. The CA_x angle correspond to angular position of the crankshaft where x% of the energy was delivered by the combustion of the fuel.

$$Q_x = \frac{x}{100}\left(Q_{gross,max} - Q_{gross,min}\right) + Q_{gross,min} \tag{2.24}$$

Where $Q_{gross,max}$ and $Q_{gross,min}$ are respectively the minimum and the maximum values of the cumulative heat release. The combustion timing is defined by the duration in CAD between the CA10 and the CA90 which are respectively defined as the beginning and the end of the combustion.

2.3.2 Calibration of experimental data

Determination of the effective compression ratio

At the TDC, due to the low volume in the cylinder, the compression ratio is pretty sensitive. However, because it influences the cylinder volume, its derivative, the HR estimation and consequently the engine performance estimation, it is necessary to use an accurate value of the compression ratio.

The Bengt method is used in order to compute the actual compression ratio in the most accurate way through the motoring pressure curves. During motoring operation, no heat is released implying that the value of the RoHR must be zero for the whole cycle. Therefore, the RoHR equation was used for different compression ratio by starting from the original 18:1. The actual compression ratio is thus the one for which the RoHR is minimum. This method was computed for every motoring test. Each of this test giving a compression, the actual compression ratio of the present application is the average of the compression obtained through the Bengt method for each motoring test. Its value is 17,5:1 and the latter was conserved for all the analyses presented in this report.

Determination of the TDC offset

The equations in Section 2.1.2 clearly show the dependence of the volume and its derivative with the angular position. It is thus very important that the value measured by the angular encoder exactly corresponds to the angular physical value, on the other hand it would imply a wrong assessment of the engine performance. In order to match the physical angular values with the crank encoder measures, the angular encoder is positioned in such a way that its reference signal is synchronized with the TDC of the first cylinder driving phase. However, it is difficult to adjust manually this device which means that the TDC offset correction is essential for the results analysis.

The method developed by Tunestål [29] has been selected thanks to its low assumptions number and ease of implementation. The latter supposed that in motoring, near the TDC the RoHR is zero and due to the small change of volume in this area, the pressure and the temperature are supposed constant implying a constant wall heat losses $\frac{dQ}{d\theta}$. Therefore, the RoHR Eq. (2.23) can be simplified for a motoring operation such that :

$$\frac{dQ_{gross}}{d\theta} = \underbrace{\frac{\gamma}{\gamma-1}}_{=0} p\frac{dV}{d\theta} \cdot + \frac{1}{\gamma-1}V\frac{dp}{d\theta} + \underbrace{\frac{dQ_{loss}}{d\theta}}_{=\mathrm{k}} \tag{2.25}$$

The cylinder volume and its derivative being known for each angular position, the offset of the TDC results in a wrong synchronization between these two known values and the pressure measurements. For an offset of a value θ_0, Eq. (2.25) can be rewritten as follows :

$$0 \approx \frac{\gamma}{\gamma-1}p(\theta+\theta_0)\frac{dV}{d\theta} \cdot + \frac{1}{\gamma-1}V\frac{dp}{d\theta}(\theta+\theta_0) + \frac{dQ_{loss}}{d\theta} \tag{2.26}$$

This equation is performed near the TDC for different angular offset and the offset giving the smallest residue of Eq. (2.26) in the least squares sense is chosen. Since the acquisition system only allowed a resolution of 0.5 [CAD], the offset of the TDC determined here can not be computed with a better precision when calculating heat release. Since the duration of the combustion phenomenon is of the order of ten CAD, this low resolution can lead to significant errors in the calculation of the RoHR.

2.3.3 Outputs

By taking into account all the calibration of experimental data and the volume according to the θ angle get from the angular encoder, it is now possible to computed all efficiencies and MEP represented on the figure 1.1. First of all, the FuelMEP is deduced from the fuel flow rate measure. Then with the calibrated experimental pressure curves in function of the crank angle, the $IMEP_{gross}$ is computed by integrating the following equation on the first half of the engine cycle:

$$IMEP_{gross} = \frac{1}{V_{cyl}} \int_{-180°}^{180°} p(\theta)\frac{dV(\theta)}{d\theta} d\theta \tag{2.27}$$

The MPRR can also be computed with the calibrated experimental pressure curves in function of the crank angle:

$$MPRR = \left(\frac{dp(\theta)}{d\theta}\right)_{max} \tag{2.28}$$

The $IMEP_{net}$ taking the pumping losses into account is obtained by integrating the same equation on the whole engine cycle:

$$IMEP_{net} = \frac{1}{V_{cyl}} \int_{-180°}^{540°} p(\theta)\frac{dV(\theta)}{d\theta} d\theta \tag{2.29}$$

The total heat exchanged between the load and the environment Q_{net} is also determined by means of the pressure curve and its derivative in function of the crank angle by integrating the following equation over a range of angles containing the combustion field.

$$\frac{dQ}{d\theta} = \frac{\gamma}{\gamma-1} p \frac{dV}{d\theta} \cdot + \frac{1}{\gamma-1} V \frac{dp}{d\theta} \tag{2.30}$$

Then both QhrMEP and QhtMEP can be derived with the Hohenberg correlation which determines the wall heat losses Q_{loss} and therefore the total amount of heat produced by the combustion of the fuel Q_{gross} . Thus, by knowing $QhrMEP$, $IMEP_{gross}$ and $QhtMEP$, the exhaust heat losses can be derived thanks to following equation connecting together all these parameters. After all the associated parameters can be computed.

$$QhrMEP = IMEP_{gross} + QhtMEP + QexhMEP \tag{2.31}$$

$$\eta_{ti} = \frac{IMEP_{gross}}{QhrMEP} \qquad \varepsilon_{ht} = \frac{QhtMEP}{QhrMEP} \qquad \varepsilon_{exh} = \frac{QexhMEP}{QhrMEP} = 1 - \eta_{ti} - \varepsilon_{ht} \tag{2.32}$$

Finally, the torque characterizing the mechanical work available at the crankshaft is measure by the torque sensor which thus allows to compute BMEP and the mechanical efficiency.

2.4 Mathematical modeling of an ORC

All the states and characteristics of the Organic Rankine Cycle were simulated within a mathematical model on MATLAB. The open-source CoolProp is a library which can be implemented with several software including MATLAB and which contains an exhaustive list of ORC fluids with their properties.

In this section, the modeling assumptions used in the 0D model to simulate the cycles will be stated. Then, the parameters of the ORC will be discussed. Finally, the numerical solving of different ORC configurations studied in this master thesis will be explained.

The ORC configurations investigated in this thesis are: the subcritical ORC without regenerator, the subcritical ORC with regenerator, the supercritical ORC without regenerator and the supercritical ORC with regenerator.

2.4.1 Model assumptions

General

As global hypothesis, the pressure losses in the pipes will be neglected and the insulation of the pipes of the ORC will be considered perfectly thermally insulated in order to prevent heat losses between the states of the cycle. Also, variations in kinetic and potential energy are neglected.

The assumptions made for the different components of the ORC are enumerated below:

Pump

The pump is characterized by an isentropic efficiency $\eta_{is,p}$. The specific volume of the organic fluid is supposed to be constant during the compression. The transformation is supposed adiabatic and the NPSH at the inlet of the pump is respected.

Steam generator

The combustion in the HCCI engine follows the Eq. (2.2.2). The coefficient of air excess is adjustable. The smoke is composed of the exhaust gases from the HCCI engine in accordance with the Eq. (2.2.2). The exhaust gases of the HCCI engine in the WHR heat the organic fluid up in an isobar way. The heat exchange in the WHR is adiabatic therefore there is no heat loss through the WHR walls.

Turbine

The turbine expansion is characterized by an isentropic efficiency $\eta_{is,T}$. The transformation is considered adiabatic. The inlet conditions of the turbine are determined by both flow rate and temperature of the exhaust gases and the optimal ORC power.

Condenser

The outlet conditions of the condenser are fixed by the temperature of the cold source. As the experimental tests are performed in the Stevin lab, the ORC cold source temperature is assumed to be at the order of 15°C.

Regenerator

There is no loss through the heat exchanger walls thus the heat exchange is adiabatic and the transformation is assumed isobaric.

2.4.2 Parameters cycle

In order to get the output power and all the efficiencies of the ORC, three key parameters have to be determined: The maximum temperature, the maximum pressure and the ORC fluid flow rate. The maximum temperature depends on the exhaust gas temperature of the HCCI engine. The maximum temperature is supposed to be close to the temperature of the exhaust gas. For all the ORC configurations of this thesis, it was assumed that the maximum temperature of the cycle is equal to the exhaust gas temperature at the inlet of the WHR minus a pinch. For a subcritical ORC, the value of this pinch is typically between the range [20-50]°C [24]. For the supercritical ORC, the value of this pinch depends both on flow rate and heat capacities of ORC fluid. The maximum pressure of the cycle can be calculated through the output power of the ORC. Indeed, the maximum pressure of the cycle is the pressure such as the power given by the ORC is maximum. The power obtained from the ORC for another maximum pressure should thus be smaller. The maximum pressure of the cycle should also not be to high to satisfy the technological, operational and economical criteria. Concerning the ORC flow rate, in the subcritical case, the maximum pressure of the cycle and the ORC flow rate are dependent on each other. Therefore, by fixing the maximum pressure cycle in order to get the maximum power, it imposes the ORC fluid flow rate of the cycle. On the contrary, in the supercritical case, the ORC fluid flow rate and the maximum pressure of the cycle are independent. However, the ORC fluid flow rate can be computed through the same way as the cycle maximum pressure. Therefore, for a fixed maximum pressure, the ORC flow rate will be the one which gives the highest ORC power.

For all ORC configurations, the determination of these three key parameters are explained below.

2.4.3 Thermodynamic states computation

The ORC numerical resolution consists in determining the state variables and the thermodynamic characteristics such as the cycle power and the different efficiencies of the ORC. The state variables are the following: the pressure [bar], the temperature [°C], the titer [/], the enthalpy [kJ/kg] and the entropy [kJ/kg K]. By using a T-s diagram, three cases are possible for the state at any position of the ORC:

- The state is outside the bell (two phases domain), all the thermodynamics characteristics can be determined when two state variables (p,T,s,h) are known.
- The state is under the bell, so the pressure and the temperature are related to each other and all the state variables can be determined with the knowledge of the pressure or temperature and one of the following state variable (x,h,s).
- The state is a saturated liquid or vapour, so the title is respectively equal to x=0 and x=1, and with one state variable (p,T,h,s), all the state variables can be determined.

The first and the third cases are showed on Figure 1.13. State 1 corresponds to the third case and states 2, 3 and 4 correspond to the first case.

Constant state

State after the condenser (1)/(5) (without/with regenerator): After the condenser, the fluid is at the saturated liquid state and its temperature is fixed by the cold source. Thus, the temperature of state (1)/(5) is equal to cold source temperature more a pinch which was fixed to 5 degrees and its title x = 0. By knowing these two variables, all the state variables of state (1)/(5) can be determined. Because the cold source is the same for all ORC's discussed in this thesis, the state after the condenser is the only state of the ORC which will remain constant whatever the ORC configuration.

Subcritical ORC without regenerator

The states of the ORC are mainly depending of the organic fluid, the maximum pressure and the maximum temperature of the cycle. These three parameters will be determined with an iterative method which will select the couple of parameters for which the ORC power is the highest one. The selection of the working fluid will also take the criteria in section 1.5.2 into account.

State after the pump (2): After the pump, the state is outside the bell thus two state variables has to be known in order to compute all the states. First, the enthalpy of this state can be calculated thanks to the isentropic efficiency of the pump.

$$h_2 = h_1 + \frac{h_{2s} - h_1}{\eta_{is,p}}$$

The pressure of state (2) is equal to the cycle maximum pressure which is a parameter. Thus the cycle maximum pressure is known and all the state (2) can be determined. **State before the turbine (3)**: After the WHR, the state is outside the bell. The pressure of state (3) is equal to the ORC maximum pressure which is known. Because only one state variable is known for this state, it is impossible to calculate all the state variables. To compute all the state (3), the maximum temperature must be known. As the organic fluid flow and the pressure of state (3) are dependent on each other, an iteration will be performed on the pressure to get at the end of the iteration the highest ORC power. After this iteration all the variables of state (3) will be known.

Iterative method

In order to compute the organic fluid flow of the ORC according to a certain pressure, the two pinches of the WHR corresponding to the Eq. (1.18) and (1.19) must be determined. In the present work, the minimum temperature difference between the ORC fluid and the smoke is fixed to ΔT_p = 15°C and the difference of temperature between the superheated steam temperature and the gas temperature at the inlet of WHR to ΔT_a = 30°C. The iteration is performed on the pressure therefore both pressure and temperature of state (3) are known and it is possible to compute all the variables of state (3). After that, the thermal balance of the evaporator-superheater unit is computed:

$$\dot{m}_{ORC}(h_3 - h_{2'}) = \dot{m}_g(h_{4g} - h_p) \tag{2.33}$$

In Eq. (2.33), as all the variables are known except the mass flow of the organic fluid, it is thus possible to calculate its value.

$$\dot{m}_{ORC} = \frac{\dot{m}_g(h_{4g} - h_p)}{(h_3 - h_{2'})} \tag{2.34}$$

Finally, the output temperature of the exhaust gases at the WHR outlet can be determined by the energy conservation at the economizer:

$$\dot{m}_{ORC}(h_{2'} - h_2) = \dot{m}_g(h_p - h_{5g}) \tag{2.35}$$

State after the turbine (4): After the turbine, the state is outside the bell. The pressure of state (4) is fixed by the cold source and is equal to the pressure of state (1). The enthalpy of state (4) can be computed thanks to the turbine isentropic efficiency and the variables of state (3).

$$h_4 = h_3 + (h_{4s} - h_3) \cdot \eta_{is,t}$$

By knowing both pressure and enthalpy of state (4), all the state variables can be determined.

ORC cycle power and efficiencies

Now, as the ORC fluid flow and all the thermodynamic variables for the whole cycle are known, the power of the subcritical ORC without regenerator can be determined:

$$P_{ORC} = \dot{m}_{ORC} \cdot (h_3 - h_4 + h_1 - h_2) \tag{2.36}$$

Once the power of the ORC is computed, the iterative loop starts again with another maximum pressure. The iteration loop, illustrated in Figure 2.7 is stopped when an increase of the cycle maximum pressure will decrease the cycle output power. At the end of this loop, both ORC fluid flow and maximum cycle pressure are the parameters that will give the maximum output power of the ORC for a given ORC fluid. Therefore, this procedure is runned for several ORC fluids and, the fluid that suits the best the criteria of Section 1.5.2 and which will give the highest power of the ORC cycle will be chosen.

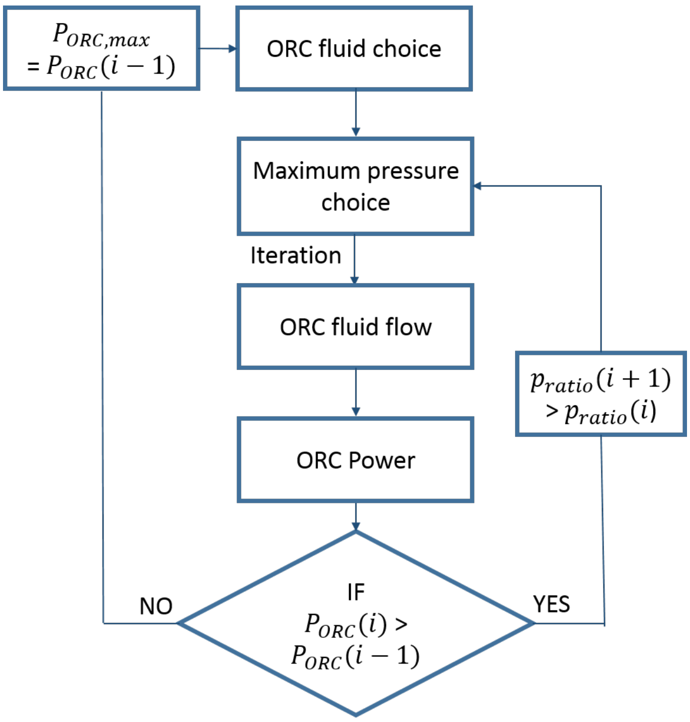

Figure 2.7: Iteration loop for the subcritical ORC cycle.

Thanks to the power of the ORC unit and the state variables of the cycle, it is possible to calculate the total energetic efficiency of the ORC unit.

$$\eta_{totenORC} = \frac{P_{ORC}}{\dot{m}_{ORC} \cdot (h_3 - h_2)} \tag{2.37}$$

ORC with a regenerator

As seen in Section 1.5.1, a solution to economize energy in the ORC and therefore to increase the total energetic efficiency of the combined cycle, is to place a heat exchanger between the fluid which is condensing and the fluid which needs to be heated. The solving of the subcritical ORC with a regenerator with through 0D model is nearly the same as the cycle solving without regenerator. However, the addition of a heat exchanger between the heating and the cooling fluid implies some modifications in numerical solving. First the numbering of the different states is made according to Figure 1.14. The states after the boiler (2), after the turbine (3), at the condenser output (5) and after the pump (6) are determined with the same method as in the subcritical ORC without regenerator.

State after the heat exchanger of the heating fluid (4): The pressure of this state is known because the heat exchange is isobaric. Therefore, the pressure of state (4) is equal to the pressure of state (5) . In order to determine all the variables of state (4), the temperature of this state must be known. In order to compute this temperature, an additional assumption has to be taken into account for the state (4), this hypothesis is:

- The heat exchanger is perfect so the temperature of the heating fluid at the heat exchanger output is exactly the same as the temperature of the cooling fluid at the heat exchanger input.

This assumption is justified because the flows of the heating and the cooling fluid in the heat exchanger are the same, thus the difference of temperature between the cooling fluid at the exchanger input and the heating fluid at the exchanger output is independent of the fluid flow. Therefore, the only parameter which will influence the heat transfer between these two fluids is the calorific capacity of each of the fluids. This is a well known fact that the calorific capacity of a fluid at the liquid state is always greater than the calorific capacity at the gaseous state. Thus with the equation of the conservation of heat, the increase of temperature of the cooling fluid will be smaller than the decrease of temperature of the heating fluid.

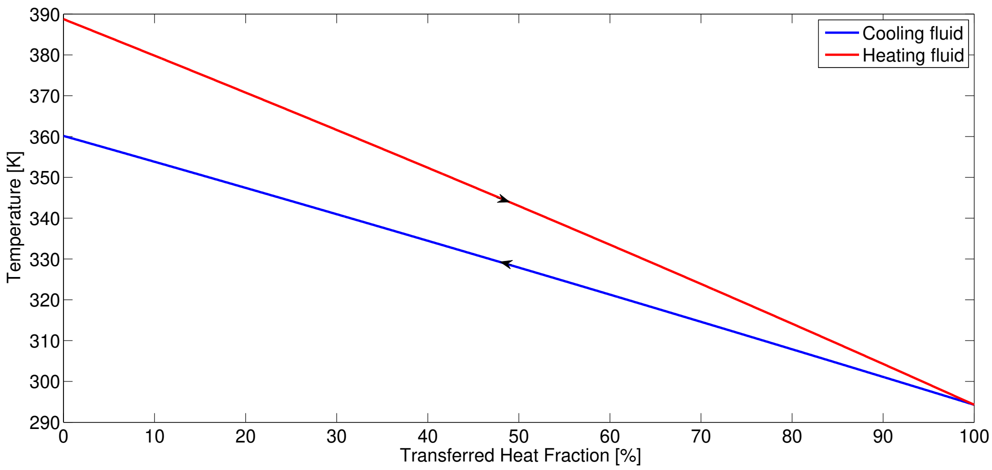

Figure 2.8: Regenerator heat exchanger diagram displaying the temperature against the transferred heat fraction.

This can be observed on Figure 2.8 where the slope of the heating fluid is greater than the slope of the cooling fluid. The result is the output temperature of the heating fluid is equal to the intake temperature of the cooling fluid which well justifies the hypothesis made above. Therefore, T(4) = T(6) and by knowing T(4), two state variables of state (4) are known so it allows to determine all the state variables of (4).

State after the regenerator (1): Thanks to the computation of state (4), all the states of the ORC are determined except state (1). First, as the heat transfer is isobaric the pressure of state (1) is equal to the maximum pressure of the cycle which is already known. The enthalpy of state (1) can be calculated thanks to the energy conservation equation for the heat exchanger. Because the heat transfer is adiabatic, the heat lost by the heating fluid is exactly the heat gained by the cooling fluid.

$$-\dot{m}_{ORC} \cdot \Delta h_h = \dot{m}_{ORC} \cdot \Delta h_c \quad \Rightarrow \quad h_1 = h_6 + h_3 - h_4$$

With the knowledge of p_1 and h_1, all the variables of state (1) can be computed.

Power and efficiencies

After the computation of all the state variables and ORC fluid flow, the power of the ORC with a regenerator can be calculated:

$$P_{ORC} = \dot{m}_{ORC} \cdot (h_2 - h_3 - h_6 + h_5) \tag{2.38}$$

To determine the maximum power of the subcritical ORC with a regenerator, the same iteration scheme as for the subcritical ORC without regenerator represented in Figure 2.7 was used. After having computed the power of the ORC cycle, the total energetic efficiency of the ORC unit is:

$$\eta_{totenORC} = \frac{P_{ORC}}{\dot{m}_{ORC} \cdot (h_2 - h_1)} \tag{2.39}$$

Supercritical ORC cycle without regenerator

The operation of the supercritical ORC is rather similar to subcritical ORC. Indeed, the state after the condenser, after the pump and after the turbine, respectively (1), (2) and (4), are determined in the same way as for the subcritical ORC. The main difference is located in the computation of state (3). Because the fluid is at the supercritical state before the turbine, the fluid no longer passes through a liquid vapor state at the equilibrium (see Figure 1.17). So the WHR no longer contains an evaporator and therefore the saturated liquid state does not exist anymore. The main consequence of this state vanishing is that a pinch between the smoke and the saturated liquid state can no longer be fixed and it results that the pressure ratio and the organic fluid flow are independent. This independence between the maximum pressure of the cycle and the ORC fluid flow implies the apparition of a second iterative loop.

Iterative method

By observing Figure 2.11, as the ORC fluid flow is independent of the maximum pressure of the cycle, there are two iteration loops. First, for each maximum pressure of the cycle, an iteration is performed on the fluid flow in order to get the one which will give the maximum ORC power for a fixed maximum pressure. Contrary to the subcritical case, the location of the pinch constraint is unknown. In the supercritical case, it will occur two different situations which are justified with the equation of conservation of energy between the

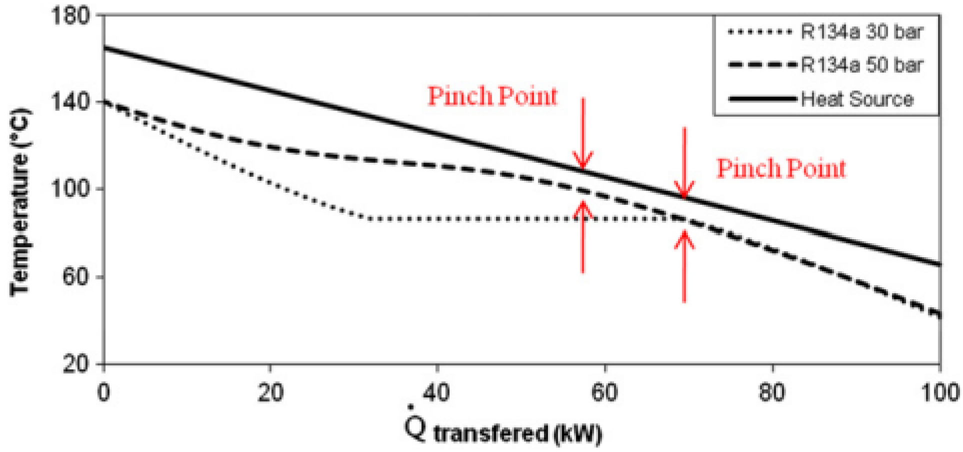

Figure 2.9: T-$\dot{Q}$ diagram of R134a. Live vapour parameters: 30 bar, 140°C (subcritical), 50 bar, 140°C (supercritical) [23].

exhaust smoke and the ORC fluid.

$$-\dot{m}_{smoke} \cdot \Delta h_h = \dot{m}_{ORC} \cdot \Delta h_c \tag{2.40}$$

By assuming the heat transfer in WHR boiler is isobaric, the equation of conservation of energy of the heat exchanger unit becomes:

$$-\dot{m}_{smoke} \cdot \bar{cp}_{smoke} \cdot \Delta T_h = \dot{m}_{ORC} \cdot \bar{cp}_{ORC} \cdot \Delta T_c \tag{2.41}$$

Where $\bar{cp}_{smoke}$ and $\bar{cp}_{ORC}$ are respectively the mean calorific capacity of the smoke between the temperature T_{4g} and T_{5g} and the mean calorific capacity of the ORC fluid between the temperature T_2 and T_3. Consequently, the two cases are:

- $\dot{m}_{smoke} \cdot \bar{cp}_{smoke} \leq \dot{m}_{ORC} \cdot \bar{cp}_{ORC}$
- $\dot{m}_{smoke} \cdot \bar{cp}_{smoke} > \dot{m}_{ORC} \cdot \bar{cp}_{ORC}$

The first case means that the temperature increase of the ORC fluid is smaller than the temperature decrease of the smoke gases. Therefore, it's the same case as on Figure 2.8. Where the slope of the smoke is greater than the slope of the ORC fluid. Thus in this case, the pinch must usually be imposed between the temperature of the ORC fluid at the WHR intake T_2 and the temperature of the smoke at the WHR output T_{5g}. There are some exceptions because some supercritical ORC have a maximum pressure very close to the critical pressure. Thus, when the temperature is close to the critical temperature, the calorific capacity of the fluid is extremely high and tends to infinity. It can be observed on a T-s diagram with the isobaric curve which becomes nearly horizontal at the neighborhood of the critical point as represented on Figure 2.10.

This can result in a modification of the location of the pinch which can no longer be between T_2 and T_{5g} but which will be closer to the critical temperature (see Figure 2.9). This is the reason why an iteration is performed on T_{5g} in order to have a minimum pinch of 15 degrees between the smoke and the ORC fluid.

The second case means that the temperature increase of the ORC fluid is greater than the temperature decrease of the smoke gases. Therefore, it is the opposite case as on Figure 2.8. The slope of the smoke is smaller than the slope of the ORC fluid. Thus in this case, the pinch must usually be imposed between the temperature of

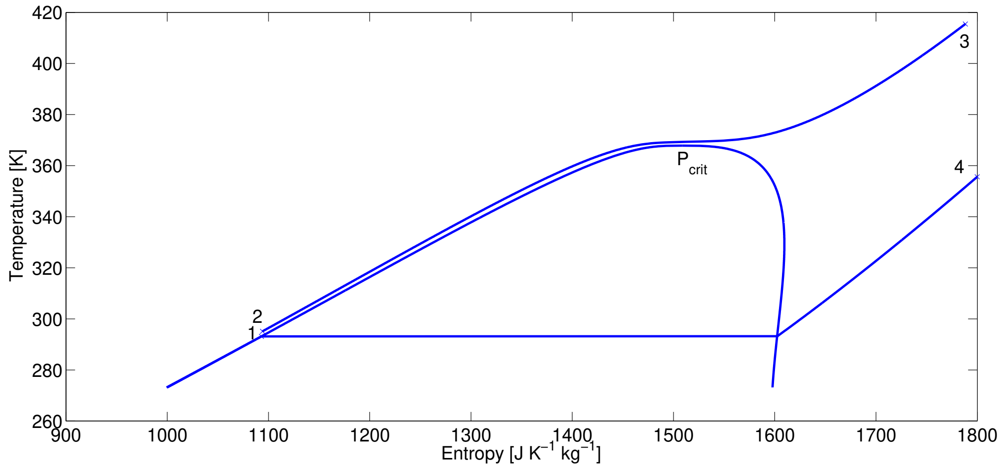

Figure 2.10: T-s diagram of the R1234yf fluid for a maximum cycle pressure of $1.03 \cdot p_{crit}$.

the fluid at the WHR output T_3 and the temperature of the smoke at the WHR intake $T4g$. There are again exceptions because of the same reason as in the first case. Thus an iteration is also performed but in this case on the temperature T_3 in order to get a minimum pinch of 15 degrees between the smoke and the ORC fluid. After the first iteration loop, for a fixed maximum pressure cycle and for a certain ORC fluid, the fluid flow which gives the maximum power is obtained $P_{ORC,flow_{max}}$. This iteration loop is performed for several maximum pressures and at the end of the two iteration loops, the code gives the maximum power for a certain ORC fluid. This procedure is runned for several fluids and exactly as the subcritical case, the fluid that suits the best the criteria of Section 1.5.2 and which gives the highest power of the ORC cycle will be chosen.

Supercritical ORC with regenerator

Exactly as for the subcritical case with a regenerator, a heat exchanger is placed between the cooling fluid and the heating fluid in order to reduce the energetic consumption of the ORC and thus increase the total efficiency of the cycle. And as for the supercritical case without regenerator, the fluid will be at the supercritical state before the turbine.

Iterative method

The iterative method used for this case is nearly the same as for the supercritical ORC without regenerator. Indeed, the state after the condenser (5), the state after the pump (6), the state before the turbine (2), the state after the turbine (3) are computed with the same way as for the supercritical ORC without regenerator and the state before the condenser (4) is computed through the same way as for the subcritical ORC cycle with a regenerator. Therefore, the only state to determine is the state after the heat exchanger (1). Because the fluid flow is independent of the maximum pressure, there are again two different cases to determine the state (1):

- $\dot{m}_{smoke} \cdot \bar{cp}_{smoke} \leq \dot{m}_{ORC} \cdot \bar{cp}_{ORC}$
- $\dot{m}_{smoke} \cdot \bar{cp}_{smoke} > \dot{m}_{ORC} \cdot \bar{cp}_{ORC}$

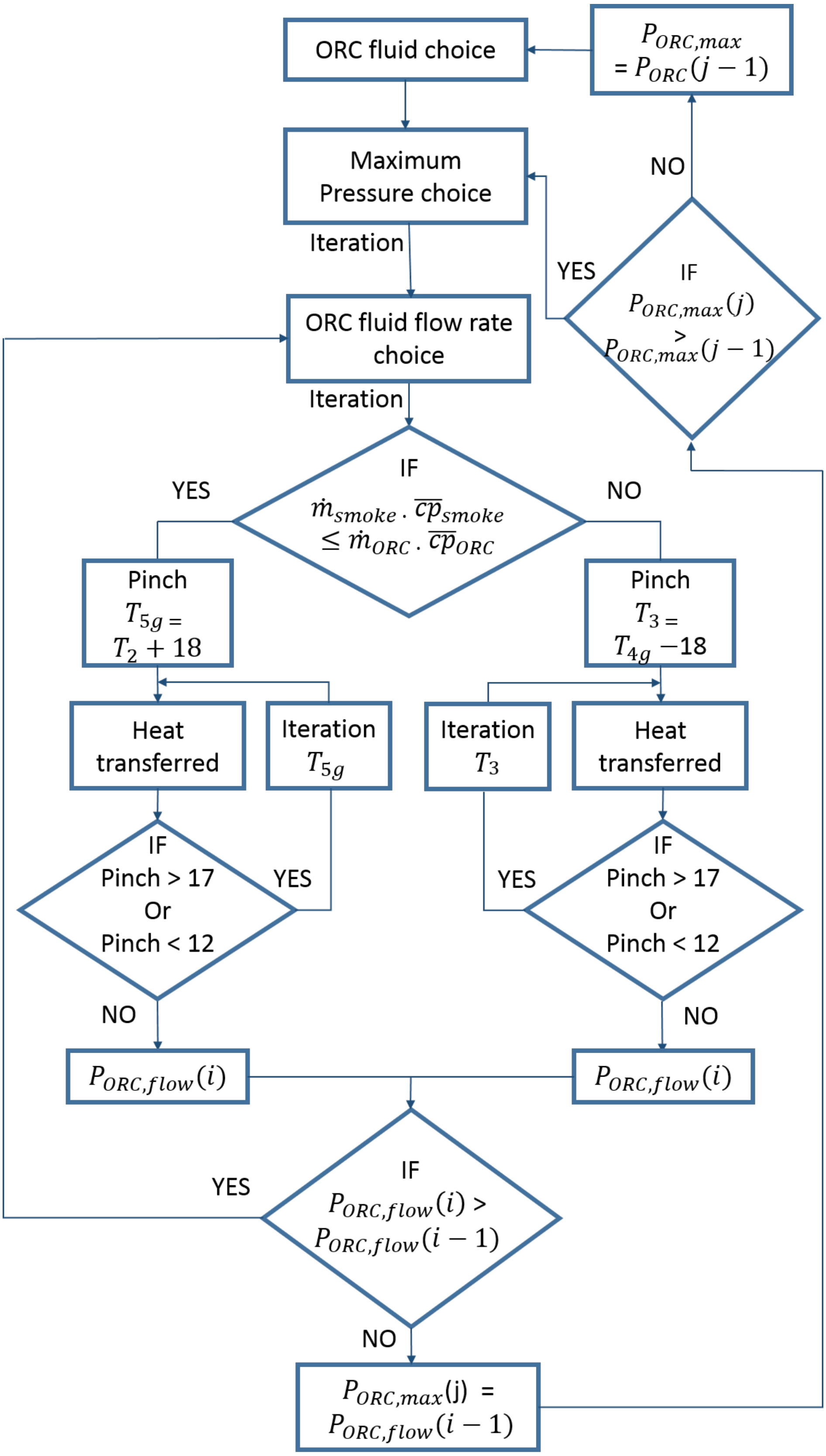

Figure 2.11: Iteration loop for the supercritical ORC cycle.

In the first case, the temperature pinch was imposed between the WHR output state of smokes (5g) and the WHR input state of the ORC fluid (1). Now the problem is that none of the two states is known. Thus a third iterative loop has to be implemented. The iteration is performed on the temperature after the heat exchanger T_1 and is runned until the difference between T_1 and T_{1guess} is smaller than a tolerance which was fixed to 0,1. With the knowledge of T_{1guess}, the WHR output temperature of the smoke is determined with the pinch of temperature.

$$T_{5g} = T_{1guess} + 15 \tag{2.42}$$

Then, the enthalpy h_{5g} with the help of JANAF can be calculated. After having determined the enthalpy of the smoke at the chimney, the enthalpy of the state before the turbine (2) can be computed through the following equation.

$$h_2 = \dot{m}_{smoke} \cdot (h_{4g} - h_{5g})/\dot{m}_{ORC} + h_{1guess} \tag{2.43}$$

Then by knowing both enthalpy and pressure of state (2), all the state variables of (2) can be determined. After this step, the pressure after the turbine (3) is already known, and the enthalpy of state (3) can be calculated with the following equation:

$$h_3 = h_2 - \eta_{is,turbine} \cdot (h_2 - h_{3s}) \tag{2.44}$$

And finally, with the help of the equation of conservation of energy applied on the heat exchanger, the enthalpy of state (1) is obtained:

$$h_1 = h_6 - h_4 + h_3 \tag{2.45}$$

With the knowledge of the enthalpy and the pressure of state (1), it allows to determine the temperature T_1 and evaluate this temperature with T_{1guess}.

In the second case, in the normal case, the pinch of temperature was imposed between the ORC fluid state at WHR output (2) and the smokes state (4g) at WHR input. The iterative loop is runned exactly as in the case without the regenerator. State (1) is determined for each fluid flow thanks to the knowledge of the pressure p_1 and the equation of the conservation of energy 2.45. For these two cases, the power is again computed for each fluid flow $P_{ORC,flow}$ through Eq. (2.38). Then the iterative method is exactly the same as in the case without regenerator (see Figure 2.11).

Total energetic efficiency of the whole cycle

Finally, with all the computations above, it is possible to compute the total energetic efficiency of the combined cycle HCCI engine + ORC:

$$\eta_{toten} = \frac{P_{HCCI} + P_{ORC}}{\dot{m}_f LHV} \tag{2.46}$$

CHAPTER 3

RESULTS AND DISCUSSION

As mentioned previously, the auto-ignition timing in HCCI combustion plays an essential role for engine performance. This timing depends on parameters that influence chemical kinetics such as fuel composition, fuel-air equivalence ratio, pressure or temperature. Many other parameters may also influence the engine performance through these first four: engine speed, compression ratio, exhaust gas recirculation (EGR), coolant temperature, etc. In the frame of this thesis, the experimental setup consists in a stationary HCCI engine running on natural gas with a constant compression ratio. Therefore, the experimental study will focus on the influence of intake pressure and temperature, fuel-air equivalence ratio, EGR rate and, to a lesser extent, coolant temperature.

This chapter first discusses operating ranges of engine intake parameters concerning boost pressure, intake temperature and equivalence ratio. The characteristics of the variable geometry turbocharger (VGT) are also studied. After that, the engine performance is investigated regarding the influence of the three intake parameters mentioned above: p_{in}, T_{in} and ϕ. The effects of EGR in HCCI combustion and its upper range limit are then explored in various ways. Following the discussion of the influence of the coolant temperature and the differences among the cylinders, the experimental part is concluded by an uncertainty analysis.

The last part concerns the coupling between the HCCI engine and the Organic Rankine Cycle (ORC). The performance of the cycle itself is discussed before investigating the HCCI-ORC system in various configurations. Finally, the expected system performance is estimated.

3.1 Operating range

Engine intake parameters that control the auto-ignition timing must remain in a certain range due to physical and technical limits. In this case, a minimum intake temperature of 170°C is needed to obtain a stable combustion. The upper limit is fixed at 190°C to respect the maximum temperature allowed by the safety valve (see P&ID in Appendix A.2). The intake pressure is constrained by the turbocharger and lies between 1 and 1.3 bar, without EGR. However, a minimum pressure boost of 0.2 bar is required for the combustion. Below this value, the heat released cannot make the combustion self-sustaining. Experiments were thus conducted with 1.2 and 1.3 bar as intake pressures. The fuel-air equivalence ratio is limited by the turbocharger performance. Below $\phi = 0.38$, the compressor cannot provide an intake pressure of 1.3 bar due to a lack of turbine power output. Under theses conditions, the combustion efficiency is too low and leads to poor engine performance. The upper limit of the equivalence ratio is determined by the peak cylinder pressure (PCP) and the maximum pressure rise rate (MPRR) associated to ringing phenomenon in HCCI engines. The PCP is here limited to 150 bar while the maximum value for the MPRR is set at 15 bar/CAD. The evolution of the PCP as a function of equivalence ratio, pressure and temperature can be seen in Figure 3.1, where values correspond to the cylinder with the highest PCP in order to be as restrictive as possible. Although its peak value increases with the intake parameters, the PCP stays below the upper limit of 150 bar. However, Figure 3.2 shows that a MPRR of nearly 15 bar/CAD is obtained at $\phi = 0.46$. The influence of the fuel-air equivalence ratio has therefore been studied between 0.38 and 0.46. The use of EGR could allow to work at higher ϕ by damping the pressure curve and thus reducing the MPRR. This should extend the operating range of the engine as it will be discussed in Section 3.4.

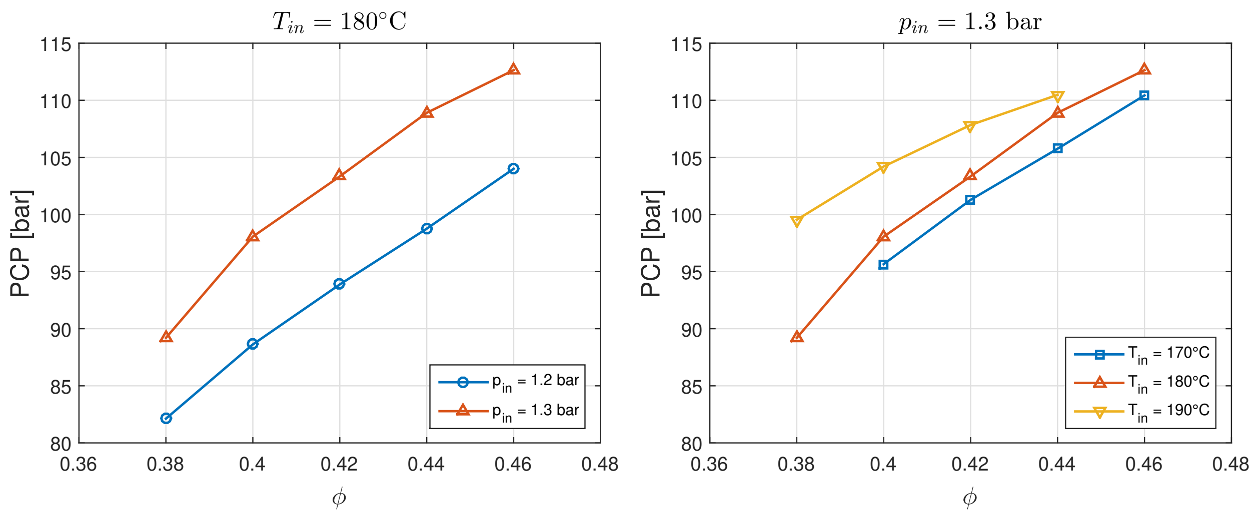

(a) For intake pressures of 1.2 and 1.3 bar at $T_{in} = 180°C$.

(b) For temperatures of 170, 180 and 190°C at $p_{in} = 1.3$ bar.

Figure 3.1: Peak cylinder pressure as a function of the fuel-air equivalence ratio.

3.2 Experimental study of the VGT

The turbocharger has been selected without precisely knowing its technical characteristics [28]. Therefore, a variable geometry turbocharger (VGT) was preferred to a fixed geometry turbocharger in order to extend its operating range. High turbine isentropic efficiencies could thus be achievable for a broader range of mass flow. Furthermore, the flexibility offered by the VGT allows to work at different intake pressures for same fuel-air equivalence ratio and intake temperature.

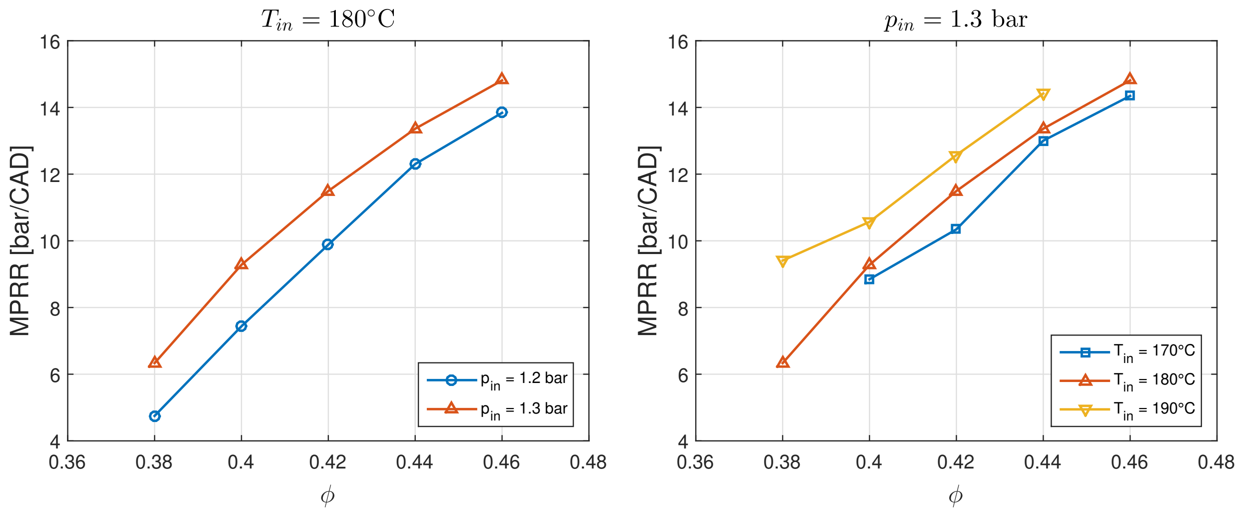

(a) For intake pressures of 1.2 and 1.3 bar at $T_{in} = 180°C$.

(b) For temperatures of 170, 180 and 190°C at $p_{in} = 1.3$ bar.

Figure 3.2: Maximum pressure rise rate as a function of the fuel-air equivalence ratio.

The global characteristics of the VGT have been determined experimentally, especially the intake and exhaust pressures of the engine. The mechanism that controls the effective turbine wheel inlet area can be divided into 20 positions. As it was explained in Section 2.2.6, the position 0 corresponds to the fully opened configuration of the turbine (highest inlet area) while the position 20 corresponds to the fully closed one (lowest inlet area). For greater accuracy, intermediate positions have also been tested. According to Figure 3.3, the intake pressure curve in motoring conditions reaches its maximum, 1.02 bar, around position 17.5 at an intake temperature of 180°C. At 190°C, the pressure curve follows the same trend despite being slightly lower than the case at 180°C. The presence of pressures below 1 bar is due to very low exhaust energy and pressure losses through the intake system.

With combustion, the exhaust enthalpy is naturally higher and provides through the turbocharger a greater intake pressure. At $\phi = 0.42$ and $T_{in} = 180°C$, a pressure of 1.33 bar can be reached at the intake. However, the optimal operating point lies near position 16.5 instead of 17.5. It has been found out that the optimal point slightly moves to the left as the fuel-air equivalence ratio increases. This corresponds to an increase of the turbine power output and thus the mass flow, as more air is sucked by the compressor. Therefore, the cross-sectional area must increase to stay at its optimum value in order to maintain a subsonic flow in the turbine and avoid high pumping losses. Finally, it can be noticed that below position 15, at $\phi = 0.42$, the boost pressure was not sufficient anymore to sustain the combustion.

Figure 3.4 depicts the evolution of the exhaust pressure as a function of the VGT position. The motoring curves at 180 and 190°C are very close to the combustion curve between positions 18 and 20, when the VGT is in closed configuration. Such high values of exhaust pressure - nearly 2.6 bar - are due to the back-pressure created by the turbine. Furthermore, the back-pressure is even greater in an HCCI engine due to its lean mixture and characteristic cold combustion. Regarding Eq. (1.14), (1.15) and (1.16), a lower exhaust temperature means that a higher exhaust pressure will be needed to obtain the same power output, and hence the same compressor boost pressure.

When the effective turbine wheel inlet area increases too much, the exhaust pressure drops sharply because the turbine power output vanishes. The consequence of that is a decrease of the compressor input power, resulting in a lower boost pressure as was discussed in Figure 3.3. Because the back-pressure increases faster than the intake pressure, the pumping losses will always be positive and lower the net indicated efficiency. In conclusion, position 17.5 will only be used in motoring conditions for engine starting while positions between 15 and 17 will be used with combustion in order to effectively control the intake pressure between 1.2 and 1.3 bar.

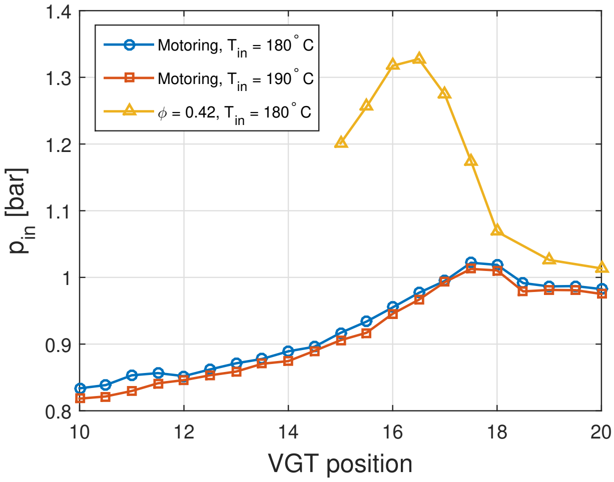

Figure 3.3: Intake pressure as a function of VGT position and intake temperature in motoring and combustion conditions.

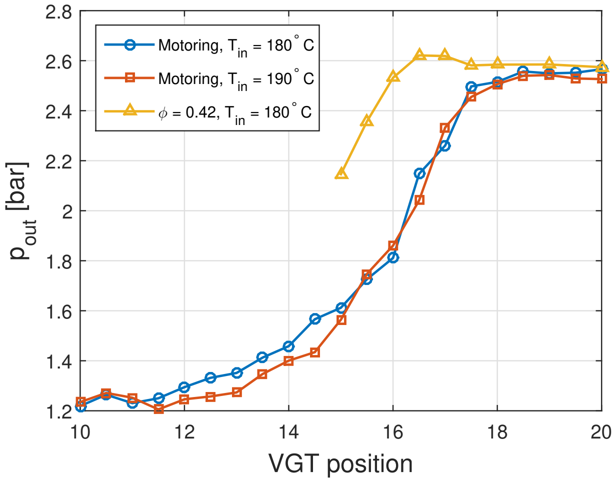

Figure 3.4: Exhaust pressure as a function of VGT position and intake temperature in motoring and combustion conditions.

At the optimal operating point, the compressor isentropic efficiency is equal to 70%, which is a common value for such applications. The computation of the turbine isentropic efficiency requires knowledge of inlet and outlet temperatures of the turbine. Because no sensors were implemented at the turbine inlet, the temperature is estimated from the average exhaust temperature of the cylinders. Without correction, a turbine isentropic efficiency of 68% is found. Instead, by considering a thermal loss of 10 degrees between the engine exhaust and the turbine inlet, the isentropic efficiency falls to 61%. This gives a more realistic value of the turbine performance. The last thing concerns the mechanical efficiency of the turbocharger which is only equal to 73%. Actually, there is no particular reason to justify such a low efficiency. However, this value could explain the relatively weak boost pressure, despite of high residual energy content at the engine exhaust.

Given the particular configuration of the test bench, reviewed in Section 2.2.3, the compressor is located after the electric heater. Therefore, the outlet temperature of the compressor must be high enough to provide the required intake temperature to the engine. The compressor inlet temperature is controlled by the electric heater and is determined by the temperature gain through the compressor, which is directly related to the power of the turbine. In such a configuration, the temperature ratio of the compressor is low. Given the isentropic relation, the pressure ratio will also be relatively low. In the other case where the compressor would be located before the heater, a higher boost pressure could be achievable. The compressor inlet temperature would be equal to the ambient temperature while the compressor outlet temperature would be known thanks to the turbine power output. In this configuration, for identical exhaust conditions, the temperature ratio across the compressor would be higher, as well as the pressure ratio.

3.3 Influence of intake parameters

This section describes the experimental investigations carried out regarding the influence of the intake parameters, p_{in}, T_{in} and ϕ, on the engine performance from fuel energy content to mechanical work expressed as MEPs (see Figure 1.1). While studying the influence of p_{in}, T_{in} is set to 180°C, whereas p_{in} is held constant at 1.3 bar when exploring the sensitivity to T_{in}. Experiments were conducted without EGR at a constant coolant temperature of 90°C. Results are obtained from the average of a sample of four consecutive tests at intervals of 15 seconds, where each sample contains 50 thermodynamic cycles. As shall be seen in Section 3.6, results may differ a lot between cylinder 1 and other cylinders. Therefore, average values of the four cylinders are used only when cylinder 1 shows variations of less than 5% in comparison with the average performance.

3.3.1 Fuel energy content

The FuelMEP represents the chemical energy of the fuel and is thus directly related to the fuel flow. Since the volumetric flow of natural gas is negligible when compared to the total volumetric flow rate ($\dot{V}_{NG} = \frac{\phi}{8.845+\phi}\dot{V}$), the air flow can be assumed to be constant at same p_{in} and T_{in}. Therefore, the mass of fuel and the resulting FuelMEP are directly proportional to the equivalence ratio as seen in Figure 3.5. Higher intake pressures lead to an increase of the charge density and provide thus a higher fuel quantity at constant ϕ. The FuelMEP also decreases with T_{in} since temperature has the opposite effect of pressure by decreasing the air intake density.

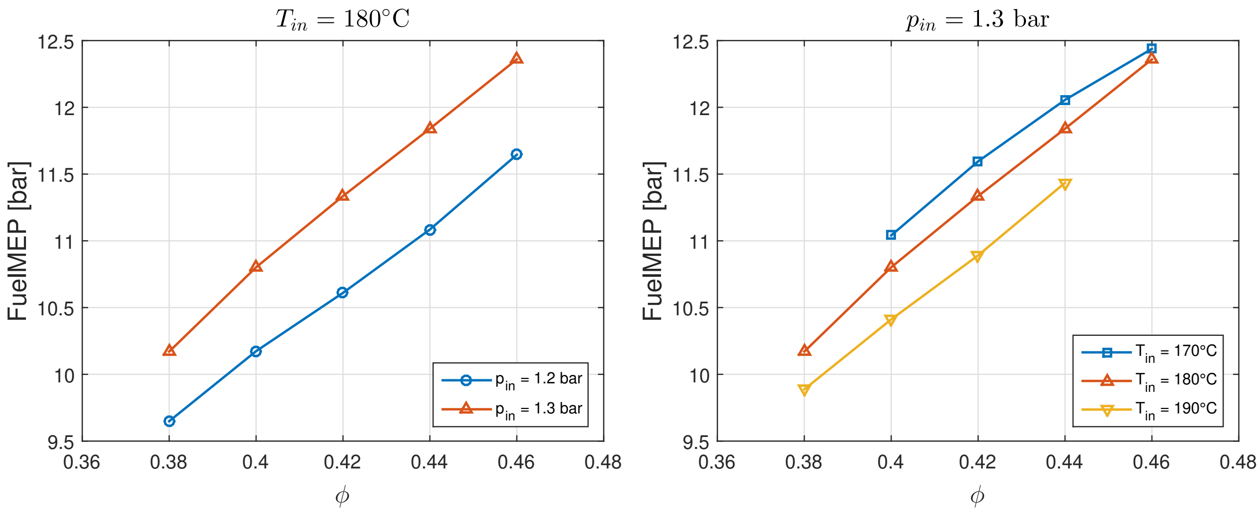

(a) For intake pressures of 1.2 and 1.3 bar. (b) For intake temperatures of 170, 180 and 190°C.

Figure 3.5: FuelMEP as a function of the fuel-air equivalence ratio.

Figure 3.6 displays the FuelMEP against the MPRR. It can be seen that at constant MPRR, a higher intake pressure allows a higher FuelMEP. It means that working under high pressures allows to increase the fuel energy content, hence the mechanical work, while avoiding ringing phenomenon.

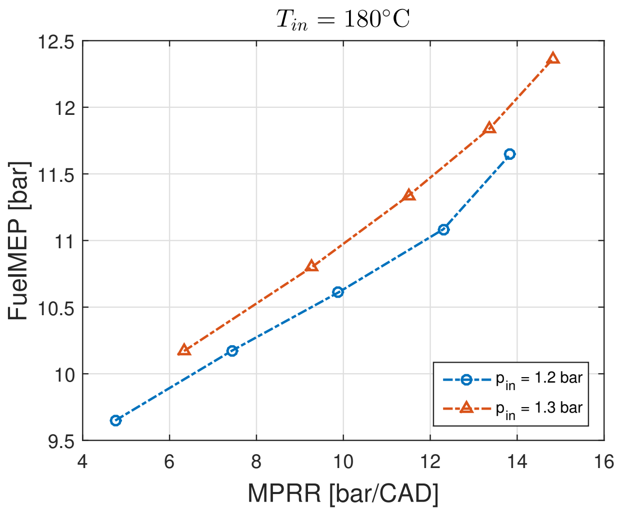

Figure 3.6: FuelMEP as a function of the MPRR with intake pressures of 1.2 and 1.3 bar.

3.3.2 Combustion efficiency

The combustion efficiency, η_c, is the efficiency in converting the fuel energy content, FuelMEP, into heat release, QhrMEP. The computation of η_c has been quite difficult due to a misalignment in the crank angle rotary encoder. Consequences of this will be detailed in the uncertainty analysis in Section 3.7.3. However, general trends can be observed in Figure 3.7. The combustion efficiency increases with ϕ and p_{in} for the reasons discussed above. Both parameters increase the fuel quantity and therefore the heat released by the combustion. As the cylinder temperature increases, this results in a higher combustion efficiency as explained is Section 1.2.1. The intake temperature is the parameter having the most significant influence on the combustion. Despite lowering the fuel quantity at constant ϕ and p_{in}, an increase in T_{in} triggers an earlier auto-ignition, resulting in higher peak cylinder temperature (PCT) and improved combustion efficiency.

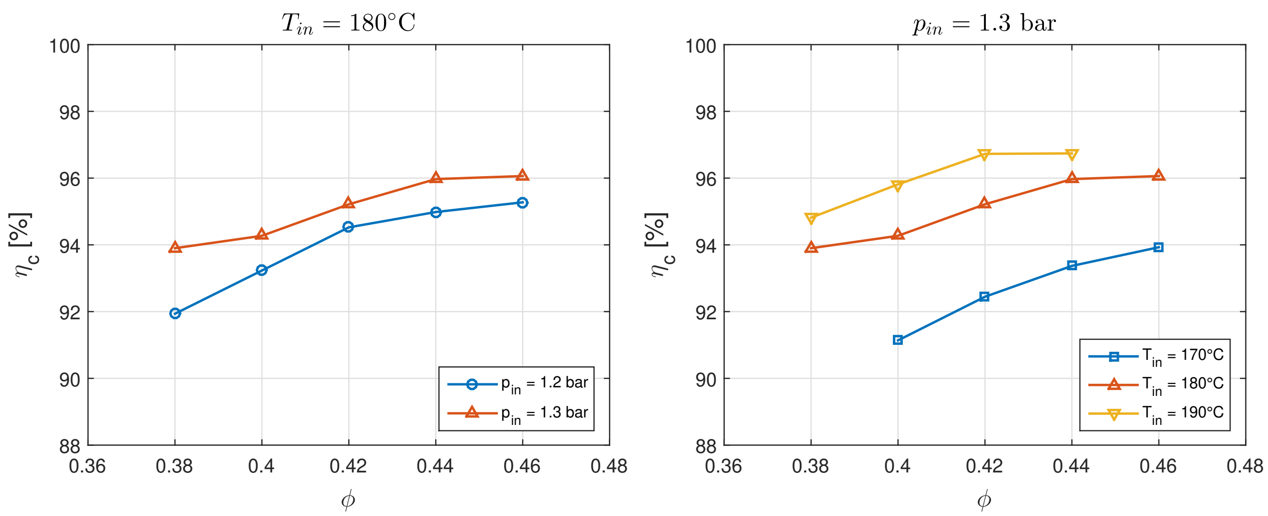

(a) For different intake pressures.

(b) For different intake temperatures.

Figure 3.7: Combustion efficiency as a function of the fuel-air equivalence ratio.

3.3.3 Combustion timing

After having characterized the completeness of the combustion, i.e. the combustion efficiency, the timing of the heat release must be analysed. In HCCI engines, the combustion timing highly depends on intake parameters and plays an essential role in the thermodynamic efficiency. If the auto-ignition occurs before the TDC, the combination of combustion and compression effects leads to higher PCP and PCT, hence higher combustion efficiency, but an increase of the compression work is observed as hot burned gases and piston motion are acting in the opposite direction. However, if the combustion occurs too late after the TDC, the cylinder pressure is lower and provides less expansion work.

The parameters CA10, CA50 and CA90 correspond to the crank angle positions where 10, 50 and 90% of the combustion heat has been released. Further, the CA_{90-10} is called the burn duration and is the absolute difference between the CA90 and CA10, considered respectively as the end and start of the combustion. The evolution of CA10, CA50 and CA_{90-10} are plotted as functions of the intake parameters in Figures 3.8, 3.9 and 3.10. Global trends are very clear as they all decrease when p_{in}, T_{in} or ϕ increases. Highest combustion efficiency is thus achieved at lowest CA50.

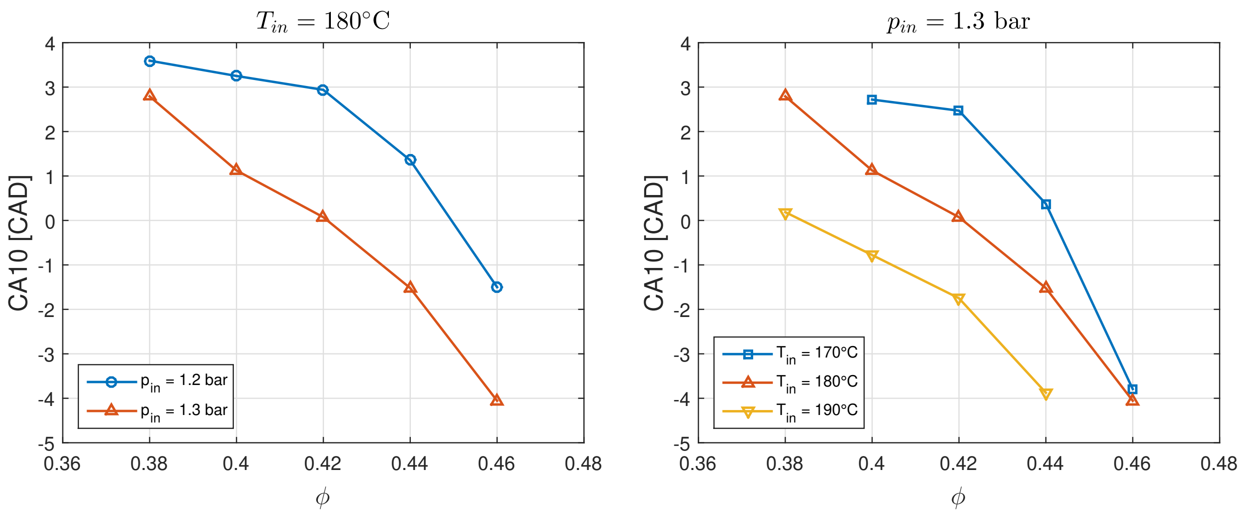

(a) For different intake pressures.

(b) For different intake temperatures.

Figure 3.8: CA10 as a function of the fuel-air equivalence ratio.

As mentioned above, the intake temperature drastically affects the combustion timing. By advancing the auto-ignition, the combustion is then accelerated by the compression of the piston, resulting in very short burn durations and advanced CA50. This earlier auto-ignition results in an increase of the MPRR as shown in Figure 3.2b. The rate of heat release (RoHR) curve displayed in Figure 3.11 can also be used to explain these results. As the fuel-air equivalence ratio increases, the heat release extends over less degrees but becomes more intense. Therefore, an increase of the fuel quantity, leading to higher cylinder temperatures, results in an earlier and shorter combustion.

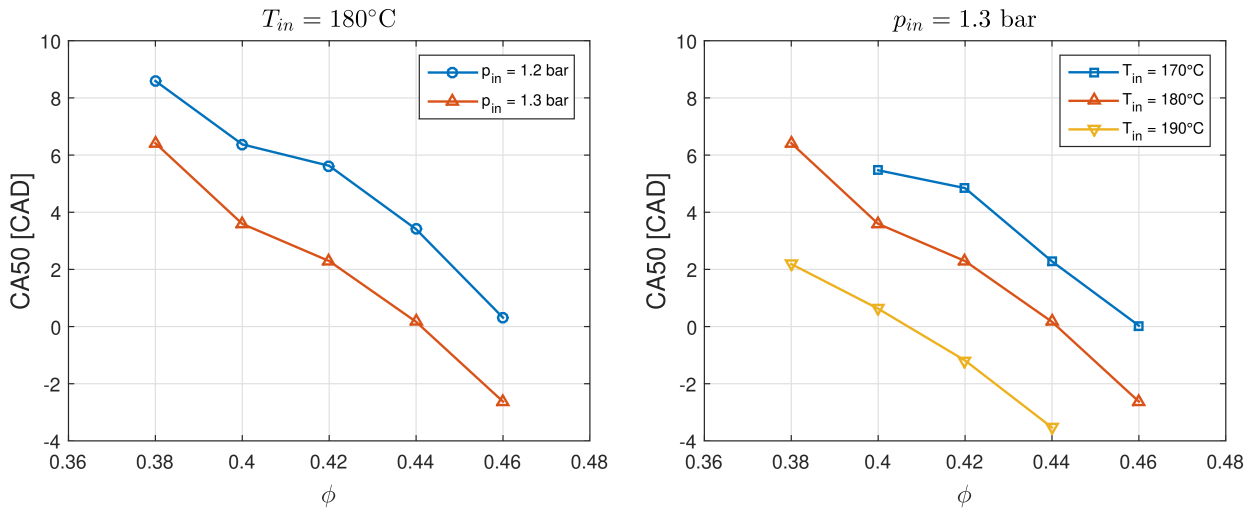

(a) For different intake pressures.

(b) For different intake temperatures.

Figure 3.9: CA50 as a function of the fuel-air equivalence ratio.

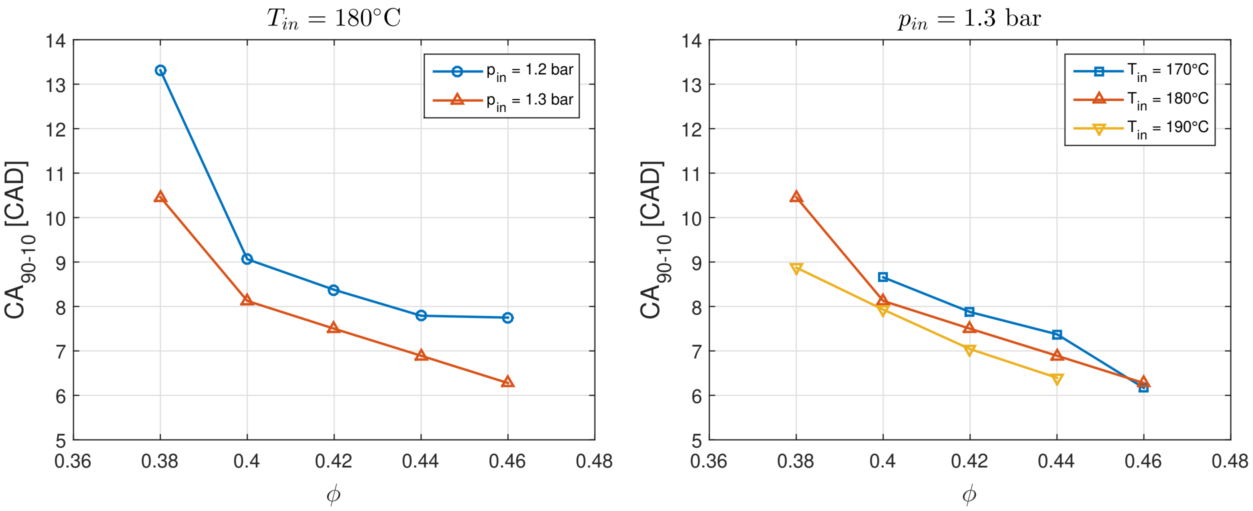

(a) For different intake pressures.

(b) For different intake temperatures.

Figure 3.10: Burn duration as a function of the fuel-air equivalence ratio.

3.3.4 Thermodynamic efficiency

The thermodynamic efficiency, η_{ti}, indicates the efficiency of the engine in converting the heat released by the combustion, QhrMEP, into cyclic work, IMEPg. Losses through this conversion include heat transfer losses, QhtMEP, and exhaust losses, QexhMEP.

Heat transfer losses are proportional to the temperature difference between the wall and the in-cylinder hot gases. As shown in Figure 3.12, the heat loss increases with the equivalence ratio but only by 10% between $\phi = 0.38$ and $\phi = 0.42$, while the gross heat release increased in the same time by 15% because a higher amount of fuel comes with a higher combustion efficiency as presented in Figure 3.7.

As the net heat release increases with the fuel quantity, the relative heat transfer losses, ε_{ht}, must decrease

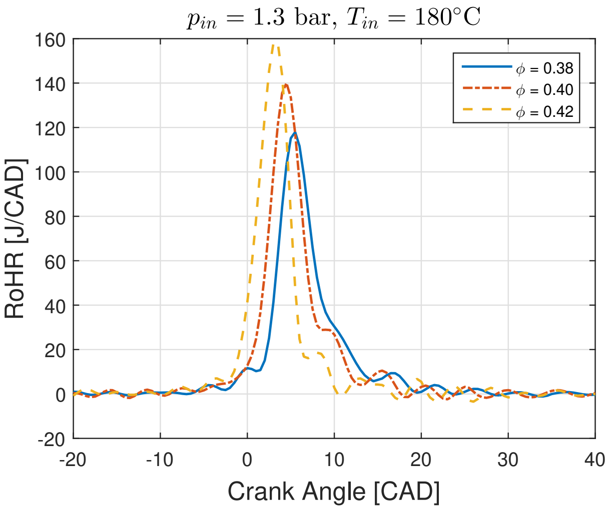

Figure 3.11: Rate of heat release as a function of the fuel-air equivalence ratio.

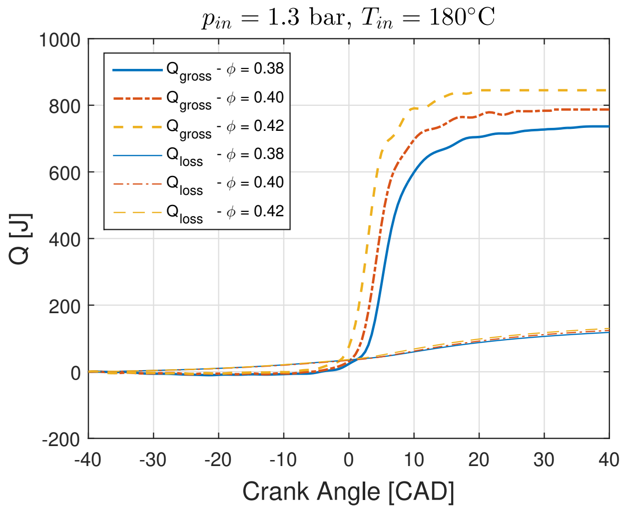

Figure 3.12: Gross heat release and in-cylinder heat loss as functions of the fuel-air equivalence ratio.

with ϕ as observed in Figure 3.13. It can also be seen that ε_{ht} decreases with p_{in} and increases with T_{in}. Higher pressures provide more fuel and air at constant ϕ which reduces even more the heat transfer losses. A higher T_{in} contributes to increase the in-cylinder temperature, hence increasing heat losses.

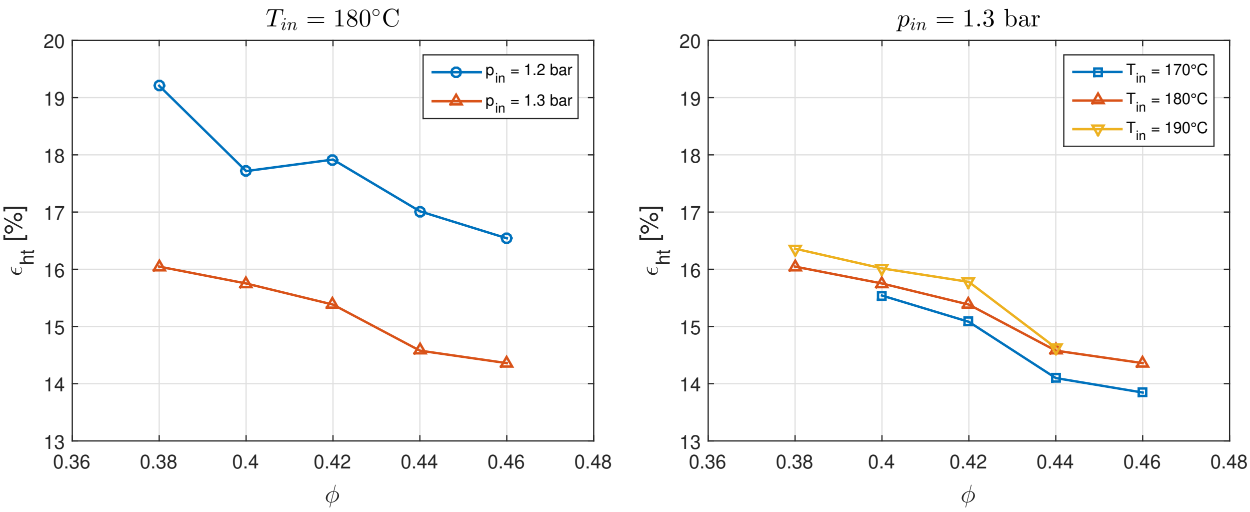

(a) For different intake pressures.

(b) For different intake temperatures.

Figure 3.13: Relative heat transfer losses as a function of the fuel-air equivalence ratio.

Figure 3.14 depicts the evolution of the relative exhaust losses, ε_{exh} which are directly linked to the exhaust temperature of the engine. The growing trend of ε_{exh} with ϕ and p_{in} is because higher exhaust temperatures are achieved when the fuel quantity increases. The same logic applies for the intake temperature.

Finally, the thermodynamic efficiency is given in Figure 3.15. The first observation is that η_{ti} decreases with the intake temperature as both ε_{ht} and ε_{exh} increase with T_{in}. In contrast, higher pressures contribute to an increase of η_{ti} as the expansion work is higher with increased charge density. The influence of the equivalence ratio is more subtle as no clear trend can be observed directly. However, an optimum point can almost be detected on each curve, meaning that there is a true correlation between the thermodynamic efficiency and the CA50. This will be discussed in further details in Section 3.3.5.

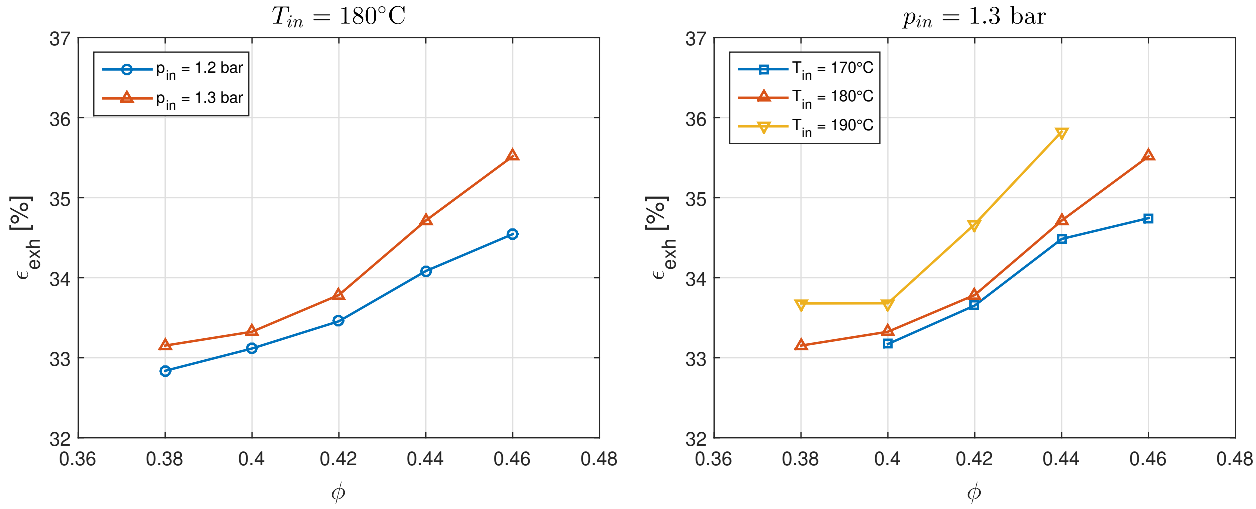

(a) For different intake pressures.

(b) For different intake temperatures.

Figure 3.14: Relative exhaust losses as a function of the fuel-air equivalence ratio.

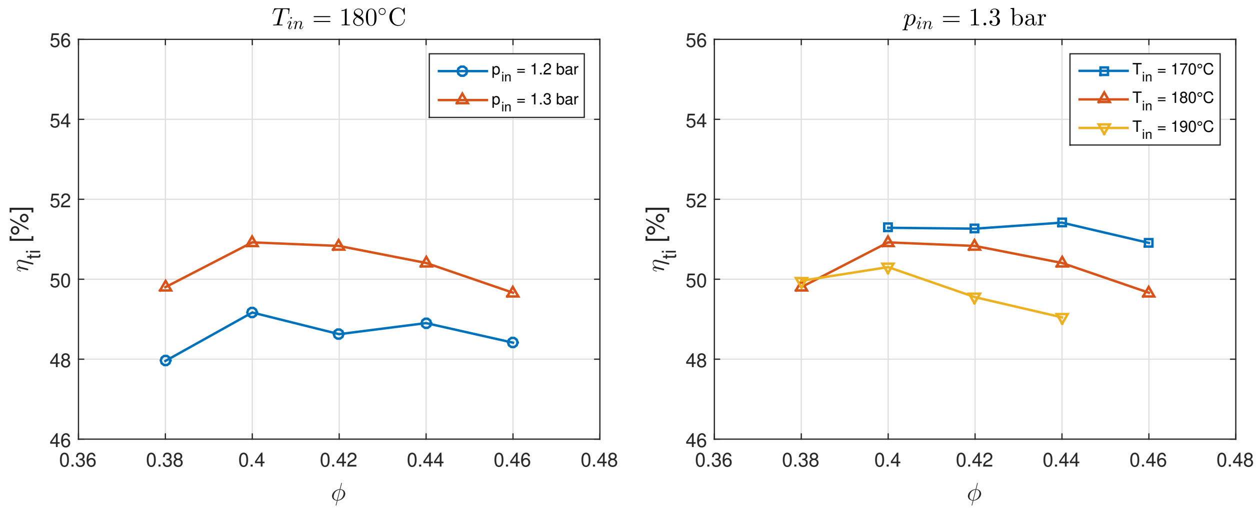

(a) For different intake pressures.

(b) For different intake temperatures.

Figure 3.15: Thermodynamic efficiency as a function of the fuel-air equivalence ratio.

3.3.5 Indicated efficiency

The indicated efficiency, which refers here to the gross indicated efficiency η_{ig}, represents the efficiency of the engine in converting the fuel energy content, FuelMEP, into cyclic work, IMEPg. This way, η_{ig} includes both combustion and thermodynamic efficiencies.

In Figure 3.16, the IMPEg seems to be proportional to the amount of fuel. Increasing p_{in} and decreasing T_{in} at constant ϕ provide higher FuelMEP resulting in an increase of the IMEPg. The advantage of increasing p_{in} rather than ϕ to obtain higher IMEPg is that pressure boosting allows lower MPRR at constant FuelMEP as seen in Figure 3.6. Particular attention should be drawn to Figure 3.16b as the curves at 170 and 180°C intersect at $\phi = 0.42$. In fact, lower temperature curves have a higher rate of increase in the IMEPg, confirming the strong influence of the CA50. The IMPEg is both impacted by the charge density, which is always better at lower temperatures, and the optimum combustion phasing, which depends on the intake parameters as discussed in Section 3.3.3.

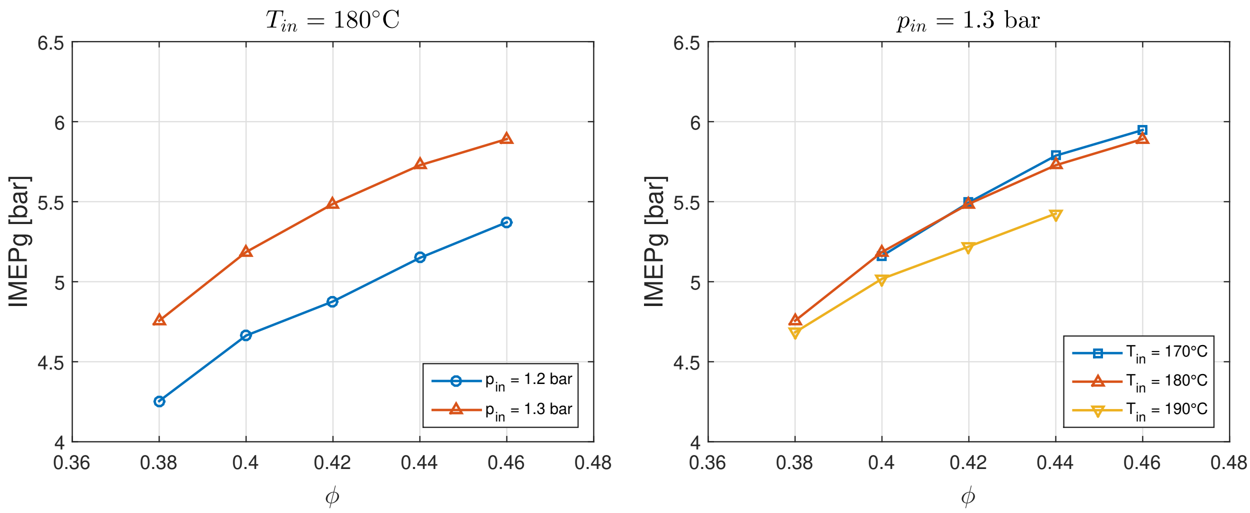

(a) For different intake pressures.

(b) For different intake temperatures.

Figure 3.16: IMEPg as a function of the fuel-air equivalence ratio.

A solution to isolate the effects of the combustion timing is to use the FuelMEP as the x-axis parameter instead of ϕ. Figure 3.17 confirms the influence of the CA50 and shows that higher IMEPg is obtained with $T_{in} = 170°C$ at higher FuelMEP while $T_{in} = 190°C$ is better at lower FuelMEP. However, highest IMEPg will always by achieved at lower temperatures. Therefore, T_{in} should be as low as possible while maintaining a decent combustion efficiency.

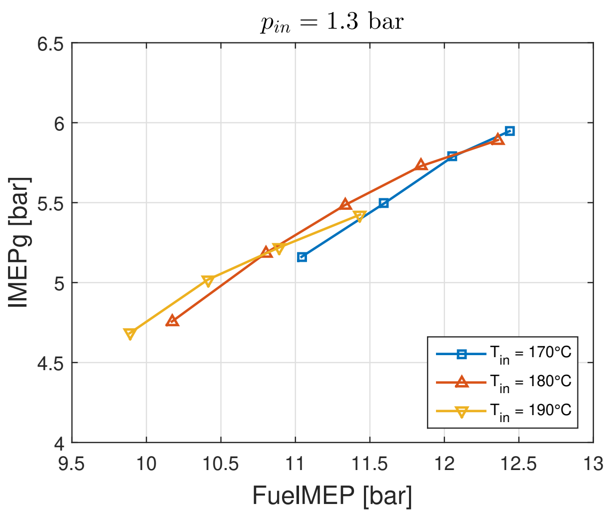

Figure 3.17: IMEPg as a function of the FuelMEP with temperatures of 170, 180 and 190°C at $p_{in} = 1.3$ bar.

The gross indicated efficiency is shown in Figure 3.18. Since both η_c and η_{ti} increase with p_{in}, the pressure dependence is quite clear. The temperature case is more difficult to analyse because η_c and η_{ti} evolve with opposite trends. However, an optimum can now be clearly seen on each efficiency curve.

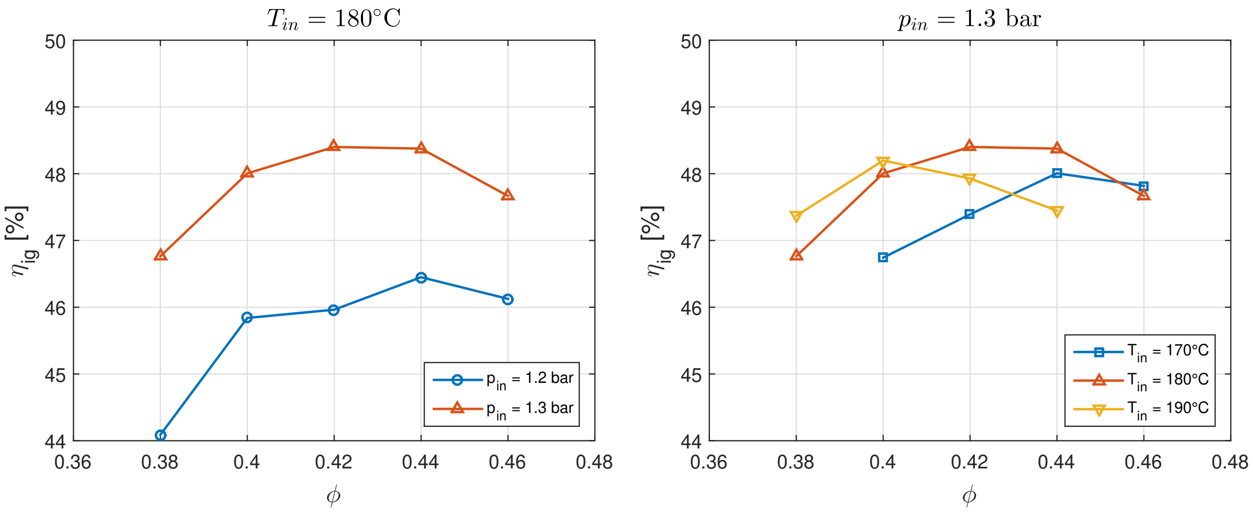

(a) For different intake pressures.

(b) For different intake temperatures.

Figure 3.18: Gross indicated efficiency as a function of the fuel-air equivalence ratio.

To better understand the influence of the combustion timing, the indicated efficiency has been displayed against the CA50 in Figure 3.19. Whatever the p_{in}-T_{in} couple, the graph indicates that the CA50 where maximum η_{ig} is achieved lies around 2 CAD after the TDC. This is a strong result as it gives the combustion phasing that ensures optimum engine performance.

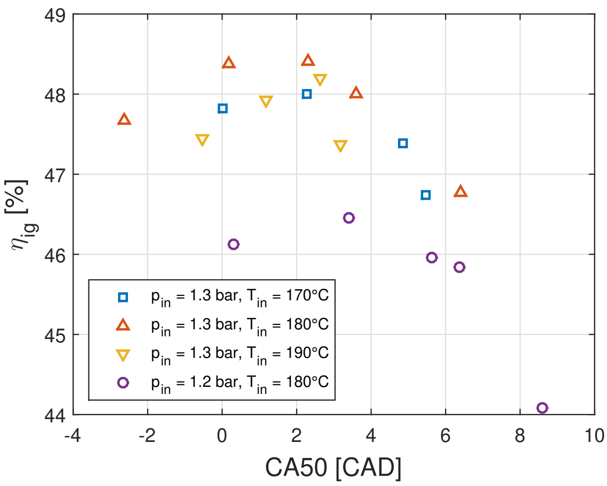

Figure 3.19: Gross indicated efficiency as a function of the CA50 for various operating conditions.

After having studied the IMEPg, it might be relevant to take into account the pumping losses occurring at the exhaust. The PMEP is exposed in Figure 3.20 and can be expressed as the difference between the exhaust and intake pressures. High values of PMEP (up to 1.5 bar) are characteristic of HCCI engines due to their low exhaust temperature, as discussed in Section 3.2. Therefore, the PMEP should slightly decrease with ϕ since higher equivalence ratios provide higher exhaust temperatures. Figure 3.20a confirms that the back-pressure rises faster than the intake pressure, leading therefore to an increase of the pumping losses with p_{in}. Finally, an increase in T_{in} lowers the intake charge density and therefore requires a higher compressor work for same boost pressure, giving then a higher PMEP.

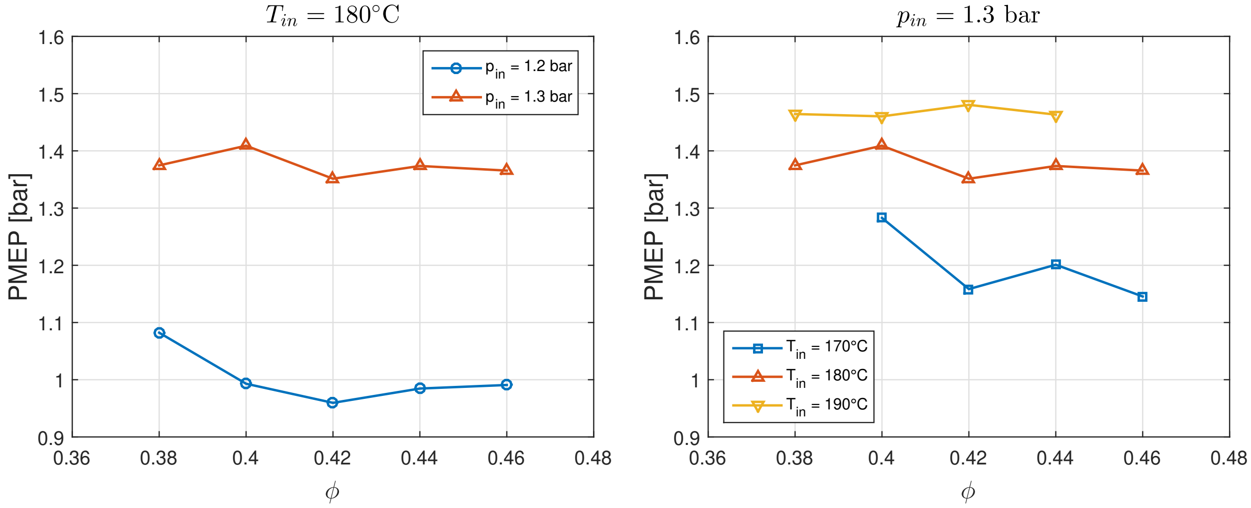

(a) For different intake pressures. (b) For different intake temperatures.

Figure 3.20: PMEP as a function of the fuel-air equivalence ratio.

The IMEPn results from the difference between the IMEPg and the PMEP. Figure 3.21 shows that the increase in the IMEPn with p_{in} has been attenuated by the pumping losses. Also, the dependence in temperature is now more visible for this range of ϕ as the IMEPn clearly increases at lower T_{in}.

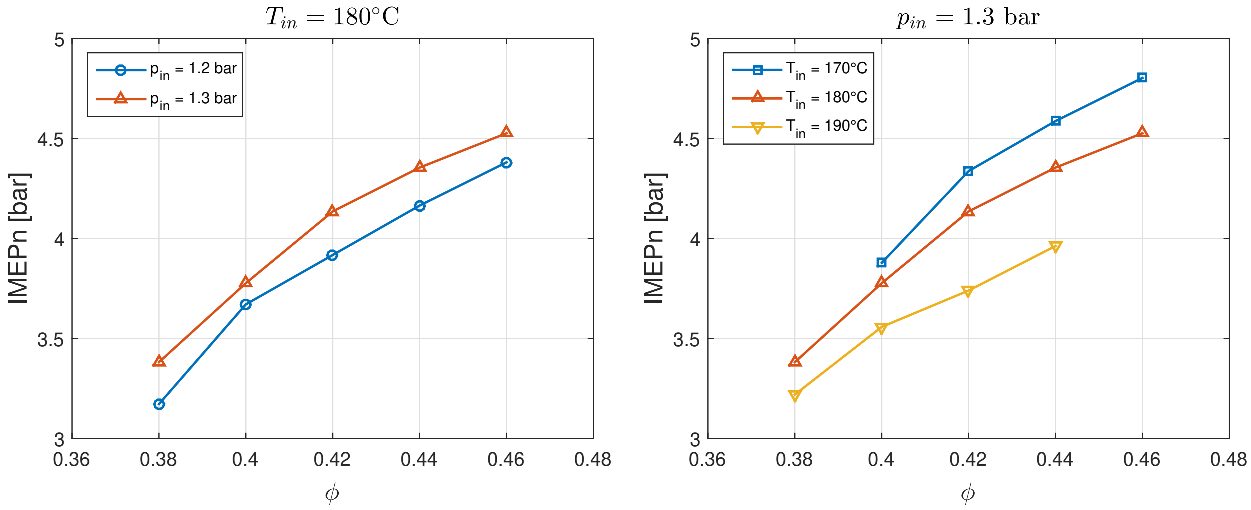

(a) For different intake pressures. (b) For different intake temperatures.

Figure 3.21: IMEPn as a function of the fuel-air equivalence ratio.

3.3.6 Brake efficiency

Arriving at the end of the energy conversion chart presented in Figure 1.1, the brake efficiency η_b indicates the efficiency of the engine in converting the fuel energy content, FuelMEP, into mechanical work, BMEP. The BMEP is directly computed from the difference between the IMEPn and the FMEP which represents the friction losses through the system.

Following the Chen-Flynn model [7], $\text{FMEP} = A + B\ p_{max} + C\ N + D\ N^2$, the FMEP should not vary too much since the engine is running at constant rotational speed and the PCP does not increase a lot with the intake parameters (see Figure 3.1). This trend is verified in Figure 3.22 as the maximum increase is only about 0.2 bar.

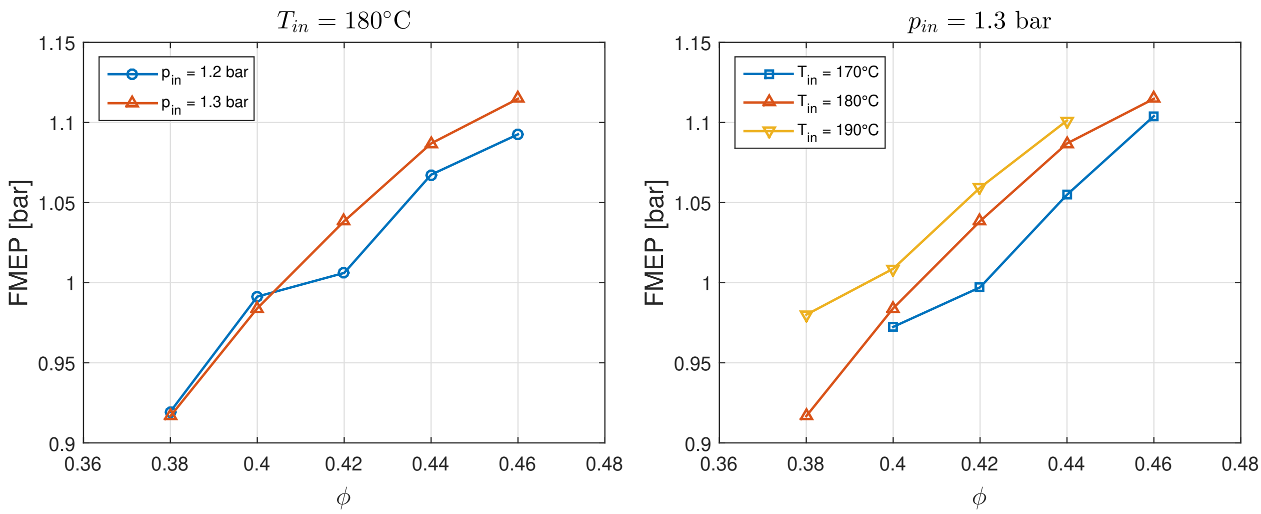

(a) For different intake pressures.

(b) For different intake temperatures.

Figure 3.22: FMEP as a function of the fuel-air equivalence ratio.

Consequently, the BMEP curves given in Figure 3.23 are very similar to those of the IMEPn. A maximum BMEP of 3.7 bar is achieved at $p_{in} = 1.3$ bar, $T_{in} = 170$°C and $\phi = 0.46$.

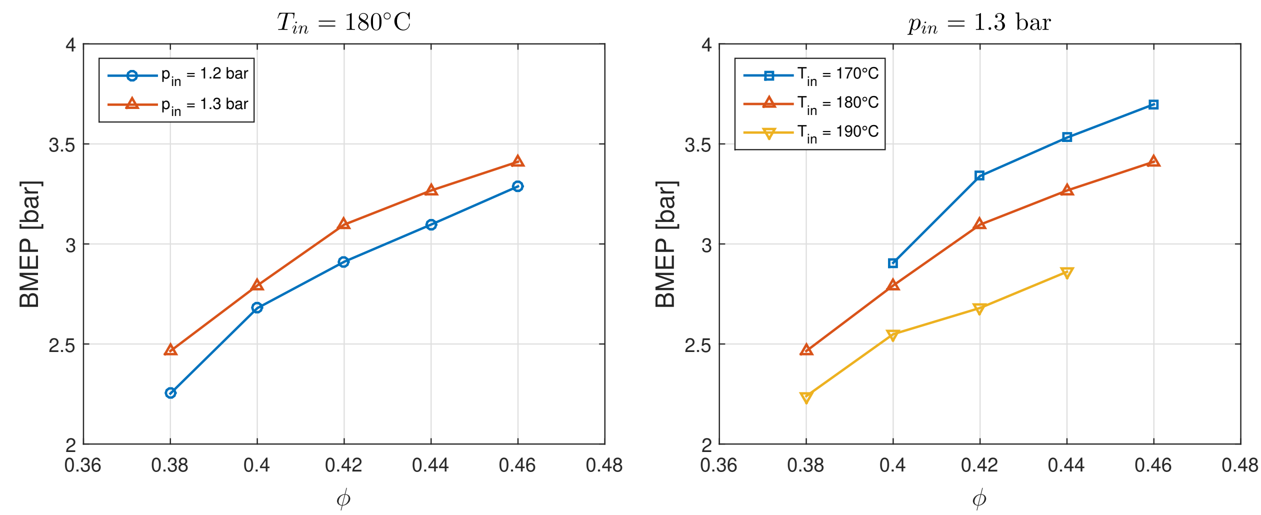

(a) For different intake pressures.

(b) For different intake temperatures.

Figure 3.23: BMEP as a function of the fuel-air equivalence ratio.

Finally, Figure 3.24 shows the brake efficiency as a function of the intake parameters. When compared to the indicated efficiency η_{ig}, the brake efficiency appears to decrease with p_{in} because of the PMEP. Hence, pressure boosting is aimed to increase the BMEP at the expense of η_b. In the same way as for the IMEPn, η_b increases with lower intake temperatures. No more optimum at CA50 = 2 CAD is observed since an increase in the BMEP with ϕ contributes to attenuate the relative weight of the pumping and friction losses. A brake efficiency of nearly 30% is achieved at $p_{in} = 1.3$ bar, $T_{in} = 170°\text{C}$ and $\phi = 0.46$. Although working at high load is always better in terms of engine performance in this range of ϕ, the rate of increase in η_b declines and suggests that a loss of performance could have happened at higher ϕ. In conclusion, the operating range in HCCI combustion is quite limited due to optimum combustion phasing, and the use of EGR therefore seems to be particularly adapted. This part will be discussed in Section 3.4.

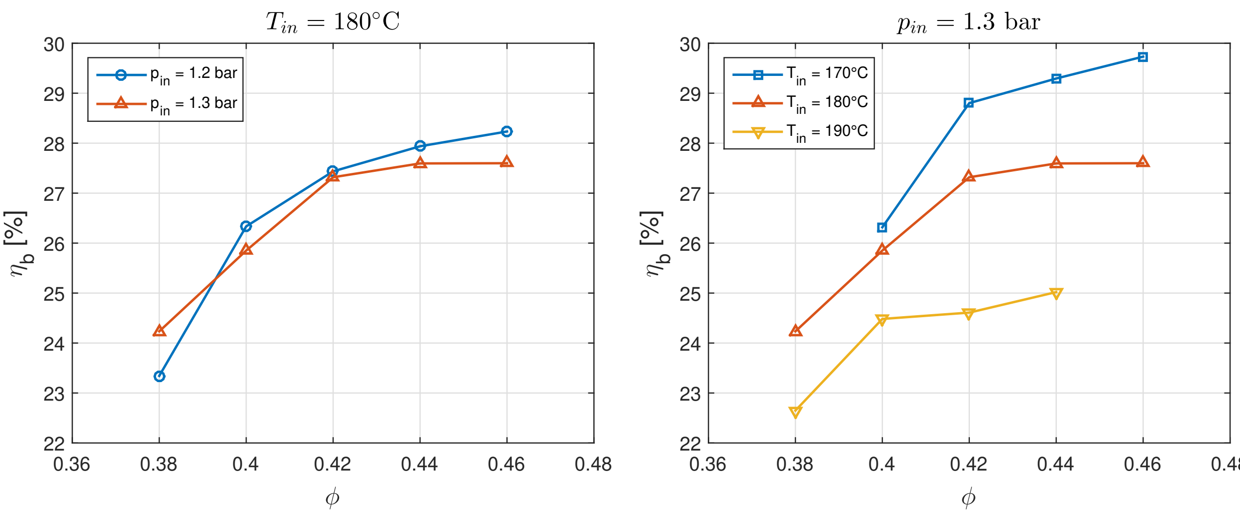

(a) For different intake pressures.

(b) For different intake temperatures.

Figure 3.24: Brake efficiency as a function of the fuel-air equivalence ratio.

3.4 Impact of EGR on engine performance

The goal of this section is to explore the effects of EGR on HCCI combustion. The experiments were carried out in position 16 of the VGT, at $T_{in} = 180°\text{C}$ and for a constant coolant temperature of 90°C. The section first discusses the influence of the use of EGR on intake conditions such as the FuelMEP and the mass flow rates. Thermal effects of EGR are then investigated at constant FuelMEP. Finally, experiments at constant CA50 of 2 CAD are conducted in order to evaluate the effectiveness of EGR as a control method for HCCI combustion.

3.4.1 Evolution of intake conditions with the EGR rate

When adding EGR to the experimental setup, a decrease of the FuelMEP was observed as presented in Figure 3.25. The loss of FuelMEP is about 21% between 0 and 30% EGR. That being said, the hypothesis made in Section 2.2.7 is not entirely correct since the use of EGR does not replace air only but also a small amount of fuel. However, Figure 3.26 shows that this loss of fuel is negligible in comparison with air and EGR mass flows. On this graph, the fuel mass flow has only lost 0.26 g/s while the air mass flow has lost 10.7 g/s with respect to the corrected intake mass flow. In fact, the initial intake flow must be corrected due to a slight decrease of the intake pressure that followed the loss of FuelMEP. Therefore, the hypothesis on the EGR flow computation is perfectly valid.

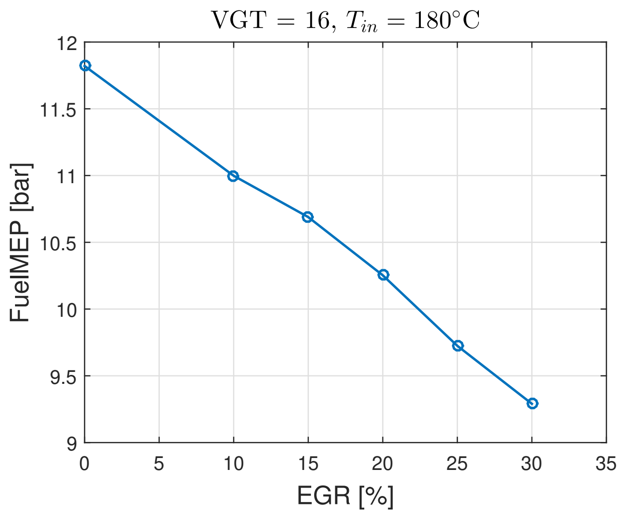

Figure 3.25: FuelMEP as a function of the EGR rate.

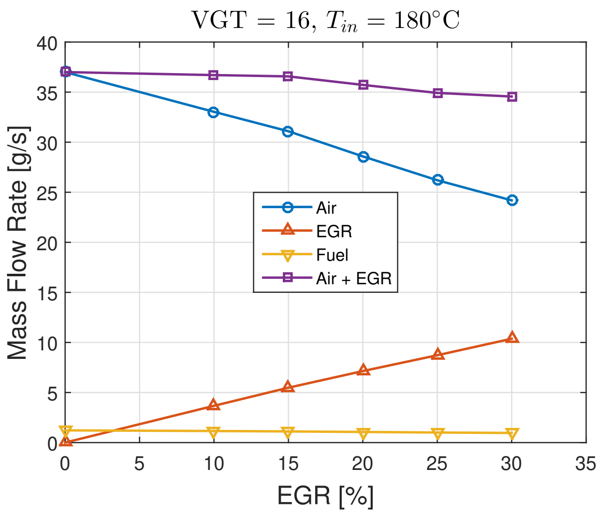

Figure 3.26: Evolution of the mass flow rates with the EGR rate.

3.4.2 Evaluation of the EGR thermal effects at constant FuelMEP

Experimental in-cylinder pressure curves are displayed in Figure 3.27 for various EGR fractions at constant FuelMEP of 12 bar. As the EGR rate increases, the increase of load thermal inertia causes important thermodynamic damping effects by slowing the combustion rate and distributing the heat release over a larger range of CAD. Therefore, the PCP positions are delayed and their magnitudes decrease.

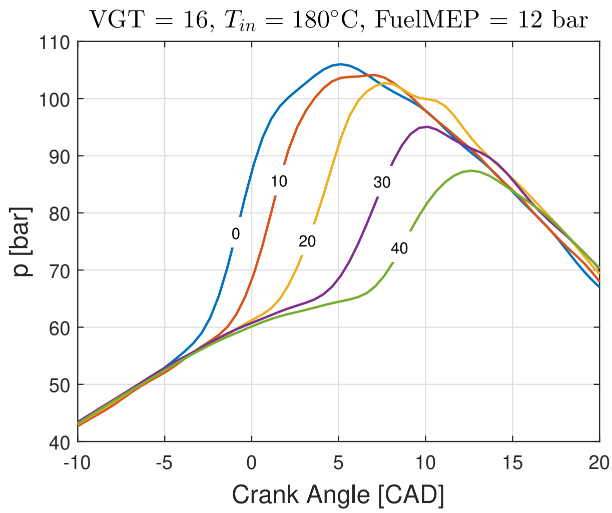

Figure 3.27: Experimental in-cylinder pressure traces at various EGR rates (in %) at FuelMEP = 12 bar.

Figures 3.28 and 3.29 confirm the influence of EGR in combustion phasing. At EGR = 0%, the heat release is completed well before the TDC causing a high MPRR. The use of EGR can effectively increase the CA50 by delaying the auto-ignition, which results in a sharp decrease of the MPRR. As a consequence of that, EGR could be used to increase the operating range of the engine by using higher ϕ while optimizing the CA50 and thus the cyclic work, IMEPg.

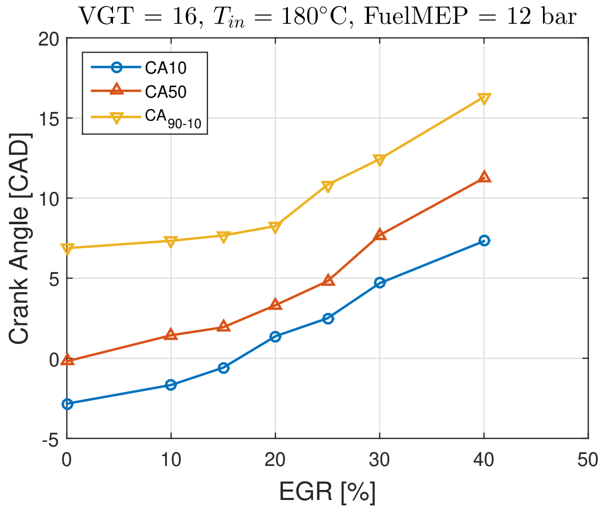

Figure 3.28: CA10, CA50 and burn duration as functions of the EGR rate at FuelMEP = 12 bar.

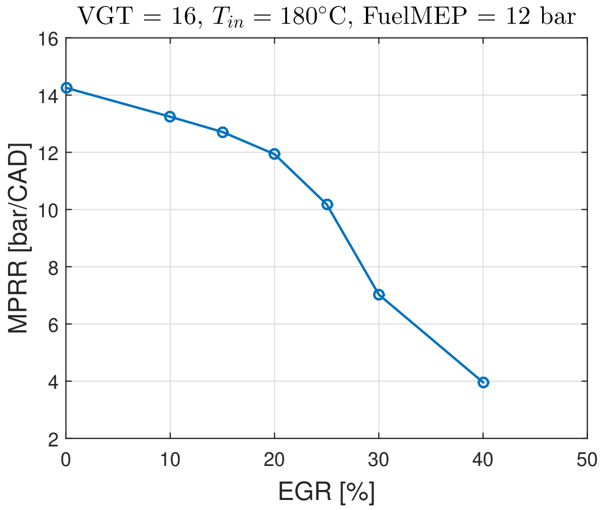

Figure 3.29: MPRR as a function of the EGR rate at FuelMEP = 12 bar.

Experiments also show a sharp decrease in the peak cylinder temperature (PCT) as seen in Figure 3.30. While increasing the EGR rate, the cylinder temperature achieved through the piston compression decreases due to higher heat capacities of the in-cylinder gases, mainly CO_2 and H_2O. This significantly affects the auto-ignition timing and results in a delayed CA50 and a lower PCT. As shown in Figure 3.31, this decrease in the PCT directly influences the combustion efficiency as less residual CO is burned at lower temperatures. However, given the EGR damping effects, higher ϕ values could be used to restore the initial combustion efficiency.

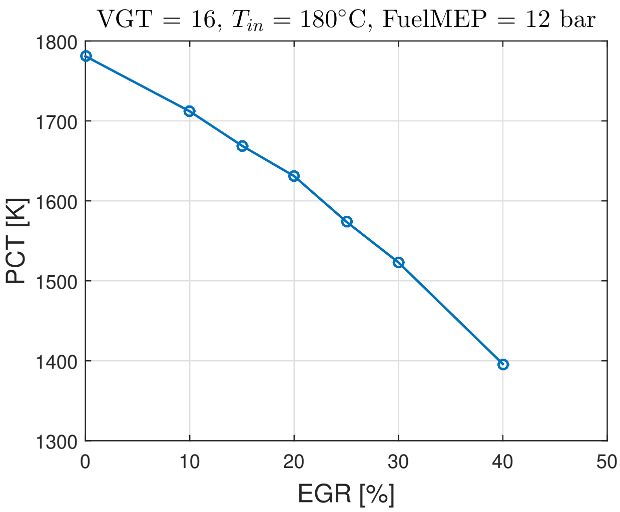

Figure 3.30: Peak cylinder temperature as a function of the EGR rate at FuelMEP = 12 bar.

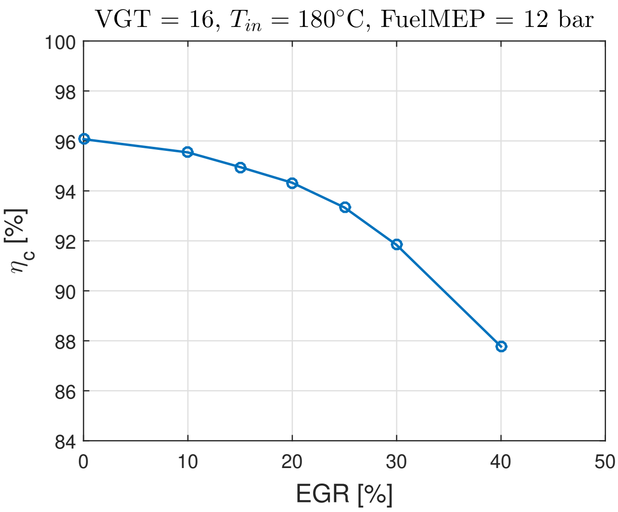

Figure 3.31: Combustion efficiency as a function of the EGR rate at FuelMEP = 12 bar.

3.4.3 EGR as a control method for HCCI combustion

To complete the EGR analysis, experiments at constant CA50 = 2 CAD were carried out to assess the capacity of EGR to control HCCI combustion. When increasing the EGR rate, the engine can work at higher ϕ while maintaining the optimum CA50 due to thermal effects discussed above. The more realistic equivalence ratio ϕ_{EGR} will be used here and has been introduced in Section 2.2.2. The objective of these experiments is to reach the theoretical optimum case where $\phi_{\mathrm{EGR}} = \phi = 1$.

In Figure 3.32, ϕ_{EGR} is plotted against the EGR rate for three different conditions: CA50 = 2 CAD, MPRR = 15 bar/CAD and a theoretical case at FuelMEP = 12 bar. As the EGR increases, the air mass flow decreases and should give an exponential trend to the constant FuelMEP curve. However, Figure 3.33 shows that the intake pressure also increases with the EGR rate and reaches 1.6 bar at EGR = 50%. Because higher EGR rates come with higher IMEPg, a greater exhaust enthalpy at the turbine allows in this case a higher boost pressure through the compressor. The resulting higher intake mass flow attenuates the exponential trend of the constant FuelMEP curve. Therefore, two cumulative effects occur for constant CA50 and MPRR curves as both the EGR and the increasing mass flow allow to work under higher FuelMEP. The only difference is that an increase in EGR gives higher FuelMEP at higher ϕ_{EGR}, hence higher MPRR, while an increase in p_{in} can give higher FuelMEP at constant MPRR (see Figure 3.6).

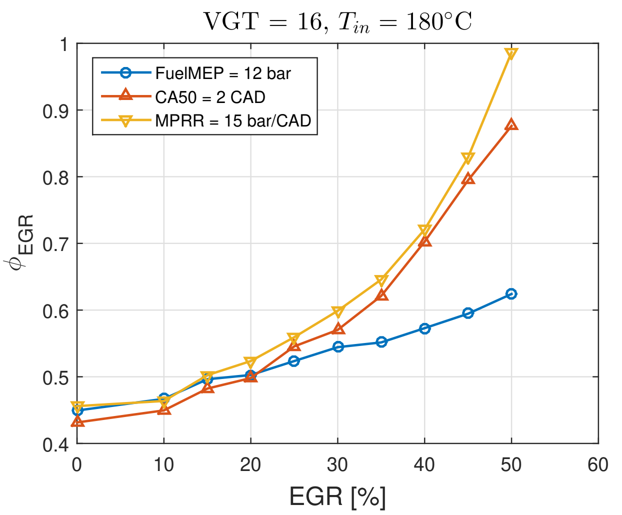

Figure 3.32: ϕ_{EGR} as a function of the EGR rate under various conditions (constant FuelMEP, CA50 and MPRR).

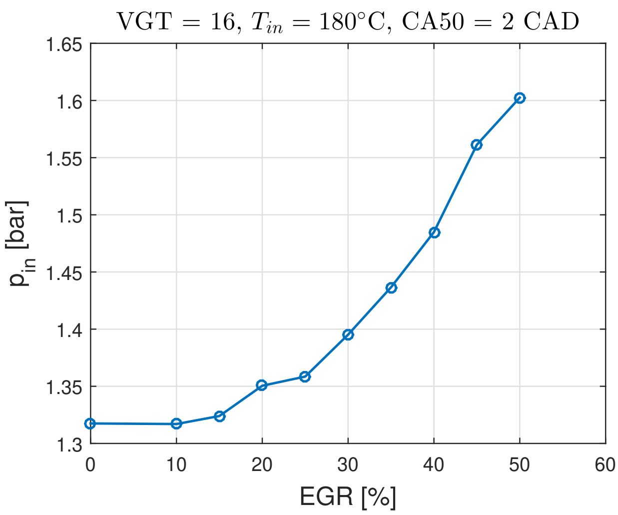

Figure 3.33: Intake pressure as a function of the EGR rate at CA50 = 2 CAD.

At EGR = 50%, ϕ_{EGR} reaches 0.88 at CA50 = 2 CAD while it already attains 0.98 at MPRR = 15 bar/CAD. In view of this, the use of EGR can drastically increase the ringing limited equivalence ratio. Theoretically, ϕ_{EGR} could further increase until 1 at higher EGR rates for the constant CA50 case. However, large variations between consecutive cycles were observed at high EGR rates. Based on the work of Bhaduri [8], the Coefficient of Variation (CoV) in the IMEPg, computed for a sample of n cycles in Eq. 3.1, was used to quantify these cyclic variations.

$$\mathrm{CoV}_{\mathrm{IMEPg}} = 100 \frac{1}{\overline{\mathrm{IMEPg}}} \sqrt{\frac{1}{n} \sum_{i=0}^{n} \left(\mathrm{IMEPg}_i - \overline{\mathrm{IMEPg}}\right)^2} \tag{3.1}$$

An upper limit of 5% in the CoV_{IMEPg} is generally accepted as representing a stable combustion [8]. Experiments with EGR rates beyond 50% showed CoVs higher than 5% even at maximum ϕ_{EGR} corresponding to MPRR = 15 bar/CAD.

Finally, the engine performance is analysed at CA50 = 2 CAD in Figures 3.34 and 3.35. The IMEPg increases from 5.6 bar to a maximum of 7.7 bar at EGR = 50%. The effect of EGR on PMEP is not very pronounced while the FMEP is nearly constant. The resulting BMEP reaches 5 bar at EGR = 50% and has increased by 58% in comparison with the case without EGR. The brake efficiency increases from 27.5% to 31.6% mainly because the PMEP and the FMEP are proportionally less important as the engine load increases.

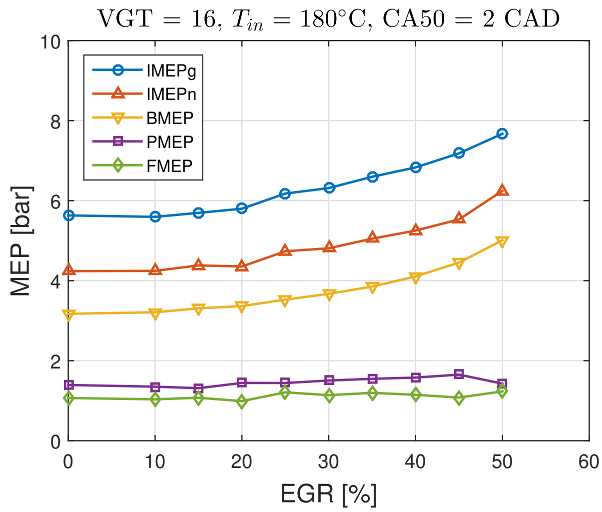

Figure 3.34: Various MEPs as functions of the EGR rate at CA50 = 2 CAD.

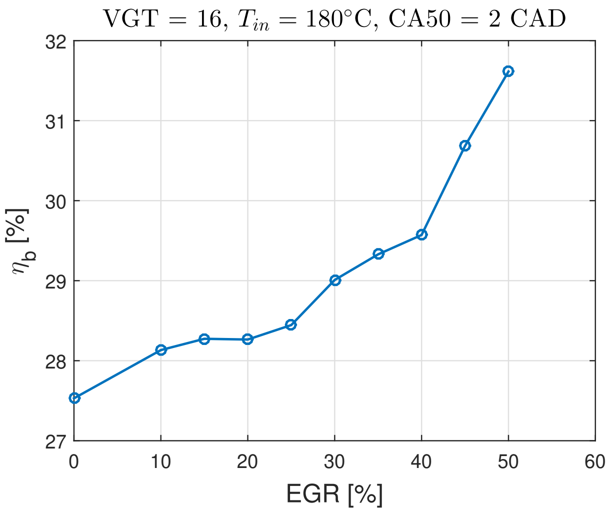

Figure 3.35: Brake efficiency as a function of the EGR rate at CA50 = 2 CAD.

3.4.4 Expected trends with ORC coupling

Although the coupling between an ORC and an HCCI engine running with EGR will be discussed in detail in Section 3.9, some expected trends can already be found out. As discussed previously, the use of EGR can drastically increase the upper limit of the engine operating range, thus allowing to achieve higher performance. However, the drawback is the decrease of the flue gas flow that would be available for the ORC, since a part of the exhaust gases is reintroduced at the engine intake. This effect is observed in Figure 3.36.

The loss of mass flow severely decreases the residual power available for the ORC. On the other hand, the EGR technique allows to use higher fueling rates which increase the exhaust temperature as shown in Figure 3.37. This contributes to an increase of the exhaust energy content and ends up in competition with the loss of mass flow at the exhaust. Therefore, only a slight decrease of the exhaust residual power is observed with the EGR rate in Figure 3.38. At the same time, the engine mechanical power output increases by around 58% with 50% EGR. In this regard, it is worth bearing in mind that higher performance will be achieved at higher EGR rates despite the loss of exhaust mass flow.

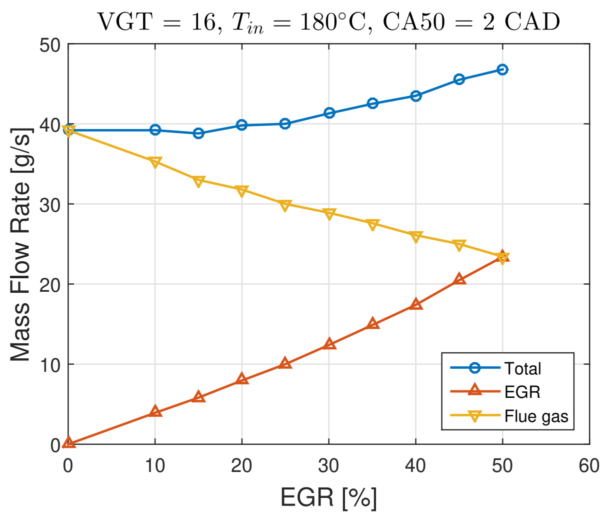

Figure 3.36: Various mass flow rates (total, EGR, flue gas) as functions of the EGR rate at CA50 = 2 CAD.

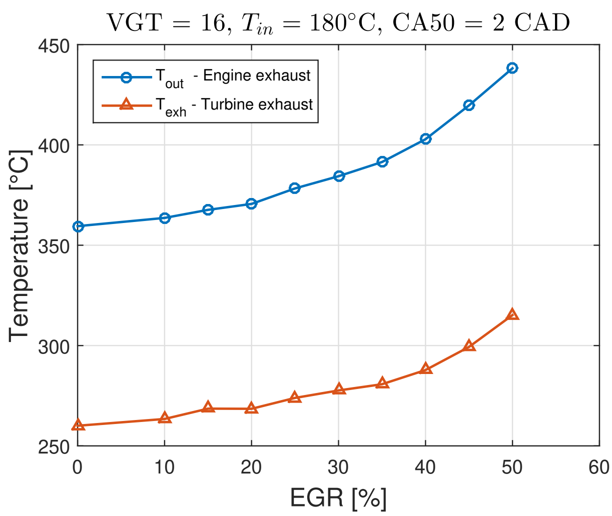

Figure 3.37: Engine and turbine exhaust temperatures as functions of the EGR rate at CA50 = 2 CAD.

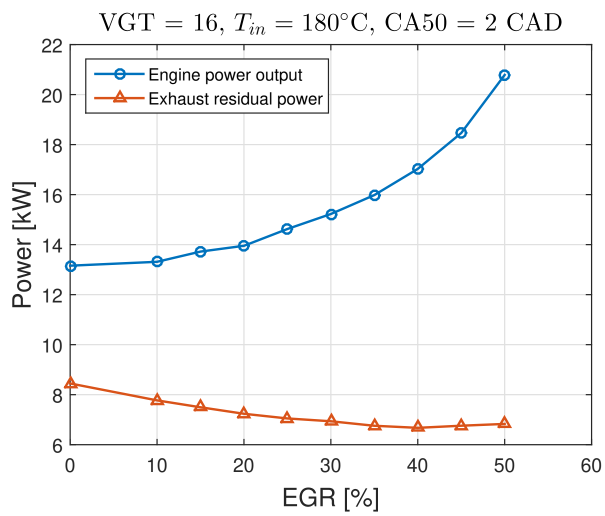

Figure 3.38: Engine power output and exhaust residual power as functions of the EGR rate at CA50 = 2 CAD. The temperature T_{5g} has been set to 60°C.

3.5 Influence of the coolant temperature

This section briefly studies the influence of the coolant temperature, which can be assimilated to the wall temperature of the engine. Experiments were conducted at $p_{in} = 1.3$ bar, $T_{in} = 180$°C and $\phi = 0.42$, for 6 coolant temperatures: 70, 75, 80, 85, 90 and 95°C. As shown in Figure 3.39, the CA50 is strongly influenced by the coolant temperature. As the cylinders wall temperature rises, higher combustion efficiency occurs in that area and leads to earlier auto-ignition, hence lower CA50. Figure 3.40 shows again the strong influence between the IMEPg and the CA50 as the maximum cyclic work is obtained at a CA50 about 2.5 CAD. However, it should be kept in mind that the coolant temperature cannot really be modified as desired.

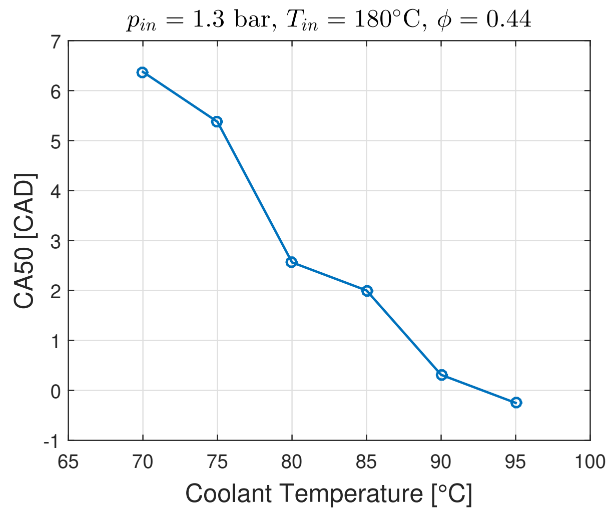

Figure 3.39: CA50 as a function of the coolant temperature.

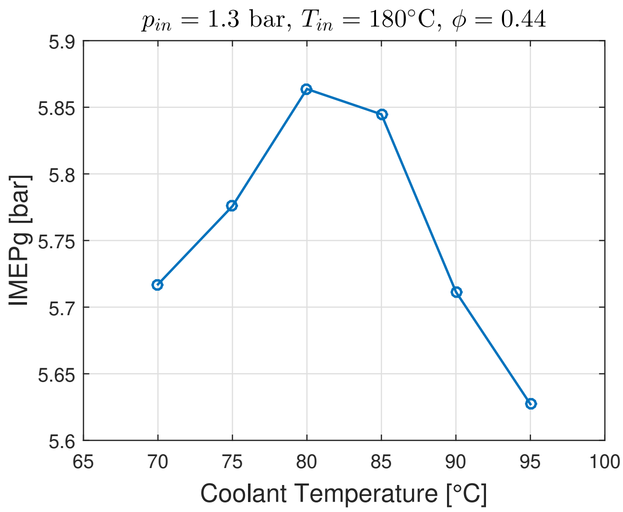

Figure 3.40: IMEPg as a function of the coolant temperature.

3.6 Variations among the cylinders

As mentioned in Section 3.3, results may differ a lot between cylinder 1 and other cylinders. Experimental in-cylinder pressure curves for each cylinder are displayed in Figure 3.41. As a first observation, the curve of the cylinder 1 seems to undergo an important damping, resulting in lower PCP and higher CA50. Figure 3.42 confirms this trend as the combustion efficiency of the cylinder 1 is much lower than that of other cylinders. This could be due to the proximity of the cylinder 1 with the cooling system since effects on the CA50 are similar. Therefore, the cylinder wall temperature should be lower and prevent a part of the fuel to burn near the wall, causing a decrease in the combustion efficiency and a delayed combustion phasing.

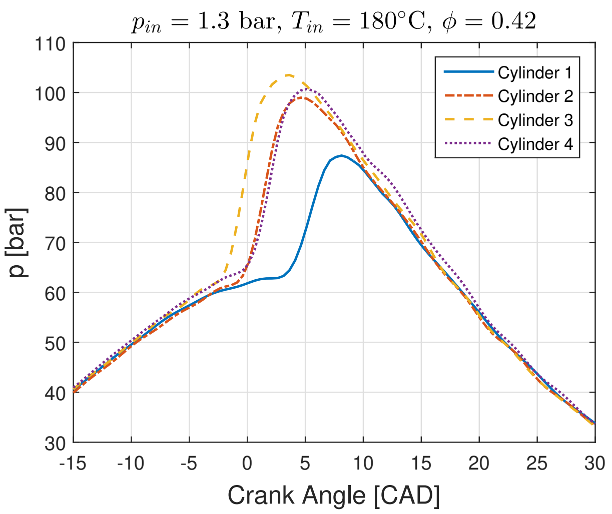

Figure 3.41: Experimental in-cylinder pressure curves for each cylinder.

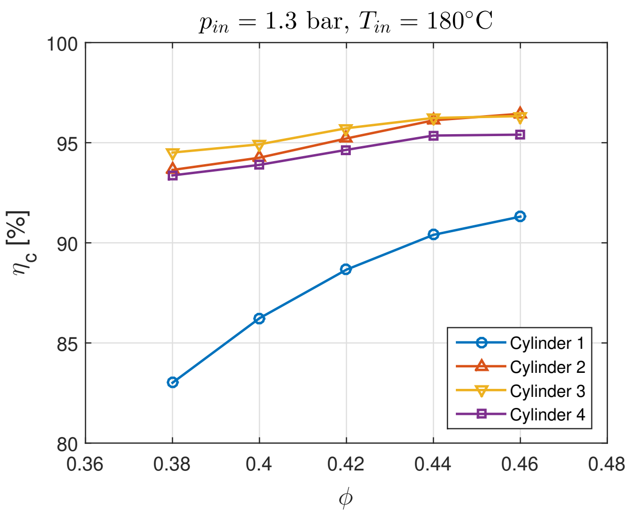

Figure 3.42: Combustion efficiency as a function of the fuel-air equivalence ratio for each cylinder.

3.7 Uncertainty analysis

After having analysed the experimental results of this thesis, it might be interesting to look at their uncertainty. The uncertainty U_x is defined as the region $\pm U$ around the nominal value for a measured or calculated quantity x. The key reason of analyzing the experimental uncertainties is to verify the reliability of the observations made in the frame of this thesis.

3.7.1 Sources of uncertainty

The sources of uncertainty and their propagation to the final results are represented in Figure 3.43. The uncertainties coming from the main instruments are listed on the left hand side. From top to bottom: air mass flow rate $\dot{m}_a$, fuel mass flow rate $\dot{m}_f$, EGR mass flow rate $\dot{m}_{\text{EGR}}$, heat losses scaling factor, α_{scale}, effective compression ratio τ, Top Dead Center offset, Pegging, pressure for 50 cycles p_{50} and finally the pressure sensor. The arrows represent the uncertainties propagation from the instrument measures to intermediate parameters which influence themselves the uncertainties computation for the final results. From top to bottom, the intermediate parameters are: cylinder volume V_{cyl}, mean filtered in-cylinder pressure $p_{cyl,mfp}$ and charge amplification $CAmp$. The final results are: equivalence ratio ϕ, equivalence ratio taking the EGR dilution effect into account ϕ_{EGR}, rate of heat release, indicated efficiency η_{ig}, Indicated Mean Effective Pressure gross and combustion efficiency η_c.

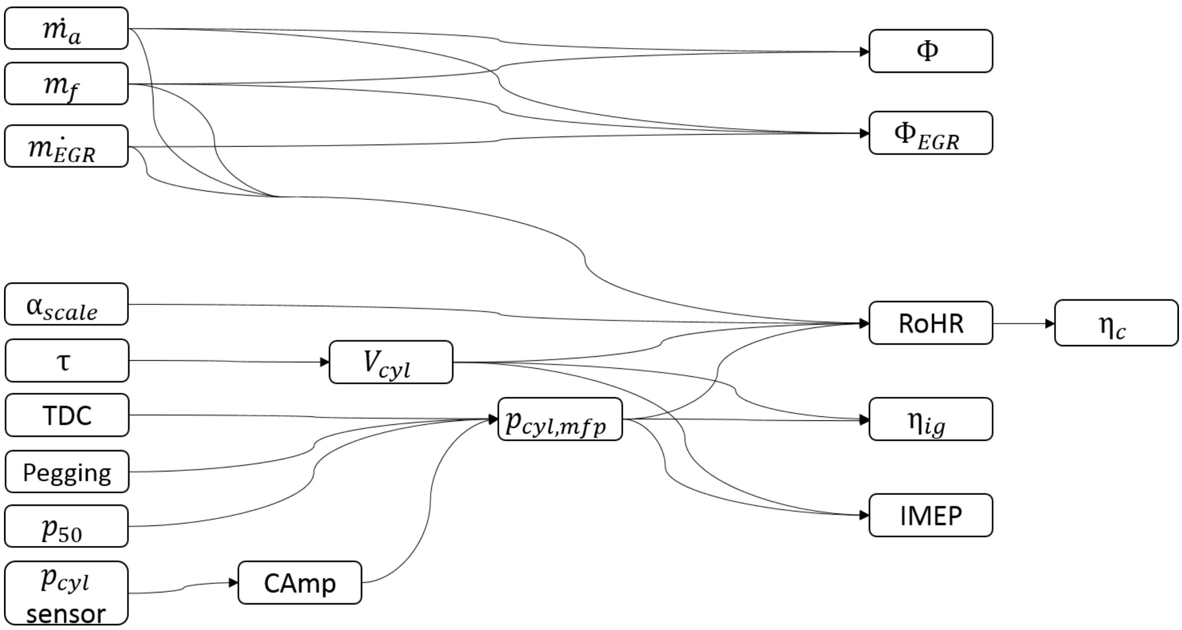

Figure 3.43: Overview of the uncertainty work flow

Estimation of the uncertainties

The first uncertainty estimation concerns the equivalence ratio whose equation is constituting of three terms: the air mass flow, the fuel mass flow and the air demand. The air flow uncertainty is computed according to the mass flow uncertainty formula from the diaphragm data sheet:

$$\frac{\delta \dot{m}_a}{\dot{m}_a} = \Bigg[\left(\frac{\delta\alpha}{\alpha}\right)^2 + \left(\frac{\delta\varepsilon}{\varepsilon}\right)^2 + 4\left(\frac{\beta^4}{\alpha}\right)^2\left(\frac{\delta D}{D}\right)^2 + 4\left(1+\frac{\beta^4}{\alpha}\right)^2\left(\frac{\delta d}{d}\right)^2 + \frac{1}{4}\left(\frac{\delta\Delta p}{\Delta p}\right)^2 + \frac{1}{4}\left(\frac{\delta\Delta\rho}{\Delta\rho}\right)^2\Bigg]^{\frac{1}{2}} \tag{3.2}$$

For the current experimental setup, this formula gives $\frac{\delta \dot{m}_a}{\dot{m}_a} = \pm 0,0063$.

For the mass fuel rate, there was assumed to be a 0.2 second discrepancy between the stopwatch reading and the gas meter dials reading. The uncertainty is therefore $\frac{\delta \dot{m}_f}{\dot{m}_f} = \pm\ 3.322 \cdot 10^{-3}$. While the air demand value is supposed to be correct. The equivalence ratio uncertainty can be computed through the quotient uncertainty formula:

$$A = \frac{B}{C} \qquad \Rightarrow \frac{\delta A}{A} = \frac{\delta B}{B} + \frac{\delta C}{C}$$
$$\frac{\delta\phi}{\phi} = \pm(3.322 + 6.3)\cdot 10^{-3} = \pm 9.622 \cdot 10^{-3}$$

3.7.2 Experiment repeatability

The repeatability of the experiments has been studied though five successive experiments at $p_{in} = 1.3$ bar, $T_{in} = 180°$C and $\phi = [0.44, 0.42, 0.40, 0.42, 0.44]$, by assuming no measurement error on these three intake parameters. Experiments have been carried out at intervals of 30 minutes to ensure as much as possible that the thermal equilibrium is reached. The purpose of theses tests is to determine whether or not the results are the same at $\phi = 0.42$ and $\phi = 0.44$.

Figures 3.44 and 3.45 show a decrease about 0.77% in the IMPEg and about 0.94% in the BMEP bewteen experiments 2 and 4 at $\phi = 0.42$. At first glance, this trend could be explained by the fact that the engine was running at a higher ϕ before test 2 while it was running at a lower ϕ before test 4. But curiously, the opposite trend occurs at $\phi = 0.44$ as the IMEPg and BMEP are higher in test 5 than in test 1. Therefore, differences are likely due to measurement errors rather than thermal equilibrium issues.

3.7.3 Crank angle rotary encoder

The method developed by Tunestål [29] has been used to correct the TDC offset occurring due to a misalignment in the crank angle rotary encoder. A precision of 0.1 CAD is required on the TDC to effectively compute the rate of heat release. However, the four high frequency sensors of the test bench give pressure measurement at a frequency of only 0.5 CAD. Therefore, calibration errors may persist after the correction as shown in Figures 3.46 and 3.47. An error of ± 0.5 CAD on the calibration would lead to an underestimation of 9.4% or an overstatement of 8.8% on the gross heat release. The consequence of this miscalculation is that very poor combustion efficiency or even combustion efficiency higher than 100% are possible.

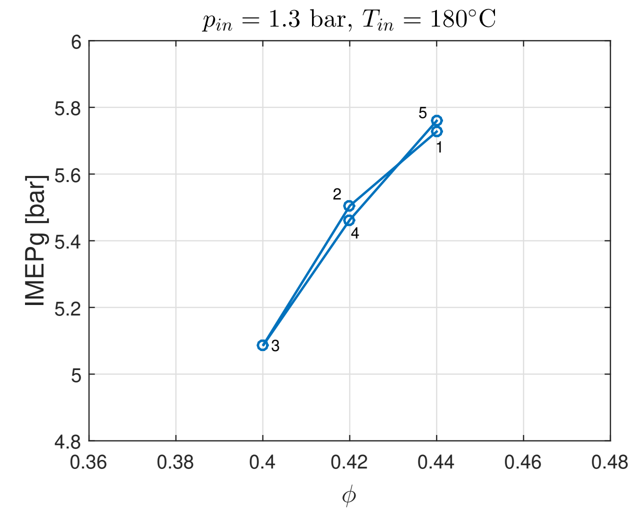

Figure 3.44: IMEPg as a function of the fuel-air equivalence ratio through successive experiments (1→5).

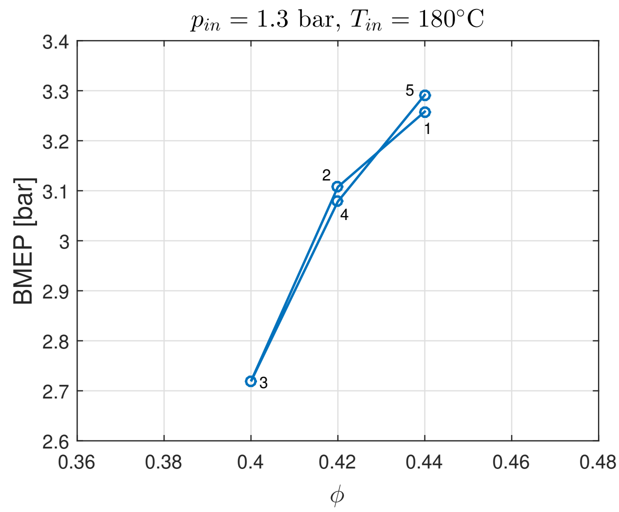

Figure 3.45: BMEP as a function of the fuel-air equivalence ratio through successive experiments (1→5).

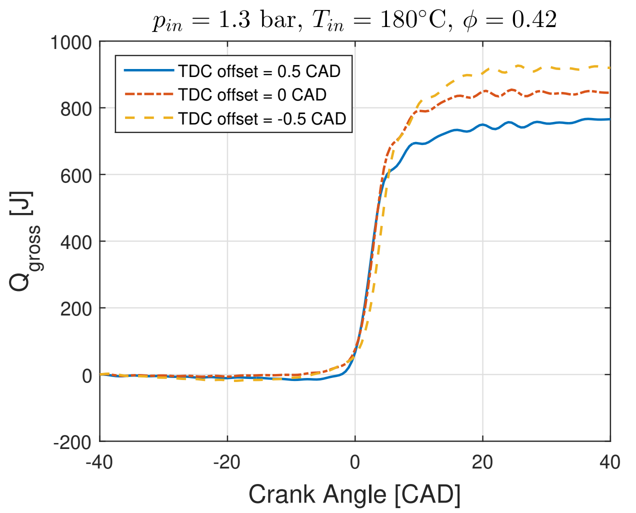

Figure 3.46: Influence of the TDC offset on the gross heat release. TDC offset = 0 CAD corresponds to the corrected case.

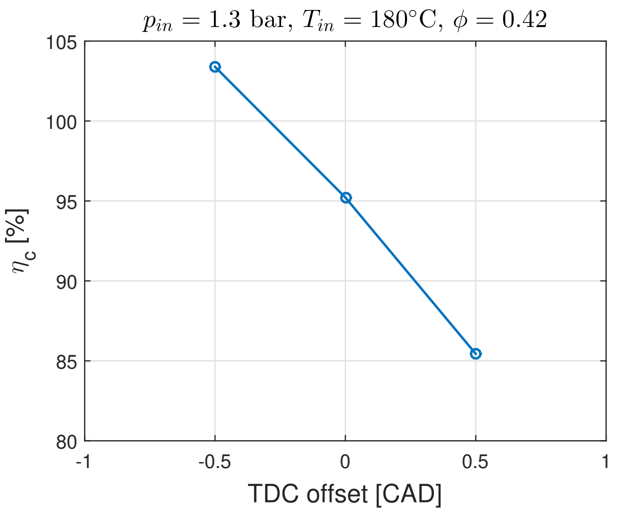

Figure 3.47: Influence of the TDC offset on the combustion efficiency. TDC offset = 0 CAD corresponds to the corrected case.

3.8 Organic Rankine Cycle

The purpose of this section is to investigate the choice of ORC fluid according to the second and third criteria reviewed in Section 1.5.2. The section first discussed about security and environmental concerns of the organic fluid. The choice of the ORC fluid according to the technological, operational and economical criteria is then tackled. Due to the large number of organic fluid, a pre-selection regrouping different organic fluid classes was realized according to [17], [23] and [20] which are scientific articles investigating organic fluids properties. The environment and security criteria is discussed by means of Table 3.1.

The second column in Table 3.1 represents the ORC fluids authorized or being phased out in Belgium according to the schedule set out in the Montreal protocol. Following the second criteria, fluids authorized by the Belgian legislation, with no inflammability, no toxicity, a low ODP and a low GWP will be preferred

ORC fluid	Belgian legislation	Inflammability	Toxicity	ODP	GWP
R123	Banned	No	Yes	0.06	77
R141b	Banned	Yes	Yes	0.11	600
R1234yf	Authorized	Yes (low)	No	0	4
R113	Banned	No	Yes	0.8	4800
R134a	Authorized	No	No	0	1430
R245fa	Authorized	No	No	0	1030
R22	Banned	No	No	0.05	1810
R717 (Ammonia)	Authorized	No	Yes	0	0
R152A	Authorized	Yes	No	0	124
Hydrogen Sulfide	Authorized	Yes	Yes	0	0
R507A	Authorized	No	No	0	3985
Sulfur Dioxide	Authorized	No	Yes	0	0
R227EA	Authorized	No	No	0	3220
R744 (Carbon dioxide)	Authorized	No	No	0	1

Table 3.1: Security and environmental criteria. [1]

for the ORC fluid choice. Therefore, by observing the results, the R744 (Carbon dioxide), Sulfur Dioxide, Hydrogen Sulfide, R717 (Ammonia) and the R1234yf seem to be the most appropriate organic fluids in an environmental and a security concern for the present application. The criteria referring the technological, operational and economical parameters of ORC fluids is investigated in Table 3.2. In a concern of coherence, all the fluid parameters contained in this table were computed according to the variables of the state before the pump (1)/(5) because this state is constant for all ORC configurations and parameters (see Section 2.4.3). According to Section 1.5.2, the fluid that better suits this criteria has the following properties : high density, reasonable vapor pressure, condensation pressure higher than the atmospheric pressure, low viscosity and high thermal conductivity. Because the vapor pressure depends on the compressor ratio, itself depending on the ORC power, the vapor pressure is presented in the tables investigating the thermodynamic criteria in Section 3.9.1.

By observing Table 3.2, it is possible to select the fluids that suit best each property of this criteria:

- Density of ORC fluids lies between [610.2-1574.9] $\frac{kg}{m^3}$. The five fluids with the biggest density are respectively in decreasing order: R113, R123, R227EA, Sulfur Dioxide and R245fa.
- Viscosity of ORC fluids belongs to a range of [0.661-6.957]e^{-4} Pa· s. The five fluids with the smallest viscosity are respectively in increasing order: R744, Hydrogen Sulfide, R22, R507A and R717.
- Heat capacity of ORC fluids lies in a range of [913.2-4744.8] $\frac{J}{kgK}$. The five fluids with the biggest heat capacity are respectively in decreasing order: R717, R744, Hydrogen Sulfide, R152A and R507A.
- The last column shows that the condensing pressure of R123, R141b and R113 is below the atmospheric pressure.

After having analyzed all the properties of this criteria, it turns out that none of the fluids suits best all the properties. However, the five next fluids, R744, the Hydrogen Sulfide, R717, R152A and sulfur dioxide seem

[1] http://www.linde-gas.com/en/products_and_supply/refrigerants/index.html, accessed on May 29, 2018.

ORC fluid	Density [kg/m^3]	Viscosity [Pa·s]	Heating capacity [J/kgK]	p_{cond} [bar]
R123	1476.6	4.426e-04	1013.5	0.756
R141b	1243.4	4.316e-04	1147.4	0.65
R1234yf	1109.9	1.544e-04	1369.3	5.917
R113	1574.9	6.957e-04	913.2	0.367
R134a	1225.3	2.074e-04	1404.9	5.717
R245fa	1351.9	4.189e-04	1305.0	1.231
R22	1209.9	1.349e-04	1235.6	9.1
R717	610.2	1.383e-04	4744.8	8.575
R152A	912	1.709e-04	1776.5	5.129
Hydrogen Sulfide	787.5	1.302e-04	2206.8	17.81
R507A	1071.7	1.374e-04	1496.8	11.218
Sulfur Dioxide	1380.9	3.584e-04	1385.8	3.307
R227EA	1408.4	2.561e-04	1166.3	3.891
R744	773.4	0.661e-04	4263.7	57.291

Table 3.2: Technological, operational and economical criteria.

to fit best the technological, operational and economical concern notably because of their high density-heating capacity product.

3.9 Expected performance for HCCI-ORC systems

As discussed in Section 2.2.3, given the particular configuration of the test bench, HCCI brake efficiency is not optimum because of the significant pumping and friction losses present in a such configuration. In order to complete the objective of this work consisting in perform the highest efficiency of a HCCI-ORC combined cycle, the HCCI brake efficiency should be optimized. HCCI performances are therefore simulated through a 0D model taking the configuration which maximizes the HCCI brake efficiency. However, to be consistent with the results, the 0D model will be fitted with the experimental data obtained from the previous experiments. In the optimal configuration implemented in the 0D model, the compressor is located before the heating resistance,resulting in higher compression efficiencies. While the FMEP is pretty hard to estimate theoretically, the value of FMEP used in the 0D model is based on previous works that have studied combustion in HCCI engines. In the present case, a value of FMEP = 1 bar [11] is chosen.

In order to fit the 0D model with experimental data, the 0D model needs the combustion efficiency η_c, the combustion timing (θ_s and θ_b) and the engine exhaust temperature T_{out}. Sometimes, parameters values are approximated through correlations based on the experimental results. For example, strong correlations exist between the engine intake parameters and the combustion timing. However, these correlations should not be used for too wide ranges. Consequently, more the CA50 is far away from the TDC, less the correlations are correct and more the uncertainties are high.

3.9.1 ORC coupling with experimental results

The study about HCCI-ORC combined cycle will first discuss the combination of the ORC abd experimental results made with and without EGR in order to achieve highest efficiency. Then the EGR impact on the combined cycle will be investigated. After that, ORC will be combined with HCCI theoretical configurations giving the highest effective efficiency where inlet parameters were estimated through correlations. The simulated HCCI configurations respect also the MPRR and PCP constraints. For each test, the optimum effective power of the combined cycle will be calculated from a purely thermodynamic point of view, namely, by coupling the highest ORC power with the HCCI power.

Experiments without EGR at highest efficiency

As shown in Figure 3.24, the experimental test without EGR having the highest effective efficiency has the following inlet parameters: ϕ=0.46, p_{in}=1.3 bar and T_{in}=170°C. The results of this test are displayed in Tabular 3.3.

ϕ [/]	p_{in} $[bar]$	T_{in} $[°C]$	θ_s [CAD]	θ_b [CAD]	η_{comb} [%]	P_{eff} $[kW]$	η_{eff} [%]	T_{smoke} $[°C]$	$\dot{m}_{smoke}$ $[g/s]$	$\dot{Q}_{smoke}$ $[kW]$	MPRR $[\frac{bar}{CAD}]$
0.46	1.3	170	-3.8	6.1	94	15.346	29.75	273.5	38	10.112	15

Table 3.3: Inlet conditions and results of the highest efficiency experimental test without EGR.

These values are inserted in the 0D code to simulate the thermodynamic results for the four ORC configurations which are represented in Tables 3.4 and 3.5.

ORC fluid	Subcritical							
	Without regenerator				With regenerator			
	P_{ORC} [kW]	η_{ORC} [%]	π_c [/]	p_{vapor} [bar]	P_{ORC} [kW]	η_{ORC} [%]	π_c [/]	p_{vapor} [bar]
R123	1.022	17.06	13.957	10.553	1.914	29.67	46.571	35.212
R141b	1.081	18.04	13.957	9.075	1.825	29.8	62.49	40.633
R1234yf	0.869	12.6	5.3478	31.644	1.6	23.88	5.1837	30.673
R113	0.982	16.43	16.348	5.996	1.607	30.97	80	29.342
R134a	0.995	15.09	6.7826	38.777	1.626	24.65	6.7755	38.736
R245fa	0.951	15.94	13.957	17.175	1.751	28.63	27.469	33.803
R22	1.141	16.88	5.3478	48.666	1.684	23.46	5.1837	47.173
R717	1.3	20.23	7.7391	66.361	2.005	23.26	11.551	99.048
R152A	1.11	18.39	8.6957	44.601	1.765	25.6	8.3673	42.917
Hydrogen Sulfide	1.295	19.51	4.8696	86.728	1.592	20.23	3.5918	63.970
R507A	0.764	9.62	2.9565	33.166	9.43	14.46	2	22.436
Sulfur Dioxide	1.277	20.03	9.1739	30.335	1.925	23.72	17.918	5.925
R227EA	0.792	12.1	7.2609	28.251	1.515	24.55	6.7755	2.636
Carbon Dioxide	NaN	NaN	NaN	NaN	NaN	NaN	NaN	NaN

Table 3.4: ORC subcritical case results for the combination with the experimental test without EGR.

ORC fluid	Supercritical							
	Without regenerator				With regenerator			
	P_{ORC} [kW]	η_{ORC} [%]	π_c [/]	p_{vapor} [bar]	P_{ORC} [kW]	η_{ORC} [%]	π_c [/]	p_{vapor} [bar]
R123	NaN	NaN	NaN	NaN	NaN	NaN	NaN	NaN
R141b	2.260	24.49	154.48	100.45	2.211	22	232.72	151.32
R1234yf	1.933	21.12	52.358	309.81	1.930	27.05	57.159	338.22
R113	2.107	24.27	278.96	102.32	2.222	25.66	332.29	121.88
R134a	2.067	22.07	36.174	206.81	2.068	27.06	48.255	275.88
R245fa	2.131	22.4	151.16	186.02	2.131	25.44	163.62	201.35
R22	2.145	23.71	20.508	186.63	2.176	26.1	23.214	211.25
R717	2.144	24.71	13.621	116.80	1.917	24.75	13.621	116.80
R152A	2.208	24.20	32.935	168.93	2.167	25.89	37.282	191.22
Hydrogen Sulfide	2.132	24.39	12.051	214.628	2.158	23.65	11.679	208.003
R507A	1.895	21.16	30.252	339.37	1.904	27.01	30.91	346.748
Sulfur Dioxide	2.179	26.81	24.566	81.232	1.991	22.92	39.847	131.76
R227EA	1.807	19.6	79.055	307.59	1.819	26.28	55.915	217.55
Carbon Dioxide	1.826	23.59	10.05	575.77	1.828	23.16	7.9267	454.13

Table 3.5: ORC supercritical case results for the combination with the experimental test without EGR.

P_{HCCI} $[kW]$	P_{ORC} $[kW]$	P_{total} $[kW]$	η_{total} $[/]$
15.346	2.222	17.568	34.06

Table 3.6: Combined cycle results for the experimental test without EGR having the highest efficiency.

Experiments with EGR at highest efficiency

As observed in Figure 3.35 , the test with the highest effective efficiency has the following inlet parameters: ϕ=0.80835, p_{in}=1.3 bar and T_{in}=170°C. The results of this test are represented in Tabular 3.7. These values

ϕ $[/]$	p_{in} $[bar]$	T_{in} $[°C]$	θ_s [CAD]	θ_b [CAD]	η_{comb} $[\%]$	P_{eff} $[kW]$	η_{eff} $[\%]$	T_{smoke} $[°C]$	$\dot{m}_{smoke}$ $[g/s]$	$\dot{Q}_{smoke}$ $[kW]$	MPRR $[\frac{bar}{CAD}]$
0.808	1.562	180	0.312	10.25	94	19.25	31.6	304	24	7.458	15

Table 3.7: Inlet conditions and results of the experimental test with EGR having the highest efficiency.

are inserted in the 0D code to simulate the thermodynamic results for the four ORC configurations which are represented in Tables 3.8 and 3.9.

Tables 3.6 and 3.10 show that the highest effective efficiency of the combined cycle by taking the experimental results of the HCCI engine reach a maximum of 35,25%. The effective efficiency of the two cycles are close to each other despite the highest efficiency of the HCCI in the case with EGR. These tables also show that the ORC power is smaller in the case with EGR. It therefore explains the higher efficiency increase for the HCCI without EGR. The impact of EGR is investigated in the next section. The pretty low efficiency of the combined cycle is mainly explained by the non-optimal test bench configuration.

ORC fluid	Subcritical							
	Without regenerator				With regenerator			
	P_{ORC} [kW]	η_{ORC} [%]	π_c [/]	p_{vapor} [bar]	P_{ORC} [kW]	η_{ORC} [%]	π_c [/]	p_{vapor} [bar]
R123	0.81	18.07	17.304	13.084	1.536	31.64	46.571	35.212
R141b	0.86	19.01	16.826	10.941	1.568	32.04	62.49	40.633
R1234yf	0.661	12.37	5.3478	31.644	1.178	25.30	5.1837	30.673
R113	0.776	17.4	20.652	7.5747	1.388	32.97	80	29.342
R134a	0.769	14.88	6.7826	38.777	1.345	26.16	6.7755	38.736
R245fa	0.748	16.75	17.304	21.294	1.329	30.33	27.469	33.803
R22	0.892	16.93	5.3478	48.666	1.327	24.98	5.1837	47.173
R717	1.06	22.02	9.1739	78.664	1.625	25.04	11.551	99.048
R152A	0.879	18.33	8.6957	44.601	1.327	27.25	8.3673	42.917
Hydrogen Sulfide	1.042	20.08	4.8696	86.728	1.234	21.56	3.5918	63.970
R507A	0.57	9.42	2.9565	33.166	0.658	15.36	2	22.436
Sulfur Dioxide	1.038	21.81	11.087	36.661	1.78	25.75	22.694	75.042
R227EA	0.605	11.78	7.2609	28.251	1.094	25.96	6.7755	26.362
Carbon Dioxide	NaN	NaN	NaN	NaN	NaN	NaN	NaN	NaN

Table 3.8: ORC subcritical case results for the combination with the experimental test with EGR having the highest efficiency.

ORC fluid	Supercritical							
	Without regenerator				With regenerator			
	P_{ORC} [kW]	η_{ORC} [%]	π_c [/]	p_{vapor} [bar]	P_{ORC} [kW]	η_{ORC} [%]	π_c [/]	p_{vapor} [bar]
R123	NaN	NaN	NaN	NaN	NaN	NaN	NaN	NaN
R141b	1.822	26.28	154.48	100.45	1.765	26.46	330.01	214.583
R1234yf	1.486	21.64	44.613	263.98	1.498	28.11	42.51	251.54
R113	1.732	23.86	349.67	128.255	1.75	28.23	332.29	121.88
R134a	1.617	23.79	65.036	371.82	1.611	27.8	71	405.914
R245fa	1.648	23.32	151.16	186.02	1.648	28.08	201.64	248.14
R22	1.709	25.29	35.368	321.86	1.714	29.14	26.728	243.23
R717	1.294	24.63	13.621	116.80	1.298	26.24	13.621	116.8
R152A	1.703	25.74	44.868	230.13	1.702	26.15	65.493	335.92
Hydrogen Sulfide	1.69	24.89	18.897	336.556	1.705	22.01	24.628	438.625
R507A	1.471	22.73	48.152	540.17	1.475	28.19	22.446	251.80
Sulfur Dioxide	1.738	27.02	24.566	81.232	1.739	20.56	55.128	182.29
R227EA	1.373	20.08	89.243	347.23	1.417	28.44	65.549	255.04
Carbon Dioxide	1.451	23.79	8.3057	475.84	1.445	24.87	8.7518	501.40

Table 3.9: ORC supercritical case results for the combination with the experimental test with EGR having the highest efficiency.

3.9.2 Influence of EGR on combined cycle performance

In this section, three HCCI configurations respectively with an EGR fraction of 0 %, 30% and 50% were coupled to ORC in order to study the impact of EGR on the combined cycle. In order to get the highest efficiency of the combined cycle, the HCCI configuration minimizing the pumping losses, namely, with the compressor before the heating resistance was chosen. The performance of HCCI configurations was study

P_{HCCI} $[kW]$	P_{ORC} $[kW]$	P_{total} $[kW]$	η_{total} $[/]$
19.25	1.822	21.47	35.25

Table 3.10: Combined cycle results for the experimental test with EGR having the highest efficiency.

through a 0D model fitted to experimental results giving the maximum HCCI engine power from Section 3.3.

α = 0%

The inlet conditions and the results of the HCCI configuration with an EGR fraction of 0% are displayed in Tabular 3.11.

ϕ_{EGR} $[/]$	p_{in} $[bar]$	T_{in} $[°C]$	θ_s [CAD]	θ_b [CAD]	η_{comb} $[\%]$	P_{eff} $[kW]$	η_{eff} $[\%]$	T_{smoke} $[°C]$	$\dot{m}_{smoke}$ $[g/s]$	$\dot{Q}_{smoke}$ $[kW]$
0.42	1.3	180	0.0729	7.5	95	18.157	39.47	328.35	38.7	12.618

Table 3.11: Inlet conditions and results of HCCI with an EGR fraction of 0%.

ORC fluid	Subcritical							
	Without regenerator				With regenerator			
	P_{ORC} [kW]	η_{ORC} [%]	π_c [/]	p_{vapor} [bar]	P_{ORC} [kW]	η_{ORC} [%]	π_c [/]	p_{vapor} [bar]
R123	1.435	18.739	20.174	15.254	2.689	33.04	46.571	35.212
R141b	1.527	19.799	19.696	12.807	2.830	33.57	62.49	40.633
R1234yf	1.135	12.127	5.3478	31.644	1.947	26.37	5.1837	30.673
R113	1.373	17.96	24	8.803	2.503	34.38	80	29.342
R134a	1.33	14.697	6.7826	38.777	2.355	27.29	6.7755	38.736
R245fa	1.319	17.267	20.174	24.826	2.350	27.55	13.143	16.174
R22	1.56	16.928	5.3478	48.666	2.424	26.12	5.1837	47.173
R717	1.92	23.179	10.13	86.863	2.902	26.36	11.551	99.048
R152A	1.546	18.234	8.6957	44.601	2.437	28.47	8.3673	42.917
Hydrogen Sulfide	1.86	20.461	4.8696	86.728	2.149	22.57	3.5918	63.97
R507A	0.966	9.2643	2.9565	33.166	1.063	16.05	2	22.
Sulfur Dioxide	1.877	23.016	12.522	41.406	3.231	27.18	22.694	75.042
R227EA	1.039	11.545	7.2609	28.251	1795	27.03	6.7755	26.362
Carbon Dioxide	NaN	NaN	NaN	NaN	NaN	NaN	NaN	NaN

Table 3.12: ORC subcritical case results for the combination with HCCI having a 0 % EGR

α = 30%

The inlet conditions and the results of the HCCI configuration with an EGR fraction of 30% are displayed in Table 3.15.

α = 50%

The inlet conditions and the results of the HCCI configuration with an EGR fraction of 50% are displayed in Table 3.19.

Tables 3.14, 3.18 and 3.22 show that the ORC power decreases when the EGR fraction increases. Indeed, the fraction of exhaust gases recirculating into the HCCI is no more recovered by the WHR of the ORC. Even if

ORC fluid	Supercritical							
	Without regenerator				With regenerator			
	P_{ORC} [kW]	η_{ORC} [%]	π_c [/]	p_{vapor} [bar]	P_{ORC} [kW]	η_{ORC} [%]	π_c [/]	p_{vapor} [bar]
R123	NaN	NaN	NaN	NaN	NaN	NaN	NaN	NaN
R141b	3.232	27.68	330.01	214.58	3.198	28.96	242.25	157.52
R1234yf	2.592	22.48	60.103	355.64	2.611	29.78	67.848	401.47
R113	3.083	25.76	596.54	218.80	3.081	31.06	345.9	126.87
R134a	2.857	25.01	84.277	481.82	2.825	31.13	74.656	426.82
R245fa	2.883	24.27	231.56	284.96	2.898	31.46	231.56	284.96
R22	3.063	26.71	27.938	254.24	3.040	29.02	42.798	389.47
R717	3.081	26.32	31.539	270.44	2.559	27.66	13.621	116.80
R152A	3.028	26.76	80.665	413.74	3.045	29.65	80.665	413.74
Hydrogen Sulfide	3.062	27.54	25.743	458.483	3.073	27.5	12.051	214.628
R507A	2.55	23.17	52.627	590.37	2.603	28.93	30.252	339.37
Sulfur Dioxide	3.143	27.07	56.882	188.09	2.864	27.37	24.566	81.232
R227EA	2.369	20.33	89.243	347.23	2.489	29.97	68.868	267.95
Carbon Dioxide	2.608	25.35	8.3057	475.84	2.641	28.2	8.3057	475.84

Table 3.13: ORC supercritical case results for the combination with HCCI having a 0 % EGR

P_{HCCI} $[kW]$	P_{ORC} $[kW]$	P_{total} $[kW]$	η_{total} [/]
18.157	3.231	21.388	46.497

Table 3.14: Combined cycle results for the HCCI configuration with 0% EGR

the exhaust gases temperature is higher, the smoke flow reduction results in a diminution of the recoverable residual enthalpy decreasing therefore the hot source power of the ORC. The diminution of the exhaust gases enthalpy $\dot{Q}_{smoke}$ with the EGR fraction is observed in Tables 3.11, 3.15 and 3.19. This result implies that the coupling with an ORC is less interesting with a HCCI using EGR but is non negligible because the combined cycle increase the efficiency of at least 4 % compared to the HCCI alone. Moreover, these tables show also that the effective efficiency of the combined cycle raises with the EGR fraction. This augmentation is mainly due to the equivalence ratio increase which boosts both HCCI power and effective efficiency.

3.9.3 ORC coupling with best theoretical HCCI configurations

This section discussed about the coupling of ORC with HCCI configurations whose combustion parameters were computed though correlations. As mentioned above, these correlations are restricted to their tolerance range. It therefore means that the engine inlet parameters must be close to the inlet parameters of the experimental tests. Consequently, the engine inlet parameters are the same of those from the experimental tests except for one inlet parameter. Correlations between the new inlet parameter and combustion parameters are used in order to estimate the combustion parameters for the new HCCI configuration. Two HCCI configurations will be investigated in the following sections: A configuration with a high equivalence ratio and another with a high inlet pressure. In this two configurations, the new inlet parameter is respectively the pressure and the equivalence ratio which was boosted compared to experimental tests. The two HCCI

ϕ_{EGR} [/]	p_{in} $[bar]$	T_{in} $[°C]$	θ_s [CAD]	θ_b [CAD]	η_{comb} [%]	P_{eff} $[kW]$	η_{eff} [%]	T_{smoke} $[°C]$	$\dot{m}_{smoke}$ $[g/s]$	$\dot{Q}_{smoke}$ $[kW]$
0.5703	1.3952	180	0.186	10.25	95	21.613	41.76	338.38	28.7	9.916

Table 3.15: Inlet conditions and results of HCCI with an EGR fraction of 30%.

ORC fluid	Subcritical							
	Without regenerator				With regenerator			
	P_{ORC} [kW]	η_{ORC} [%]	π_c [/]	p_{vapor} [bar]	P_{ORC} [kW]	η_{ORC} [%]	π_c [/]	p_{vapor} [bar]
R123	1.15	18.92	21.13	15.976	2.138	33.59	46.571	35.212
2 R141b	1.224	20.15	21.13	13.739	2.272	34.15	62.49	40.633
R1234yf	0.896	12.04	5.3478	31.644	1.515	26.8	5.1837	30.673
R113	1.1	18.17	25.435	9.329	2.008	34.93	80	29.342
R134a	1.054	14.62	6.7826	38.777	1.857	27.73	6.7755	38.736
R245fa	1.054	17.50	21.609	26.592	1.906	28.7	14.735	18.133
R22	1.241	16.92	5.3478	48.666	1.962	26.57	5.1837	47.173
R717	1.551	23.97	11.087	95.069	2.328	26.88	11.551	99.048
R152A	1.233	18.19	8.6957	44.601	1.980	28.95	8.3673	42.917
Hydrogen Sulfide	1.492	20.60	4.8696	86.728	1.789	22.98	3.5918	63.970
R507A	0.759	9.20	2.9565	33.166	0.822	16.33	2	22.436
Sulfur Dioxide	1.516	23.43	13	42.987	2.606	27.74	22.694	75.042
R227EA	0.821	11.45	7.2609	28.251	1.394	27.45	6.7755	26.362
Carbon Dioxide	NaN	NaN	NaN	NaN	NaN	NaN	NaN	NaN

Table 3.16: ORC subcritical case results for the combination with HCCI having a 30 % EGR

ORC fluid	Supercritical							
	Without regenerator				With regenerator			
	P_{ORC} [kW]	η_{ORC} [%]	π_c [/]	p_{vapor} [bar]	P_{ORC} [kW]	η_{ORC} [%]	π_c [/]	p_{vapor} [bar]
R123	NaN	NaN	NaN	NaN	NaN	NaN	NaN	NaN
R141b	2.572	28.04	417.78	271.65	2.550	29.61	242.25	157.52
R1234yf	2.045	22.49	60.103	355.64	2.094	30.63	52.358	309.81
R113	2.455	26.18	721.86	264.76	2.454	31.58	596.54	218.80
R134a	2.267	25.16	84.277	481.82	2.252	32.33	74.656	426.82
R245fa	2.299	25.3	472.76	581.78	2.298	30.34	231.56	284.96
R22	2.432	27.44	35.368	321.86	2.443	31.66	35.368	321.86
R717	2.538	28.11	31.539	270.44	2.181	24.56	13.621	116.80
R152A	2.424	27.10	104.53	536.14	2.433	30.29	68.732	352.53
Hydrogen Sulfide	2.467	27.02	18.897	336.556	2.404	29.12	12.051	214.628
R507A	2.014	22.67	39.202	439.77	2.072	30.55	30.252	339.37
Sulfur Dioxide	2.531	28.87	56.882	188.09	2.308	28.67	24.566	81.232
R227EA	1.869	20.35	89.243	347.23	1.989	30.71	58.681	228.32
Carbon Dioxide	2.106	26.67	11.795	675.75	2.117	28.58	11.795	675.75

Table 3.17: ORC supercritical case results for the combination with HCCI having a 30 % EGR

configurations studied are respectively characterized by a high equivalence ratio and a low pressure boost and by a low equivalence ratio boost and a high pressure. The aim of these two configurations is to study which parameter between the pressure and equivalence ratio influences the most the combined cycle efficiency.

P_{HCCI} $[kW]$	P_{ORC} $[kW]$	P_{total} $[kW]$	η_{total} $[/]$
21.612	2.605	24.217	46.794

Table 3.18: Combined cycle results for the HCCI configuration with 30% EGR

ϕ_{EGR} $[/]$	p_{in} $[bar]$	T_{in} $[°C]$	θ_s [CAD]	θ_b [CAD]	η_{comb} $[\%]$	P_{eff} $[kW]$	η_{eff} $[\%]$	T_{smoke} $[°C]$	$\dot{m}_{smoke}$ $[g/s]$	$\dot{Q}_{smoke}$ $[kW]$
0.8761	1.6025	180	0.312	10.25	95	26.239	44.49	371.45	22	9

Table 3.19: Inlet conditions and results of HCCI with an EGR fraction of 50%.

ORC fluid	Subcritical							
	Without regenerator				With regenerator			
	P_{ORC} [kW]	η_{ORC} [%]	π_c [/]	p_{vapor} [bar]	P_{ORC} [kW]	η_{ORC} [%]	π_c [/]	p_{vapor} [bar]
R123	1.103	19.77	25.913	19.593	1.988	35.29	46.571	35.212
R141b	1.178	21.01	25.435	16.539	2.161	35.95	62.49	40.633
R1234yf	0.823	11.78	5.3478	31.644	1.324	28.15	5.1837	30.673
R113	1.053	18.90	31.174	11.434	1.905	36.61	80	29.342
R134a	0.975	14.35	6.7826	38.777	1.662	29.15	6.7755	38.736
R245fa	1.005	18.2	26.87	33.066	1.896	31.78	19.51	24.009
R22	1.163	16.87	5.3478	48.666	1.923	28	5.1837	47.173
R717	1.529	25.64	13	111.472	2.231	28.51	11.551	99.048
R152A	1.156	18.07	8.6957	44.601	1.955	30.47	8.3673	42.917
Hydrogen Sulfide	1.433	21.02	4.8696	86.728	1.763	24.26	3.5918	63.970
R507A	0.688	9	2.9565	33.166	0.708	17.23	2	22.436
Sulfur Dioxide	1.49	25.04	15.391	50.893	2.531	29.48	22.694	75.042
R227EA	0.755	11.16	7.2609	28.251	1.215	28.8	6.7755	26.362
Carbon Dioxide	NaN	NaN	NaN	NaN	NaN	NaN	NaN	NaN

Table 3.20: ORC subcritical case results for the combination with HCCI having a 50 % EGR

HCCI configuration: $\phi = 0.44$, $p_{in} = 1.4$ bar, $T_{in} = 170°$C

In this configuration, a slightly higher inlet pressure compared to experimental tests, the same temperature and same equivalence ratio as those of experimental tests are took. And as said above, the equivalence ratio is high. By simulating several configurations in the 0D model, the configuration with the highest effective efficiency respecting the MPRR constraint and with its inlet parameters in the tolerance range of the correlations between the inlet and the combustion parameters is: ϕ =0.44, p_{in}=1.4 bar, T_{in}=170°C. Because it was not possible to reach an inlet pressure with experimental test bench, the combustion parameters were evaluated thanks to figures of Section 3.3 . The point with the same equivalence ratio, the same inlet temperature and with a inlet pressure of 1.3 bar serves as reference. By observing Figures 3.8a and 3.10a, a pressure increase of 0.1 bar seems advance the combustion start of 2.5 CAD, reduce the combustion timing of 0.9 CAD and increase the combustion efficiency of 0.01. The inlet parameters and results of this test are represented in tabular 3.23. All these parameters are inserted in the 0D model to simulate the thermodynamic results for the four ORC which are displayed in Tables 3.24 and 3.25.

ORC fluid	Supercritical							
	Without regenerator				With regenerator			
	P_{ORC} [kW]	η_{ORC} [%]	π_c [/]	p_{vapor} [bar]	P_{ORC} [kW]	η_{ORC} [%]	π_c [/]	p_{vapor} [bar]
R123	NaN	NaN	NaN	NaN	NaN	NaN	NaN	NaN
R141b	2.46	29.48	417.78	271.65	2.44	33.22	330.01	214.58
R1234yf	1.917	23.27	75.593	447.30	1.992	31.06	67.848	401.47
R113	2.326	27.16	721.86	264.76	2.314	33.91	596.54	218.80
2 R134a	2.107	25.95	113.14	646.83	2.133	33.68	74.656	426.82
R245fa	2.136	25.73	271.76	334.43	2.167	33.65	271.59	334.22
R22	2.335	28.61	50.228	457.08	2.324	32.54	42.763	389.15
R717	2.448	28.74	49.458	424.09	1.632	30.7	31.417	269.39
R152A	2.308	27.74	80.665	413.74	2.290	31.61	104.49	535.94
Hydrogen Sulfide	2.413	29.85	25.743	458.483	2.256	27.84	12.004	213.791
R507A	1.888	22.98	34.727	389.57	1.976	31.53	30.252	339.37
Sulfur Dioxide	2.506	29.88	89.199	294.95	2.253	28.17	24.327	80.442
R227EA	1.750	21.25	140.18	545.41	1.896	32.27	89.243	347.23
Carbon Dioxide	2.024	28.15	13.54	775.72	2.063	32.32	8.3057	475.84

Table 3.21: ORC supercritical case results for the combination with HCCI having a 50 % EGR

P_{HCCI} $[kW]$	P_{ORC} $[kW]$	P_{total} $[kW]$	η_{total} [/]
26.239	2.53	28.742	48.734

Table 3.22: Combined cycle results for the HCCI configuration with 50% EGR

HCCI configuration: $\phi = 0.32$, $p_{in} = 1.9$ bar, $T_{in} = 165°$C

As mentioned in Section 3.1, the inlet pressure lies between 1 and 1.3 bar without EGR. Therefore the correlation between the combustion parameters and the pressure are only valid in a close range to the one of the pressure. This small tolerance range limits therefore the coupling with ORC because the HCCI configurations are restricted. Therefore, to couple ORC with HCCI configurations whose its inlet conditions are out of correlations tolerance range, previous master thesis can be used. Indeed, Boveroux and Gramme [3], investigated the performance of the HCCI engine with methane for different ranges of pressure and equivalence ratio and for another inlet temperature. By taking the experimental data of [3], the theoretical test giving the highest effective efficiency is obtained by testing several configurations with the 0D model. The configuration with the highest effective efficiency respecting the MPRR constraint and and with its inlet parameters in the tolerance range of the correlations between the inlet and the combustion parameters is: ϕ=0.32, p_{in}=1.9 bar, T_{in}=165°C. Boveroux and Gramme [3] did not test this equivalence ratio because they fixed the maximum MPRR to 10 bar/CAD, but as the maximum MPRR of this thesis is 15 bar/CAD, this test can be combined with the ORC cycles. However, the combustion parameters must again be evaluated through correlations made from their thesis figures. The point with the same inlet pressure, the same inlet temperature and with an equivalence ratio of 0.28 serves as reference. By observing thefigure displaying θ_s and θ_b according to the equivalence ratio, an equivalence ratio increase of 0.2 seems advance the CA50 of 1 CAD, reduce the combustion timing of 1.2 CAD, advance the combustion start of 0.8 CAD and increase the combustion efficiency of 0,01. The results of this test are represented in Tabular 3.27. All these parameters

ϕ [/]	p_{in} $[bar]$	T_{in} $[°C]$	θ_s [CAD]	θ_b [CAD]	η_{comb} $[\%]$	P_{eff} $[kW]$	η_{eff} $[\%]$	T_{smoke} $[°C]$	$\dot{m}_{smoke}$ $[g/s]$	$\dot{Q}_{smoke}$ $[kW]$	MPRR $[\frac{bar}{CAD}]$
0.44	1.4	170	-2	6.6	95	22.91	43.27	356.32	42.6	15.25	12.36

Table 3.23: Results of the HCCI configuration: ϕ =0.44, p_{in}=1.4 bar, T_{in}=170°C

ORC fluid	Subcritical							
	Without regenerator				With regenerator			
	P_{ORC} [kW]	η_{ORC} [%]	π_c [/]	p_{vapor} [bar]	P_{ORC} [kW]	η_{ORC} [%]	π_c [/]	p_{vapor} [bar]
R123	1.821	19.37	23.522	17.785	3.334	34.53	46.621	35.250
R141b	1.942	20.54	23.043	14.983	3.554	35.13	61.793	40.180
R1234yf	1.387	11.9	5.3478	31.644	2.125	25.99	4.4828	26.526
R113	1.74	18.55	28.304	10.381	3.028	29.12	18.138	6.6527
R134a	1.638	14.47	6.7826	38.777	2.694	27	5.7241	32.725
R245fa	1.663	17.82	24	29.534	3.087	29.82	15.655	19.265
R22	1.943	16.9	5.3478	48.666	3.092	25.94	4.4828	40.794
R717	2.494	24.86	12.043	103.27	3.754	27.91	11.931	102.31
R152A	1.934	18.09	8.6957	44.601	3.209	29.65	8.2069	42.094
Hydrogen Sulfide	2.367	20.84	4.8696	86.728	3.157	25.75	4.4828	79.839
R507A	1.167	9.09	2.9565	33.166	1.225	16.82	2	2.436
Sulfur Dioxide	2.433	24.18	13.957	46.152	4.018	28.73	23.103	76.395
R227EA	1.271	11.29	7.2609	28.251	2.115	28.44	6.9655	27.101
Carbon Dioxide	NaN	NaN	NaN	NaN	NaN	NaN	NaN	NaN

Table 3.24: ORC subcritical case results for the combination with HCCI configuration: ϕ =0.44, p_{in}=1.4 bar, T_{in}=170°C

are inserted in the 0D model to simulate the thermodynamic results for the four ORC's which are displayed in Tables 3.28 and 3.29.

Tables 3.26 and 3.30 show that the equivalence ratio has a more significant impact on the combined cycle efficiency than the pressure. This is explained because the ORC power is greatly influenced by the maximum cycle temperature. As mentioned in this thesis, the maximum cycle temperature is directly influenced by the exhaust gases temperature. Because the exhaust gases temperature increases more with the equivalence ratio than the inlet pressure, the equivalence ratio is therefore a key parameter for the combined cycle power.

3.9.4 Choice of the combined cycle configuration and discussion

By observing all tables displaying ORC results, it is possible to draw some conclusions:

- The beneficial effect of the regenerator is particularly valuable in the subcritical case. Indeed the regenerator allows to heat a higher ORC flow rate which is traduced by a power and cycle efficiency increase and to reduce pressure ratio. The regenerator improves therefore the ORC according to the first and the third criteria. The regenerator effect has a smaller impact in the supercritical case where it only reduces the pressure ratio and therefore the cycle maximum pressure.
- The power obtained in the supercritical case is higher than in the subcritical case. However, the compression ratio and the vapor pressure are much higher in the supercritical case.

ORC fluid	Supercritical							
	Without regenerator				With regenerator			
	P_{ORC} [kW]	η_{ORC} [%]	π_c [/]	p_{vapor} [bar]	P_{ORC} [kW]	η_{ORC} [%]	π_c [/]	p_{vapor} [bar]
R123	NaN	NaN	NaN	NaN	NaN	NaN	NaN	NaN
R141b	4.062	28.86	330.01	214.51	4.075	32.20	357.22	232.19
R1234yf	3.221	23.46	91.084	538.94	3.296	32.68	46.173	273.21
R113	3.896	26.93	721.86	264.92	3.868	33.51	450.81	165.45
R134a	3.537	25.80	84.277	481.81	3.544	33.05	61.902	353.89
R245fa	3.597	26.11	472.76	582.01	3.605	32.88	239.66	295.02
R22	3.907	27.81	35.368	321.85	3.874	32.81	40.781	371.11
R717	4.004	28.97	31.539	270.45	4.019	32.73	28.62	245.42
R152A	3.836	27.98	92.597	474.93	3.837	32.65	65.493	335.91
Hydrogen Sulfide	3.977	28.73	25.743	458.48	3.989	30.02	14.916	265.65
R507A	3.188	23.35	43.677	489.97	3.215	34.78	33.026	370.49
Sulfur Dioxide	4.081	28.59	56.882	188.11	4.082	26.26	85.69	283.38
R227EA	2.909	20.69	109.62	426.53	3.145	30.68	70.366	273.78
Carbon Dioxide	3.346	27.83	13.54	775.72	3.413	31.17	9.5768	548.66

Table 3.25: ORC supercritical case results for the combination with the HCCI configuration: ϕ =0.44, p_{in}=1.4 bar, T_{in}=170°C.

P_{HCCI} $[kW]$	P_{ORC} $[kW]$	P_{total} $[kW]$	η_{total} $[\%]$
22.91	4.082	26.992	50.98

Table 3.26: Combined cycle results for the HCCI configuration: ϕ =0.44, p_{in}=1.4 bar, T_{in}=170°C.

- For each test, the ORC fluid and ORC configuration that seems to be the most appropriate in a thermodynamic and pressure ratio concern is the subcritical ORC with a regenerator using sulfur dioxide. Indeed this configuration allows the highest ORC power for a reasonable pressure ratio.

By observing Tables 3.6, 3.26 and 3.30, it appears that the exhaust gases temperature, i.e. the hot source temperature, has an higher impact on the ORC power than the exhaust gases residual enthalpy. Indeed, the ORC power obtained from the experimental test without EGR and the test whose HCCI configuration is: ϕ=0.44, p_{in}=1.4 bar, T_{in}=170°C are both higher than the ORC power obtained from the test whose HCCI configuration is: ϕ=0.32, p_{in}=1.9 bar, T_{in}=165°C even if the residual enthalpy of the exhaust gases (Tables 3.3, 3.23 and 3.27) was higher in that case. However, as mentioned in Section 3.9.2 the residual enthalpy of the exhaust gases contributes also to the ORC power. It can also be observed on the above figures that the efficiency of the ORC increases with its maximum heat source temperature. The greatest ORC efficiency reached is 35.951% (see Table 3.20). The maximum heat source temperature of this test is the highest compared to all the other tests performed. This result confirms the hot source temperature is a key parameter for ORC. By analyzing all the tables displaying the combined cycle results, it is important to notice that the combined cycle highest efficiency obtained is 50.98 % (Table 3.26). The HCCI configuration giving the combined cycle highest efficiency is the configuration whose inlet parameters are: ϕ = 0.44, T_{in} =170° and p_{in} = 1.4 bar. There is no EGR in this configuration. The HCCI configuration using EGR which gives the highest combined cycle efficiency is the one with a 50% EGR fraction. Its results are displayed in Table 3.22.

ϕ [/]	p_{in} $[bar]$	T_{in} $[°C]$	θ_s [CAD]	θ_b [CAD]	η_{comb} [%]	P_{eff} $[kW]$	η_{eff} [%]	T_{smoke} $[°C]$	$\dot{m}_{smoke}$ $[g/s]$	$\dot{Q}_{smoke}$ $[kW]$	MPRR $[\frac{bar}{CAD}]$
0.32	1.9	165	-1.7	7	96	22.577	42.15	282.69	5.88	15.99	12.31

Table 3.27: Results of HCCI configuration: ϕ=0.32, p_{in}=1.9 bar, T_{in}=165°C.

ORC fluid	Subcritical							
	Without regenerator				With regenerator			
	P_{ORC} [W]	η_{ORC} [%]	π_c [/]	p_{vapor} [bar]	P_{ORC} [W]	η_{ORC} [%]	π_c [/]	p_{vapor} [bar]
R123	1.652	17.38	14.913	11.276	3.119	30.3	46.571	35.212
R141b	1.75	18.39	14.913	9.697	3.053	30.53	62.49	40.633
R1234yf	1.39	12.52	5.348	31.644	2.540	24.32	5.1837	30.673
R113	1.586	16.8	17.783	6.522	2.696	31.61	80	29.342
R134a	1.599	15.03	6.783	38.777	2.672	25.11	6.776	38.736
R245fa	1.535	16.2	14.913	18.352	2.797	29.16	27.469	33.803
R22	1.839	16.9	5.348	48.666	2.681	23.93	5.184	47.173
R717	2.120	20.83	8.217	70.463	3.270	23.82	11.551	99.048
R152A	1.797	18.38	8.696	44.601	2.810	26.11	8.3673	42.917
Hydrogen Sulfide	2.107	19.7	4.87	86.728	2.557	20.64	3.592	63.970
R507A	1.213	9.56	2.956	33.166	1.466	14.74	2	22.436
Sulfur Dioxide	2.081	20.53	9.652	31.917	3.341	24.42	21.102	69.778
R227EA	1.267	12.01	7.261	28.251	2.386	24.99	6.776	26.362
Carbon Dioxide	NaN	NaN	NaN	NaN	NaN	NaN	NaN	NaN

Table 3.28: ORC subcritical case results for the combination with HCCI configuration: ϕ=0.32, p_{in}=1.9 bar, T_{in}=165°C

This can be observed that despite the highest power of the combined cycle its efficiency is lower than the efficiency of the test without EGR. However, the inlet temperature of both HCCI configurations are not the same. As mentioned previously, the diminution of the HCCI inlet temperature has a positive impact of both HCCI power and efficiency because it allows a better filling. Therefore the HCCI configuration with a 50% EGR fraction, with an inlet temperature of 170°C could give the highest effective efficiency of the combined cycle. Unfortunately, this experimental test was not performed in this thesis.

After having analyzed several configurations of the combined cycle, it is possible to choose the optimal configuration, namely, the configuration with the greatest effective efficiency and whose ORC fulfill the most the organic fluid criteria. First it is necessary to choose the ORC configuration according to the organic fluid criteria 1.5.2. The thermodynamic criteria will have a higher impact than the others on the choice of the fluid because the purpose of this master thesis is to maximize the combine cycle power. As mentioned above, the subcritical ORC with a regenerator using sulfur dioxide gives the highest ORC power for a reasonable maximum cycle pressure and pressure ratio. This configuration satisfies therefore best the thermodynamic criteria. Section 3.8 shows that sulfur dioxide satisfies also well the second and the third criteria. Therefore the ORC configuration choice for the combined cycle of this thesis is the subcritical ORC with a regenerator using sulfur dioxide. As seen in the previous section, the HCCI configuration giving the maximum effective efficiency of the combine cycle is the configuration whose inlet parameters are: ϕ = 0.44, T_{in} =170°C and p_{in} = 1.4 bar. Therefore the combination of this HCCI configuration and the subcritical ORC using sulfur dioxide constitutes the combined cycle of this thesis. Its effective power and efficiency raises respectively to

ORC fluid	Supercritical							
	Without regenerator				With regenerator			
	P_{ORC} [kW]	η_{ORC} [%]	π_c [/]	p_{vapor} [bar]	P_{ORC} [kW]	η_{ORC} [%]	π_c [/]	p_{vapor} [bar]
R123	NaN	NaN	NaN	NaN	NaN	NaN	NaN	NaN
R141b	3.67	25.06	154.48	100.45	3.693	28.55	66.715	43.38
R1234yf	3.095	21.92	44.613	263.98	3.076	28.17	31.523	186.53
R113	3.625	24.46	220.58	80.904	3.603	27.32	273.04	100.15
R134a	3.365	24	65.036	371.82	3.335	27.93	52.804	301.89
R22	3.48	24.46	20.508	186.63	3.531	26.56	26.728	243.23
R245fa	3.437	23.24	271.76	334.43	3.418	26.73	201.64	248.14
R717	3.231	24.04	13.621	116.80	3.373	20.78	22.094	189.45
R152A	3.564	24.58	44.868	230.13	3.535	25.93	48.566	249.10
Hydrogen Sulfide	3.493	24.39	12.051	214.63	3.505	23.25	14.916	265.65
R507A	3.029	21.06	25.777	289.17	3.046	28.41	30.91	346.75
Sulfur Dioxide	3.509	25.52	24.566	81.232	3.497	18.83	39.847	131.76
R227EA	2.859	20.04	79.055	307.59	2.880	27.89	36.646	142.58
Carbon Dioxide	3.039	23.71	8.3057	475.84	3.027	24.71	8.7518	501.40

Table 3.29: ORC supercritical case results for the combination with HCCI configuration: ϕ=0.32, p_{in}=1.9 bar, T_{in}=165°C.

P_{HCCI} $[kW]$	P_{ORC} $[kW]$	P_{total} $[kW]$	η_{total} $[\%]$
22.577	3.693	26.27	49.04

Table 3.30: Combined cycle results for the HCCI configuration: ϕ=0.32, p_{in}=1.9 bar, T_{in}=165°C.

26.928 kW and 50.18%.

Following the work of Ando et al. [30], a comparison between the Solid Oxide Fuel Cell-Micro Gas Turbine (SOFC-MGT) hybrid system, with an overall efficiency of 55%, and the HCCI-ORC system can be made. The HCCI-ORC combined cycle could therefore be considered as a promising way to produce energy, as its efficiency only differs by 5% in comparison with the SOFC-MGT efficiency.

However, in order to not draw too hasty conclusion, let's remind that the HCCI configuration of this combined cycle was estimated though correlations and the ORC was simulated with some assumptions. The results obtained through the 0D model constitute therefore an upper limit which means that the actual efficiency of the combined cycle should therefore be slightly lower.

Furthermore, the power of the electrical heater has not been taken into account. Actually, high-energy exhaust gases could be used to preheat the intake load but this recycling solution comes on top of the three downstream cycles: turbocharging, EGR and ORC. Thus, this external power source should be deduced from the total power of the system.

To increase its efficiency and outperform the SOFT-MGT system, some ways of improving need still to be studied. However, the HCCI-ORC system seems to be a promising technology in stationary power generation.

CONCLUSION

This thesis has addressed three ways to extend the operating range of an HCCI engine: turbocharging, exhaust gas recirculation and Organic Rankine Cycle.

The first chapter of this work presents the theoretical concepts to understand the technology behind HCCI combustion, turbocharging, EGR and ORC. The second chapter explains the methodology used in the frame of this work to obtain the final results. A 0D model was developed to simulate the processes that occur in the engine. Experiments were conducted on a stationary natural gas HCCI engine, equipped with both turbocharging and EGR. A mathematical model was implemented for the theoretical study of the ORC.

The final chapter gathers all the results obtained through experiments and theoretical simulations. It has be found out that the optimum CA50 of the engine would lie around 2 CAD, resulting in high IMEPg along with high indicated efficiency. A maximum brake efficiency of nearly 30% would be achieved at $p_{in} = 1.3$ bar, $T_{in} = 170$°C and $\phi = 0.46$, giving a BMEP of 3.7 bar. The use of EGR could drastically extend the operating range of the engine. Indeed, with 50% EGR, a BMEP of 5 bar is obtained, with a brake efficiency of 31.6%.

A higher brake efficiency of 43.3% is reached when the engine is simulated through the 0D model. When coupling with the Organic Rankine Cycle, the whole system could achieve an overall efficiency of 50.2%, which makes it quite competitive with the SOFC-MGT system and its 55% efficiency. Despite some assumptions made in the frame of this thesis, the HCCI-ORC system seems to be a promising technology in stationary power generation.

BIBLIOGRAPHY

[1] Bengt Johansson. Towards High Efficiency Engine. Lund University, Division of Combustion Engines, 2015.

[2] Arnaud Rouanet. Turbocharging and Exhaust Gas Recirculation on a Stationary Natural Gas HCCI Engine: Theoretical Analysis. Master's thesis in Engineering Sciences, under the supervision of Prof. Hervé Jeanmart, Université catholique de Louvain, 2015.

[3] François Boveroux and Amaury Gramme. Développement expérimental d'un moteur HCCI au gaz naturel. Master's thesis in Engineering Sciences, under the supervision of Prof. Hervé Jeanmart, Université catholique de Louvain, 2016.

[4] S. Aceves and D. Flowers. Engine Shows Diesel Efficiency without the Emissions. *Sci Technol Rev*, pages 17–19, 2004.

[5] P. Amneus, D. Nilsson, F. Mauss, M. Christensen, and B. Johansson. Homogeneous Charge Compression Ignition Engine: Experiments and Detailed Kinetic Calculations. *The Fourth International Symposium on Diagnostics and Modeling of Combustion in Internal Combustion Engines*, 1998.

[6] K. Kobayashi, T. Sako, Y. Sakaguchi, S. Morimoto, S. Kanematsu, K. Suzuki, T. Nakazono, and H. Ohtsubo. Development of HCCI natural gas engines. *Journal of Natural Gas Science and Engineering*, 3 (5):651–656, 2011.

[7] Hervé Jeanmart. LMECA2220 – Internal Combustion Engines. Université catholique de Louvain, 2017.

[8] Subir Bhaduri. Experimental Studies on HCCI Combustion of Biomass Syngas Towards Tar Tolerant Operation. Doctoral thesis in Engineering Sciences, under the supervision of Prof. Hervé Jeanmart, Université catholique de Louvain, 2015.

[9] Maxime Pochet, Véronique Dias, Hervé Jeanmart, Sebastian Verhelst, Julien Blondeau, and Francesco Contino. Multifuel HCCI Engine: Numerical Study of the Operating Range for Hydrogen, Ammonia, Methane, Methanol and Their Blends. 2017.

[10] Maxime Pochet, Ida Truedsson, Fabrice Foucher, Hervé Jeanmart, and Francesco Contino. Ammonia-Hydrogen Blends in Homogeneous-Charge Compression-Ignition Engine. *SAE International*, 2017.

[11] Magnus Christensen, Bengt Johansson, Per Amnéus, and Fabian Mauss. Supercharged Homogeneous Charge Compression Ignition. *SAE Transactions, Journal of Engines*, 107(SAE Technical Paper 980787), 1998.

[12] Nicolas C. Baines. *Fundamentals of Turbocharging*. Concepts NREC, 2005.

[13] Hermann Hiereth, Klaus Drexl, and Peter Prenninger. Charging the internal combustion engine. *Springer Science & Business Media*, 2007.

[14] Youngsoo Park and Choongsik Bae. Experimental study on the effects of high/low pressure EGR proportion in a passenger car diesel engine. *Applied Energy*, 133:308–316, 2014.

[15] Subir Bhaduri, Hervé Jeanmart, Ernst Breuer, , and Francesco Contino. Studies of EGR in Biomass Syngas Fuelled Tar Tolerant HCCI Engines. 2015.

[16] Gequn Shu, Mingru Zhao, Hua Tian, Haiqiao Wei, Xingyu Liang, Yongzhan Huo, and Weijie Zhu. Experimental investigation on thermal OS/ORC (Oil Storage/Organic Rankine Cycle) system for waste heat recovery from diesel engine. *Energy*, 107:693–706, 2016.

[17] A. Rettig, M. Lagler, T. Lamare, S. Li, V. Mahadea, S. McCallion, and J. Chernushevich. Application of Organic Rankine Cycles (ORC). *World Engineer's Convention*, 2011.

[18] S. Saadon and A. R. Abu Talib. An analytical study on the performance of the organic Rankine cycle for turbofan engine exhaust heat recovery. *IOP Conference Series: Materials Science and Engineering*, 152(1), 2016.

[19] Richard L. Powell. CFC phase-out: have we met the challenge? *Journal of Fluorine Chemistry*, 114: 237—250, 2002.

[20] Huijuan Chen, D. Yogi Goswami, and Elias K. Stefanakos. A review of thermodynamic cycles and working fluids for the conversion of low-grade heat. *Renewable and Sustainable Energy Reviews*, 14(9): 3059–3067, 2010.

[21] Yann Bartosiewicz and Miltiadis Papalexandris. Lmeca1855 — thermodynamique et énergétique. Université catholique de Louvain, 2017.

[22] James M Calm. Options and outlook for chiller refrigerants. *International Journal of Refrigeration*, 25 (6):705–715, 2002.

[23] Sotirios Karellas, Andreas Schuster, and Aris-Dimitrios Leontaritis. Influence of supercritical ORC parameters on plate heat exchanger design. *Applied Thermal Engineering*, 33–34:70–76, 2012.

[24] D. Jonhson, J. Martin, and P. Wauters. *Thermal Power Plants - Energetic and exergetic approaches*. DUC - Presses universitaires de Louvain, 2016.

[25] B. Johansson, O. Andersson, P. Tunestål, and M. Tunér. MVKN50 – Introduction to Combustion Engines. Lund University, 2014.

[26] H.S. Soyhan, H. Yasar, H. Walmsley, B. Head, G.T. Kalghatgi, and C. Sorusbay. Evaluation of heat transfer correlations for HCCI engine modeling. *Applied Thermal Engineering*, 29(2–3):541–549, 2009.

[27] Stijn Broekaert, Thomas De Cuyper, Kam Chana, Michel De Paepe, and Sebastian Verhelst. Assessment of Empirical Heat Transfer Models for a CFR Engine Operated in HCCI Mode. *SAE Technical Paper*, 2015.

[28] Martin Golard and Mathieu Rosar. Analyse expérimentale d'un moteur HCCI turbocompressé avec recirculation des gaz d'échappement. Master's thesis in Engineering Sciences, under the supervision of Prof. Hervé Jeanmart, Université catholique de Louvain, 2017.

[29] Per Tunestål. TDC Offset Estimation from Motored Cylinder Pressure Data based on Heat Release Shaping. *Oil & Gas Science and Technology - Revue d'IFP Energies nouvelles*, 66(4):705–716, 2011.

[30] Yoshimasa Ando, Hiroyuki Oozawa, Masahiro Mihara, Hiroki Irie, Yasutaka Urashita, and Takuo Ikegami. Demonstration of SOFC-Micro Gas Turbine (MGT) Hybrid Systems for Commercialization. *Mitsubishi Heavy Industries Technical Review*, 52(4):47–52, 2015.

APPENDIX A

TEST BENCH

A.1 Engine technical data

YANMAR

4TNV98T

Engine Technical Data Revision: 0

	Unit	4TNV98T-GGE
General Data		
Number of Cylinders	-	4
Engine Type	-	Inline, Water-Cooled, 4 Stroke Diesel
Bore x Stroke	mm x mm	98 x 110
Total Displacement	cc	3.318
Combustion type	-	Direct Injection
Aspiration	-	Turbocharged Aspiration
Valves per Cylinder	-	4
Compression ratio	-	18.1
Firing Order	-	1-3-4-2
Performance Data		
Net Intermittent Power	HP [kW] / rpm]	67.2 [50.09]/1800, 55.5 [41.42]/1500
Net Continuous Power	HP [kW] / rpm]	60.8 [45.3]/1800, 50.5 [37.69]/1500
Net Max Torque	ft-lb [Nm]/rpm	-
Low Idle Speed	rpm	1500+/-25
High Idle Speed	rpm	1900+/-25
Physical Data		
Direction of rotation	-	Counter Clockwise (view from flywheel)
Length - Inches	Inches [mm]	31.06 [789]
Width - Inches	Inches [mm]	21.85 [555]
Height - Inches	Inches [mm]	32.95 [837]
Dry Weight	lbs [kg]	606 [275]
PTO System		
Flywheel	-	SAE #3
Flywheel Housing	-	SAE #3 (125 mm Depth)
Gear Case	-	without SAE Hydraulic Pump Flange
Lubrication System		
Inclination, Continuous	degrees	30
Inclination, 3 minutes Max.	degrees	35
Lubrication Oil Filter Type	-	Paper Element
Oil Capacity, Effective	Liters	4.5
Total System Capacity	Liters	10.5
Oil Change Interval, Hours	hr	250 (50, initial)
Recommended Oil Type	API	CD, CE, CF or higher grade
Cooling System		
Fan Type	-	Pusher
Fan Diameter	Inches [mm]	16.9 [430]
Number of Blades	-	6
Fan Pulley Diameter	Inches [mm]	4.3 [110]
Crank Pulley Diameter	Inches [mm]	5.1 [130]
Fuel System		
Fuel Filter Type	-	Paper Element
Fuel Injection Pump Type	-	Distributor Type
Water Separator (Standard)	-	Mesh size: 100-mesh/inch, water reservoir 150 cc
Electrical System		
System Voltage	Volts	12 V
Electric Stop Device	-	Stop Solenoid
Alternator	-	12V-40A
Starting Aid Device	-	Air Heater, 12V 400W
Standard pre-heat time	Seconds	15
Starting Motor Type	-	Reduction
Starting Motor Power	kW	2.3

A.2 Piping and instrumentation diagram (P&ID)

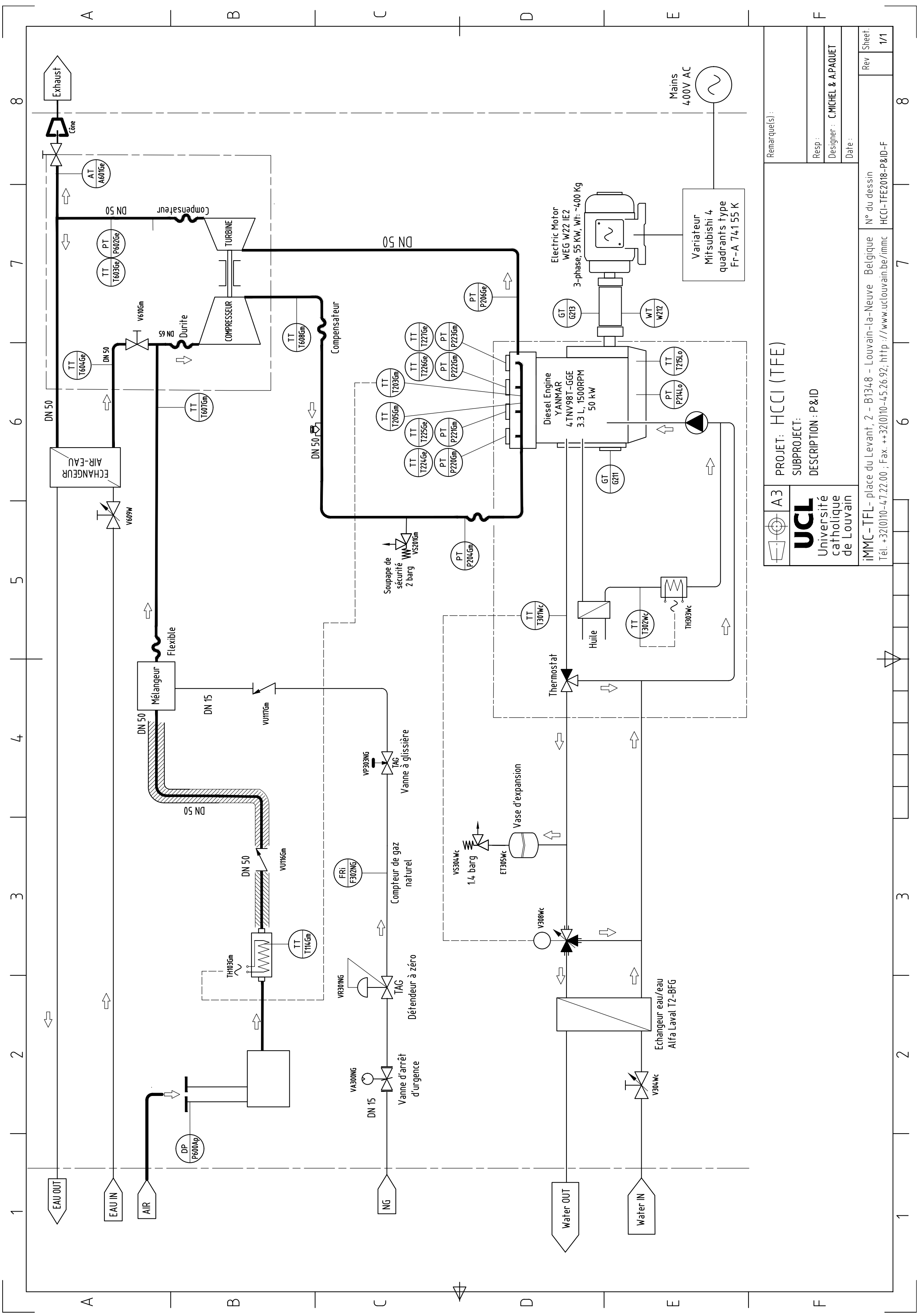

A.3 LabVIEW user interface

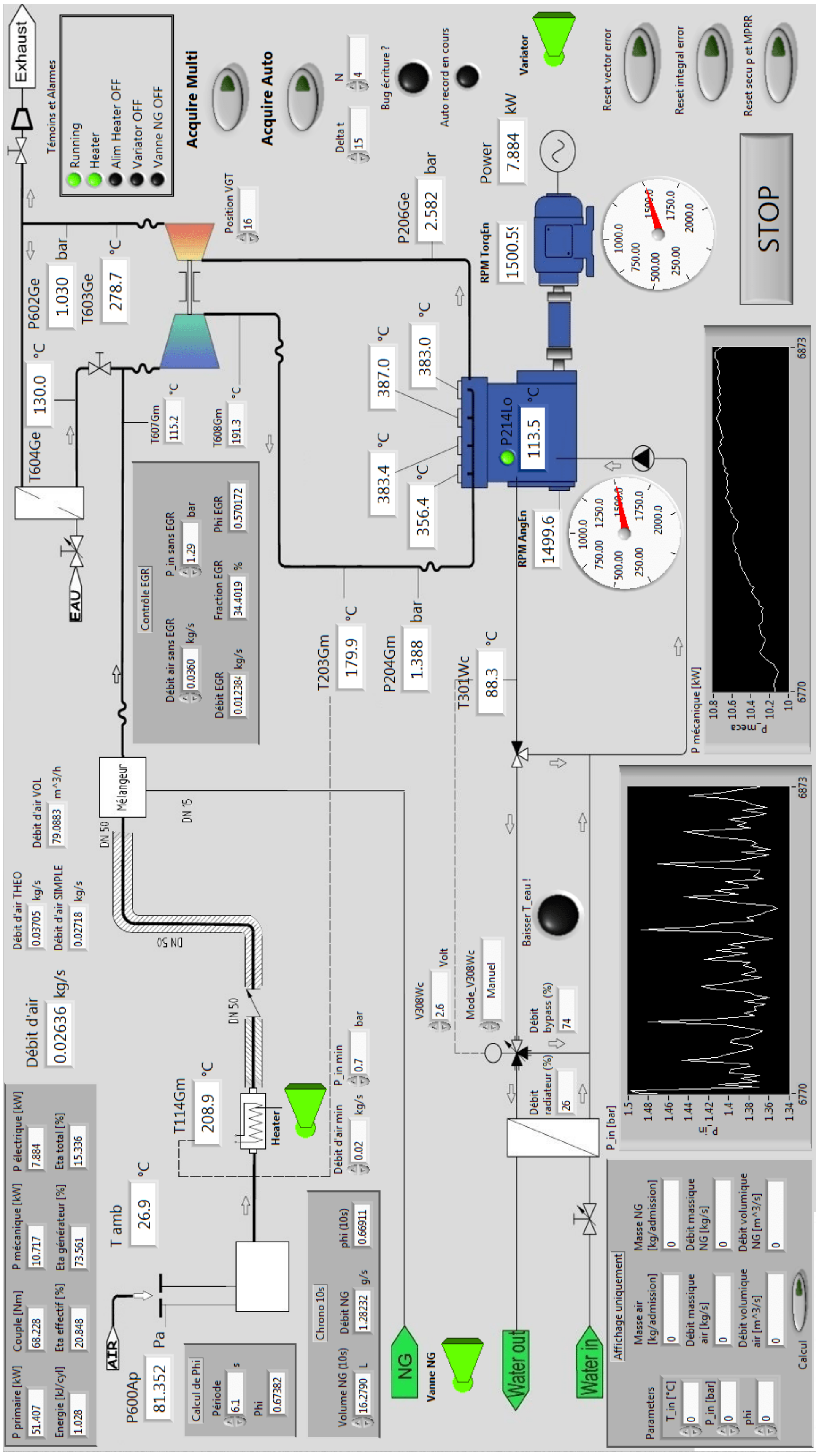

Rue Archimède, 1 bte L6.11.01, 1348 Louvain-la-Neuve www.uclouvain.be/epl